RECOVERY ACT: Efficient Regeneration of Physical and Chemical Solvents for CO_2 Capture

FINAL REPORT

Reporting Period Start Date: 12/1/2009

Reporting Period End Date: 5/30/2013

Principal Authors: Brian Tande, Wayne Seames, Steve Benson

Report Date: December 2013

Award Number: DE-FE0002196

University of North Dakota
241 Centennial Dr. Stop 7101
Grand Forks, ND 58201

ABSTRACT

The objective of this project was to evaluate the use of composite polymer membranes and porous membrane contactors to regenerate physical and chemical solvents for capture of carbon dioxide (CO_2) from synthesis gas or flue gas, with the goal of improving the energy efficiency of carbon capture. Both a chemical solvent (typical for a post-combustion capture of CO_2 from flue gas) and a physical solvent (typical for pre-combustion capture of CO_2 from syngas) were evaluated using two bench-scale test systems constructed for this project. For chemical solvents, polytetrafluoroethylene and polypropylene membranes were found to be able to strip CO_2 from a monoethanolamine (MEA) solution with high selectivity without significant degradation of the material. As expected, the regeneration temperature was the most significant parameter affecting the CO_2 flux through the membrane. Pore size was also found to be important, as pores larger than 5 microns lead to excessive pore wetting. For physical solvents, polydimethyl-siloxane (PDMS)-based membranes were found to have a higher CO_2 permeability than polyvinylalcohol (PVOH) based membranes, while also minimizing solvent loss. Overall, however, the recovery of CO_2 in these systems is low – less than 2% for both chemical and physical solvents – primarily due to the small surface area of the membrane test apparatus. To obtain the higher regeneration rates needed for this application, a much larger surface area would be needed. Further experiments using, for example, a hollow fiber membrane module could determine if this process could be commercially viable.

Table of Contents

Table of Figures

Acronyms and Abbreviations

Abbreviations

AMP	2-amino-2-methyl-1-propanol
ATR	Attenuated Total Reflectance
CA	Cellulose Acetate
CE	Cellulose Ester
CFD	Computational Fluid Dynamics
DEA	Diethanolamine
DMPEG	Dimethyl ethers polyethylene glycol
DOE	Department of Energy
DSC	Differential Scanning Calorimetry
EIA	Energy Information Administration
FID	Flame Ionization Detector
FTIR	Fourier Transform Infrared Spectroscopy
GC	Gas Chromatography
IR	Infrared
LEPW	Liquid Entry Pressure of Water
MD	Membrane Distillation
MDEA	N-methyldiethanolamine
MEA	Monoethanolamine
NDIR	Non-dispersive Infrared
PA	Polyamide
PDMS	Polydimethylsiloxane
PE	Polyethylene
PES	Polysulfone
PETE	Polyethylene terephthalate
PTFE	Polytetrafluoroethylene
PVOH	Polyvinylalcohol
PVDF	Polyvinylidene fluoride
SEM	Scanning Electron Microscopy
TPC	Temperature Polarization Coefficient
TCD	Thermal Conductivity Detector
UV-vis	Ultraviolet–visible

Chemical Species

CO	Carbon Monoxide
CO_2	Carbon Dioxide
H_2	Hydrogen
H_2O	Water
HCl	Hydrochloric Acid
He	Helium
N_2	Nitrogen
N_2O	Nitrous Oxide
O_2	Oxygen

Se	Selenium
Zn	Zinc

Symbol and Meaning

A	Absorbance
B	Geometry factor
C	Concentration
$\mathrm{c_p}$	Specific heat
d_p	Diameter of pores
D	Diffusivity coefficient
$\mathrm{D_k}$	Knudsen diffusivity
$\mathrm{D_G}$	Diffusivity in the gas phase
$\mathrm{D_E}$	Combination of Knudsen and molecular diffusivity coefficient
h	Heat transfer coefficient
K	Equilibrium constant
$\mathrm{k_B}$	Boltzmann constant
k_L	Mass transfer coefficient through melt
k_E	Mass transfer coefficient at surface
k_U	Mass transfer coefficient through pores
K	Equilibrium constant
s	Solubility coefficient
k_G	Gas mass transfer coefficient
k_L	Liquid mass transfer coefficient
k_M	Membrane mass transfer coefficient
k_{OL}	Overall mass transfer coefficient
M_i	Molecular weight of species i
m_s	Sample weight (gr)
P	Pressure
P_1	Physical solvent Sampling module pressure after evacuation (psi)
P_2	Physical solvent Sampling module final pressure after sample injection (psi)
R	Gas constant
t	Time
T	Absolute temperature
$\mathrm{T_f}$	Viscous Flow Temperature
$\mathrm{T_g}$	Glass Transition Temperature
$\mathrm{T_m}$	Melting Point
V	volume
V_T	Sampling module total volume($\mathrm{cm^3}$)

V_s	Sample volume (cm^3)
X_{CO2}	Mole fraction of CO2 in physical solvent

Dimensionless Numbers

E	Enhancement factor
H	Henry's constant
Re	Reynolds number
Sc	Schmidt number
Sh	Sherwood number
Re	Reynolds number

Greek Symbols

α	CO_2 loading
κ/ε	Lennard-Jones parameter
μ_γ	Viscosity
π	3.14159….
ρ	Density
σ	Collision diameter
ε	Membrane porosity
τ	Membrane tortuosity
θ	Contact angle
λ	Mean free path

1 Executive Summary

The overall objective of this project was to evaluate the use of composite polymer membranes and porous membrane contactors for the recovery of carbon dioxide (CO_2) from CO_2-rich solvent streams. The development of materials and processes is necessary to reduce the capital and operating costs of the solvent regeneration process, in particular, the energy expended in regeneration. These membrane systems have the potential to help meet this goal because they can reduce the thermal and/or pressure cycling requirements of traditional solvent regeneration systems and because they facilitate CO_2 transport out of the solvent by increasing the interfacial contact area for mass transfer. The specific goals of this project were as follows:

1) Train graduate students in carbon capture technologies through fundamental research that includes a primary research experience.
2) Fabricate a continuous bench-scale test system to measure membrane performance.
3) Assess the capability of a range of composite polymer membranes and porous membrane contactors to regenerate physical and chemical solvents for CO_2 capture.
4) Perform a commercial feasibility study.

A total of three graduate students collectively received nearly 5000 hours of training throughout the course of this project. This training included the design, construction, and operation of test equipment, the planning and analysis of experiments, and the oral and written communication of results.

Two bench-scale test systems were constructed. The first was designed to evaluate membranes for the regeneration of chemical solvents, specifically monoethanolamine (MEA). It contained an absorber, an in-line heater, a membrane fixture and two analytical tools used to characterize the flux of CO_2 through the membrane material being tested: a gas chromatograph (for high concentrations) and an infrared (IR) detector (for low concentrations). The second system was designed to evaluate membranes for the regeneration of physical solvents, specifically Selexol. It was similar to the first system, except that it was designed to operate at higher pressures – requiring, among other changes, a different absorber, membrane fixture, and circulation pump. Both systems were tested to validate their ability to continuously circulate the solvent from the absorber through the membrane module, while measuring the flux of CO_2 through the membrane.

For chemical solvents, a wide variety of porous, polymeric membranes were evaluated to determine which materials would be suitable for this application. Of those tested, polytetrafluoroethylene and polypropylene were able to strip CO_2 from an MEA solution with high selectivity without excessive swelling or fouling. As expected, the temperature was, by far, the most significant parameter affecting the CO_2 flux through the membrane. A detailed study of the effect of membrane pore size revealed that a pore size of 0.6 µm resulted in the highest selectivity, allowing substantial CO_2 flux while minimizing solvent loss. In general, membranes with a pore size smaller than 2.5 µm showed excellent hydrophobicity with no wetting, while pore sizes of 5 µm and 10 µm were wetted by the solvent, slowing mass transfer.

Physical solvent regeneration was evaluated using two types of dense (nonporous) composite membranes: polyvinyl alcohol (PVOH) and polydimethylsiloxane (PDMS). PDMS-based membranes had a higher CO_2 permeability than PVOH based membranes. One PDMS membrane (PERVAP 4060) had the highest overall flux with a minimal loss of Selexol. Unlike chemical solvents, it was determined that increasing the solvent temperature does not affect the CO_2 flux through the membrane. However, the pressure did appear to have a significant effect, presumably by increasing the driving force for mass transfer.

For both systems studied, the rate of mass transfer is controlled by transport through the membrane. Overall, the recovery of CO_2 in these systems is rather low. For chemical solvents, less than 1% of the CO_2 in MEA was recovered, while for physical solvents, the recovery was less than 2%. While the membrane surface area for our test system was small- just a few square centimeters- the results suggest that a very large surface area would be needed to obtain the high regeneration rates needed for this application. Further experiments using, for example, a hollow fiber membrane module could determine if this process were commercially viable.

2 Background

2.1 Chemical Solvents for Post-Combustion Capture

Chemical solvents, such as alkanolamines, used in CO_2 capture rely on a chemical reaction with acidic gases. The most common alkanolamine currently in use for application is MEA. It has been widely used as a CO_2 absorption solvent for over 70 years in natural gas sweetening and gas scrubbing facilities (Wallace, 2006). Other commonly used alkanolamines include: 2-amino-2-methyl-1-propanol (AMP), diethanolamine (DEA) and N-methyldiethanolamine (MDEA) (Alvarez, Rendo, Sanjurjo, Sanchez-Vilas, & Navaza, 1998). These amines are usually divided into three main categories–primary, secondary, and tertiary–according to the number of carbon-nitrogen bonds. For example, MDEA is a tertiary amine because it has three carbon-nitrogen bonds; DEA is a secondary amine because it has two carbon-nitrogen bonds whereas MEA is a primary amine as it has only one.

MEA is the alkanolamine with the highest alkalinity (S. A. Freeman, Davis, & Rochelle, 2010). A hydroxyl group on the molecule makes MEA ready to be dissolved into polar solvents such as water, and 10 to 30 wt % aqueous solutions of MEA are most commonly used. The basic amine group of an MEA molecule reacts very rapidly with CO_2 to form a carbamate and a proton. This reaction occurs very efficiently below 60°C with an exothermic heat load of 72 kJ per mole of CO_2 absorbed (30 wt % MEA) (Yeh, Pennline, & Resnik, 2001).

Below the CO_2 saturation point, the rate of reaction with MEA usually determines the overall absorption rate. MEA is favored for complete CO_2 removal due to its fast reaction rate. The MEA and CO_2 chemistry (Hook, 1997) is illustrated in Figure 2.1. Yeh et al. (Yeh et al., 2001) found no significant difference in absorption ability in the range 38-50°C for a 20 wt% aqueous MEA solution. The principle behind the regeneration process is the fact that the MEA–CO_2 reaction is reversed by supplying heat to the system to raise the temperature to 70°C and higher. CO_2 regeneration at 120°C requires a heat load of 165 kJ per mole of CO_2 (Yeh et al., 2001). Up to 80 % of the total cost of absorption/desorption can be attributed to the regeneration process even with effective integration of waste heat (Yeh et al., 2001).

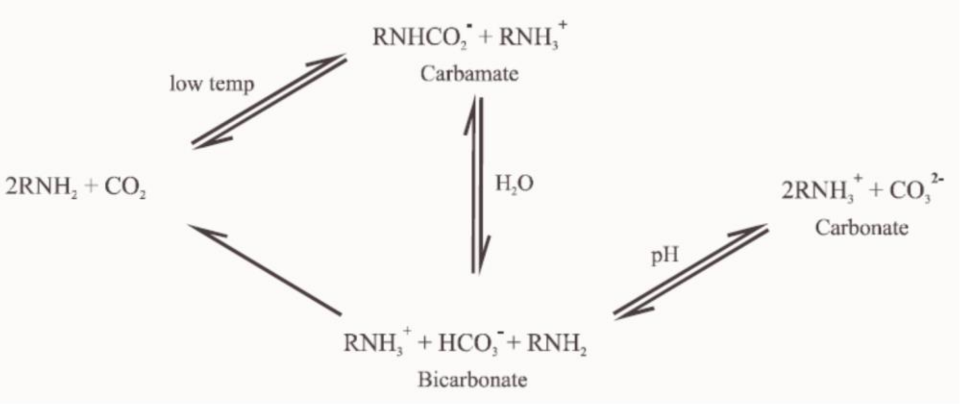

Figure 2.1 MEA-CO_2 chemistry illustration (Wallace, 2006), RNH_2 stands for an amine, where $R=CH_2CH_2OH$ represents MEA.

Besides the heavy energy consumption of this process, there are operational issues that arise from using MEA for CO_2 capture. Corrosion of the equipment as well as oxidative or thermal degradation of the solvent are the most significant problems (Davis, 2009; S. A. Freeman et al., 2010; Kittel et al., 2009). MEA, upon exposure to a certain amount of free O_2, usually found in flue gas streams, can react to form corrosive degradation products (Kittel et al., 2009). Inhibitors are often used with MEA to improve solvent performance (Goff & Rochelle, 2006). Selected physical properties of MEA are summarized and compared with water in Table 2.1.

Table 2.1Selected propertied of MEA and water (Wallace, 2006)

Property	MEA	Water	Unit
Molecular Formula	C_2H_7NO	H_2O	N/A
Molecular Weight	61.08	18.02	g/mol
pH	12.5	7	N/A
Density	1012	1000	kg/m^3
Boiling Point	171	100	°C (1atm)
Melting Point	10.5	0	°C (1 atm)
Specific Heat	3200	4182	J/kg.K (25°C)
Thermal Conductivity	0.299	0.598	W/m-K (25°C)
Absolute Viscosity	0.021	0.001	Pa.s (25°C)
Surface Tension	0.048	0.073	N/m (25°C)
Vapor Pressure	0.05	2.3	kPa (25°C)
Vapor Pressure	10 (110°C)	101.3 (100°C)	kPa

2.2 Physicals solvents for Pre- or Post-Combustion Capture

2.2.1 Physical absorption

The major concern regarding using the typical chemical solvents such as amines is the heat requirement for solvent regeneration which can decrease the plant efficiency significantly. This is the primary motive to develop processes that employ nonreactive solvents, such as physical solvents. Unlike chemical solvents, physical solvents do not react with the solute but rather physically dissolve the acid gases, which are then stripped, without the need to be heated, by means of pressure swing techniques.

The performance of a physical solvent depends on its capacity to dissolve different gases. The solubility of an individual gas follows Henry's law—the solubility of a compound in the solvent is directly proportional to its partial pressure in the gas phase. Hence, the capacity of a physical solvent can be enhanced by increasing the partial pressures of gases. This is one of the major advantages of physical solvents over chemical solvents for removal of acid gases from high pressure syngas. As shown in

Figure 2.2, chemical solvents have higher absorption capacity than physical solvents at relatively low acid gas partial pressures. However, their absorption capacities are less than that of a physical solvent at higher partial pressures. The solubility of an acid gas in physical solvents increases linearly with its partial pressure. Therefore, chemical solvent technologies are favorable at low acid gas partial pressures and physical solvents are favored at high acid gas partial pressures. Furthermore, the physical absorption allows for the solvent to be partially regenerated by pressure reduction, which reduces the energy requirement compared to chemical solvents.

The Rectisol process was the earliest physical solvent commercial process used for synthesis gas applications. The trend of physical solvents accelerated in 1960 with the introduction of the Fluor solvent process, which was followed by several other physical solvent processes (Kohl & Nielsen, 1997).

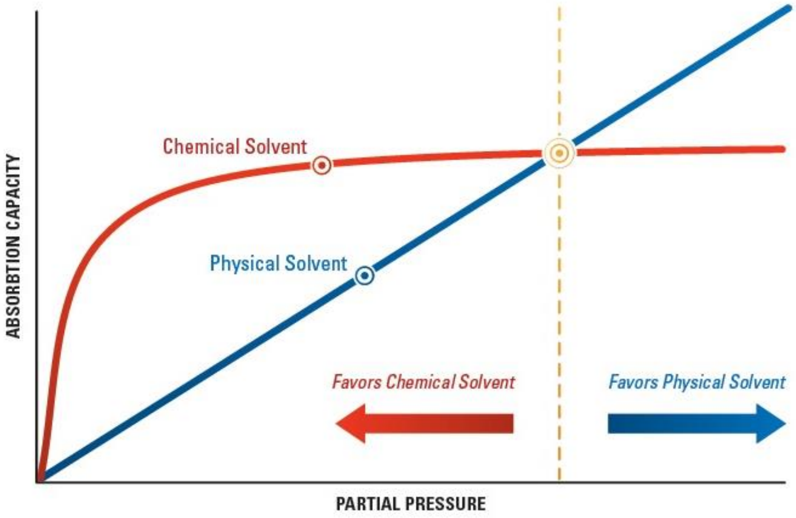

Figure 2.2. Absorption capacity of physical and chemical solvents (NETL, May 2011).

Table 2.2 shows a list of major physical solvents that have been or are currently used commercially.

Table 2.2. Physical Solvent Processes (Epps, R. Union Carbide Chemicals & Plastics Technology Corporation, 1992).

Process Name	Solvent	Process Licensor
Flour Solvent	Propylene carbonate	Fluor Daniel
SELEXOL	Dimethyl ether of polyethylene glycol(DMPEG)	Union Carbide
Sepasolv MPE	Methyl isopropyl ether of polyethylene glycol (MPE)	Badische (BASF)
Purisol	NMP	Lurgi and Linde AG
Ifpexol	Methanol	Institut Francais du petrole (IFP)
Etasolvan	Tributyl phosphate	IFP/Uhde
Methylcyanoacetate	Methylcyanoacetate	Unocal
Rectisol	Methanol	Lurgi

As mentioned earlier, the most important parameter in designing and selecting the type of process and its associated solvent is the solubility of the gaseous impurities to be absorbed. In order to be practical, the solvents must have an equilibrium capacity for acid gases several times of that of water, coupled with a low capacity for the primary constituents of the synthesis gas stream, e.g, hydrocarbons and hydrogen. Additionally, they must have low viscosity to minimize the amount of required work for recirculating the solvent throughout the plant. They must be noncorrosive to common metals as well as nonreactive with all components in the gas (Kohl & Nielsen, 1997). To minimize the amount of solvent loss and reduce the need to scrub the flue gas for solvent recovery, they must have a very low vapor pressure at ambient temperature and eventually they must be commercially available at a reasonable price. Physical solvent processes are used primarily for acid-gas removal from high-pressure natural-gas streams and for carbon dioxide removal from crude hydrogen and ammonia synthesis gases produced both by partial oxidation and steam-hydrocarbon reforming.

As the molecular weight of the hydrocarbon increases, the solubility also increases. Consequently, hydrocarbons heavier than ethane are also removed to a large extent.

This is one of the main reasons why physical solvents are mainly used in the case of gasification when the syngas has no significant amount of hydrocarbon. Physical solvent processes are generally not commercial for the treatment of hydrocarbon streams that contain a substantial amount of pentane-and-heavier hydrocarbons (Kohl & Nielsen, 1997). In their simplest form, physical solvent processes require an absorber, an atmospheric flash vessel and a recycle pump.

After regenerating the solvent by pressure letdown, the lean solution contains acid gas in an amount corresponding to equilibrium at 1atm acid-gas partial pressure is recycled back to the absorber. To obtain higher degree of purification, vacuum or inert gas stripping or heating of the solvent must be implemented. Design equations and simulation models commonly used for hydrocarbon separations are generally applicable to physical solvent gas purification. The key requirement is adequate liquid/vapor equilibrium data covering all components and conditions appearing in the process. The selectivity of a physical absorption process can be enhanced by the use of more than one stripping and absorption stage. Many different flow schemes have been developed to meet specific requirements and to take advantage of the properties of specific solvents.

One of the key parameters in designing a physical solvent process is the solvent circulation rate since it affects the size and the cost of every piece of equipment, including the absorber, piping, circulation pumps and flash drums. The main parameter that affects solvent circulation rate is the contact temperature. At lower temperatures, solvent capacity for acid gases increases and thus less solvent needs to be recirculated. The other advantage of lower temperature is to minimize the amount of hydrocarbon loss due to the fact that acid-gases solubility increases much more than hydrocarbon solubility as temperature decreases. It should be kept in mind that the temperature to which a solvent may be cooled is limited primarily by its increased viscosity and the resulting decrease in solvent heat and mass transport capabilities.

As outlined by Kohl and Nielsen (Kohl & Nielsen, 1997), the most important factors in selecting a physical solvent process are:

- Process performance in terms of acid gas composition and treated gas purity
- Loss of light and heavy hydrocarbons,
- Experience and ingenuity of the designer and adapting the process to the case at hand
- Method of dealing with impurities such as COS, NH_3, aromatic hydrocarbons etc.
- Consideration of corrosion, foaming and other operating problems
- Cost of initial solvent charge
- Cost of replacement solvent
- Energy and /or stripping cost
- Process royalty cost

A comparison of common physical solvent processes in terms of power requirement, removal efficiency and equipment required was given by (Burr & Lyddon, 2008). Among the common physical solvents, Selexol is one of the most widely used both in natural gas processing and gasification applications. Selexol has a very low vapor pressure (9.73×10^{-5} kPa) and a relatively high capacity for CO_2 absorption. In addition, Selexol has an acceptable range of operating temperature and good selectivity for CO_2

and H_2S removal. More details of the solubility data in common physical solvents are available in literature (Bucklin & Schendel, 1985; Doctor, Molburg, & Thimmapuram, 1994; Epps, R. Union Carbide Chemicals & Plastics Technology Corporation, 1992; Korens, Simbeck, Wilhelm, Longanbach, & Stiegel, 2002; Newman, 1985; Rousseau, Matange, & Ferrell, 1981). Although different research groups are working in the field of synthesizing new physical solvents with improved capability for absorbing acid gases (Heintz, Sehabiague, Morsi, Jones, & Pennline, 2008; Porter, Sitthiosoth, & Jenkins, 1991), the primary focus of this research is on the application of Selexol process to the IGCC power plants. More details of the Selexol process will be discussed in next section.

2.2.2 Selexol process

2.2.2.1 Selexol process history and current practices

The Selexol process, patented by Allied Chemical Corp., has been used since the late 1960s. The process was sold to Norton in 1982 and then bought by Union Carbide in 1990 (R. Epps, 1994). The Dow Chemical Co. acquired gas processing expertise, including the Selexol process, from Union Carbide in 2001. The process is offered for license by several engineering companies-the most experienced of which is Universal Oil Products (UOP) (Breckenridge, Holiday, Ong, & Sharp, 2000). Over 60 Selexol units have been put into commercial services (*UOP* 2009), which cover a wide variety of applications, ranging from natural gas to synthetic gas. Moreover, increasing interests in controlling CO_2 emission may lead to a wider adoption of the Selexol process, particularly for coal gasification plants. Relevant experiences for gasification are Sarlux - Italy (IGCC- Power plus H_2), API-Italy (IGCC Power), Coffeyville Resources – USA (NH_3/urea ammonium nitrate), OptiCanada - Oil Sands Canada (H_2 plus fuel) (*UOP*

2009). The 100 megawatt (MW) Texaco/Cool Water (California) 1,000 tons per day coal gasifier plant for IGCC demonstration was operated continuously for about five years in the 1980s and the Selexol unit performed extremely well. The Tennessee Valley Authority/Muscle Shoals (Alabama) 200 tons per day coal gasifier demonstration plant was operated continuously for about five years in the early 1980s, using the Selexol process. In addition, multiple large units are in engineering phase such as Residue gasification for H_2 production (Oil Sands Canada) and other gasification projects. According to Union Carbide as of 1992, a total of 53 Selexol plants had been installed. These comprise 10 for CO_2 removal from various synthesis gas, 12 for CO_2 removal from natural gas, 15 for selective H_2S removal, 8 for desulfurization of synthesis gas and 8 for landfill gas purification (Kohl & Nielsen, 1997).

2.2.2.2 Solvent properties

The solvent used in the Selexol acid removal system is a mixture of dimethyl ethers of polyethylene glycol (DMPEG) (with the formulation of $CH_3(CH_2CH_2O)_nCH_3$, where n is between 3 and 9. The size of the molecule enables the solvent to have vapor pressure and viscosity values low enough to inhibit evaporative losses and lower pumping costs respectively. The oligomers' end groups are methyl ether groups rather than hydroxyl groups. The oxygen of the methyl ether group increases the CO_2 solubility by providing an additional site for Lewis acid: Lewis base interaction with CO_2. Selexol solvent is a yellow to brown liquid with a mild odor. The general properties of the DMPEG are given by (Newman, 1985; Sciamanna & Lynn, 1988) and summarized in Table 2.3.

Table 2.3. DMPEG Basic properties.

Property	Value
Vapor pressure, kPa @25 °C	9.73×10^{-5}
Viscosity, cp @25 °C	5.8
Maximum feasible operating temperature, °C	175
Density, kg/m^3	1,030
Boiling point, °C	240
Freezing point, °C	-28
Molecular weight	250

Solvents containing DMPEG are licensed and/or manufactured by several companies including Coastal Chemical Company, Dow (Selexol) and UOP (Selexol). Other process suppliers such as Clariant GmbH of Germany offer similar solvents (Burr & Lyddon, 2008). The performance of a physical solvent can be predicted by its solubility.

As explained previously, the solubility of a physical solvent follows Henry's law. This explains the reason why physical solvents are favorable in gasification application where the partial pressure of acid-gas is high enough so that the solvent capacity for acid gases increases. The major advantage of Selexol over other physical solvents is that it has a favorable solubility for the acid gases versus other light gases. Table 2.4 shows the relative solubility of different compounds in Selexol solvent (Doctor et al., 1994). As shown in Table 2.4, CO_2 is 75 times more soluble than H_2, and H_2S is 670 times more soluble than H_2 in Selexol. Also H_2S solubility is almost 9 times the CO_2 solubility. This characteristic facilitates the use of the Selexol solvent in removing H_2S and CO_2 selectively from the gas stream that needs to be purified. DMPEG also dehydrates the gas and removes HCN.

Table 2.4. Relative solubility of gases in Selexol solvent (Doctor et al., 1994).

Gas	CO_2	H_2	CH_4	CO	H_2S	COS	SO_2	NH_3	N_2	H_2O
Solubility	1	0.0133	0.0667	.028	8.93	2.33	93.3	4.87	0	733

The regeneration step for Selexol can be carried out by either thermally, or flashing, or stripping gas depending on the process design, treated gas required specifications and acid-gas composition. In addition to the advantage of high capacity for acid-gases, other advantages of the Selexol solvent are:

1. Very low vapor pressure that limits its losses to the treated gas
2. Low viscosity to avoid large pressure drop
3. High chemical and thermal stability
4. Nontoxic, non-corrosive and inherently non-foaming
5. Compatibility with gasifier feed gas contaminants
6. High solubility for HCN and NH_3
7. Low heat requirements for regeneration
8. High flash point ensures ease and safety in handling
9. Requires no mixing, formulating, diluting or activating agents and can be used as received.
10. A fairly wide range of operating temperature (-18 to 175 ^{o} C)
11. High loadings at high CO_2 partial pressure- reduces recirculation rate
12. High affinity for water so it simultaneously dehydrates the gas stream

2.2.2.3 Selexol process flow schemes

The design and configuration of a Selexol process depends on the requirements for the level of H_2S/CO_2 selectivity, the depth of sulfur removal, the need for bulk CO_2 removal, and whether the gas needs to be dehydrated or not. However, all the Selexol processes have some elements in common, including sour gas absorption, solvent regeneration/sour gas recovery, and solvent cooling and recycle. The Selexol process has been discussed extensively in literature (Epps, R. Union Carbide Chemicals &

Plastics Technology Corporation, 1992; Judd, 1978; Kohl & Nielsen, 1997; Raney, 1976; J. W. Sweny, 1976; J. W. Sweny, 1980; J. Sweny, 1976). Due to the diversity of the flow schemes and design configurations the two most common flow schemes are discussed in more detail.

1.2.2.4 **Selexol process for H_2S and CO_2 removal**

The Selexol solvent processes can be configured to capture H_2S and CO_2 together with high levels of CO_2 recovery. This is usually achieved by staging absorption for a high level of H_2S removal, followed by CO_2 removal. Figure 2.3 shows a Selexol process for synthesis gas treating where a high level of both sulfur and CO_2 removal are required. H_2S is selectively removed in the first column by a lean solvent, and CO_2 is removed from the H_2S-free gas in the second absorber. The second-stage solvent can be regenerated with air or nitrogen if very deep CO_2 removal is required. Solvent regeneration is carried out both by air stripping for CO_2 and applying heat to regenerate the absorbed H_2S.

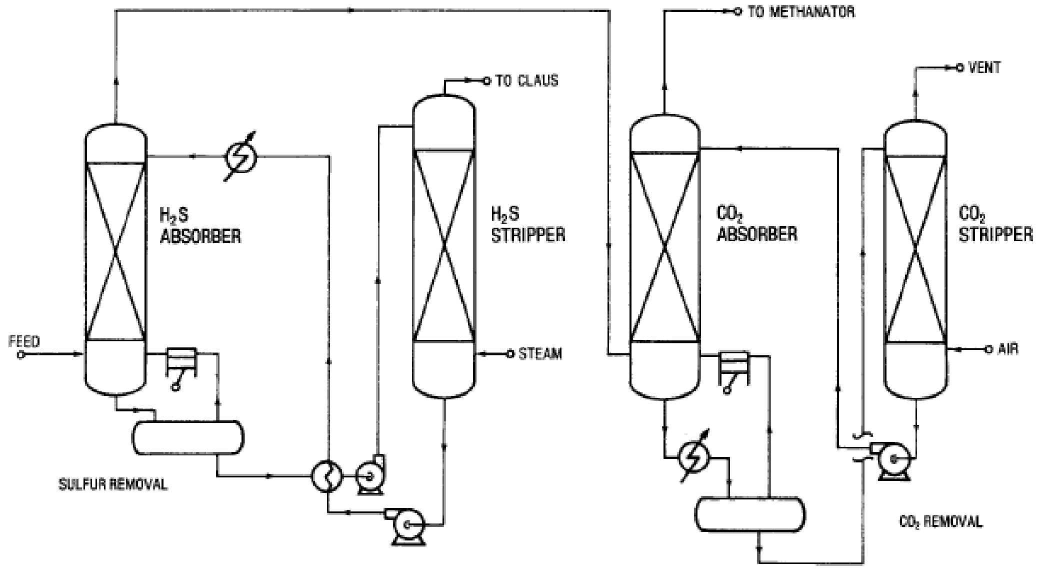

Figure 2.3. Selexol process for CO_2 and Sulfur removal (Kohl & Nielsen, 1997).

1.2.2.5 An optimal design for Selexol process for sulfur and CO_2 capture

The following is a description of an optimal design of a Selexol process which removes sulfur and CO_2 from syngas from Integrated Gasification Combined Cycle (IGCC) systems. Recent DOE/NETL systems analysis studies assume a Water Gas Shift (WGS) reactor combined with a two-stage Selexol process is used for CO_2 capture in IGCC applications. This optimal design is based on modifying an original design by UOP, for H_2S and CO_2 removal from syngas for the production of ammonia from IGCC systems. A simplified schematic diagram of this design is showed in Figure 2.4 (NETL, May 2011).

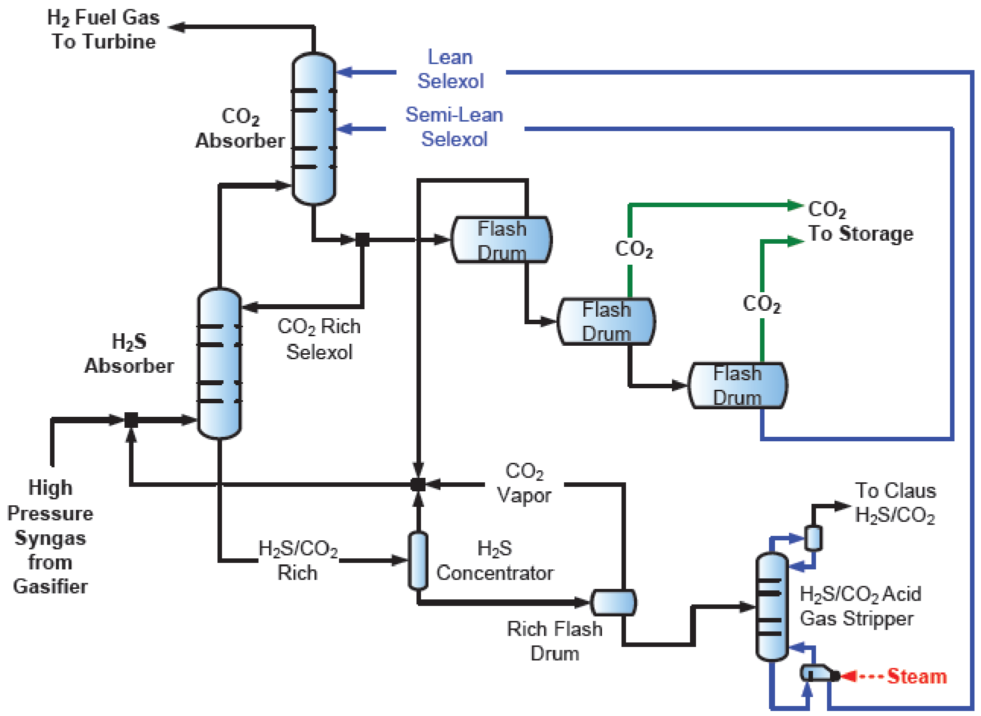

Figure 2.4. Schematic diagram of CO_2 pre-combustion capture with Selexol (NETL, May 2011).

Untreated syngas enters the H_2S absorber and is brought into contact with solvent that is preloaded with CO_2 in the CO_2 absorber and H_2S is preferentially removed using CO_2-rich solvent. The use of pre-loaded solvent prevents additional CO_2 absorption in the H_2S absorber, and it also minimizes the temperature rise across the tower. The H_2S absorber overhead stream enters the CO_2 absorber where CO_2 is absorbed into the fresh solvent. The rich solvent from the H_2S absorber is fed to the H_2S solvent regeneration facility. The H_2S regeneration facility consists of an H_2S concentrator where its pressure is set so that if any CO_2 has been absorbed into the solvent would be degassed from the rich solvent and recirculated back to the feed gas stream. Then the rich solvent from the H_2S concentrator passes through a stripping column where H_2S is regenerated from the solvent by using high pressure steam. The rich solvent at the bottom of the CO_2 absorber is partially sent through the H_2S absorber and the other proportion is regenerated by consecutive flash drums. The flash drums operate at progressively lower pressures, ranging from several hundreds of pounds per square inch (psi) down to near-atmospheric pressure in the final flash drum. Because a significant fraction of the CO_2 is produced at elevated pressure, the total compression energy requirement is lower than for post-combustion processes that typically generate their entire CO_2 product stream at near atmospheric pressure. As explained previously, the key factor in designing the absorption towers as well as the regeneration facilities is the solubility data of the gas components in the solvent at different conditions that may be encountered in the plant. In the case of the Selexol process, many studies have been performed regarding the solubility of different gases in the Selexol solvent (Gainar & Anitescu, 1995; Henni, Tontiwachwuthikul, & Chakma, 2006; Miller et al., 2009). More details on the design conditions and simulations of the Selexol process can be found in (*Power plant carbon capture with CHEMCAD.*; Strube & Manfrida, 2011)

2.2.3 Challenges and barriers of the current physical solvent technology

Despite low energy required to regenerate the physical solvents and their high capacity to capture and separate acid gases from the syngas produced in a gasification plant, physical solvents have some disadvantages as outlined below:

1. CO_2 pressure is lost during flash recovery. If the captured CO_2 needs to be transported and sequestered in geological formations it has to be at some certain conditions such as dry, near pure CO_2 at high pressures approximately 13000 kPa. Since pressure swing technique is often used to regenerate physical solvents, the last flash drum is usually operating at atmospheric pressure. As a result of that, more energy is required to compress the CO_2 to meet the pipeline specifications.

2. In order to increase the solubility of acid gases and minimize the solvent circulation rate, physical solvent absorption usually takes place at ambient temperatures or even lower temperatures. This requires the syngas to be cooled down and then heated back up again and re-humidifed for firing the gas turbine. This can impose energy penalties on the plant performance significantly.
3. Absorption process may require some refrigeration.
4. Another disadvantage of physical solvents, not as important as previous ones, but still challenging is the energy required to circulate the solvent from the atmospheric pressure (outlet of the last flush drum) to high pressures of the absorber column.
5. Simultaneous absorption of the heavier hydrocarbons exists in the process gas stream.
6. Some hydrogen may be lost with the CO_2.

The main challenges of physical solvents involve the regeneration step. Novel techniques for regenerating physical solvents which reduce the pressure lost at both the solvent side and CO_2 side needs to be investigated.

This project studies the use of polymeric membranes for the regeneration of both chemical and physical solvents. The goal of this work will be the development of materials and processes that reduces the capital and operating costs of the solvent regeneration process; particularly the energy expended in regeneration. The primary advantage of membranes over other vapor-liquid mass transfer processes is its significantly higher interfacial contact area. While packed and trayed columns possess

~30-300 m^2/m^3 of interfacial area, membranes can provide over 6000 m^2/m^3. In the next section, a more detailed description of the membrane technology will be given.

2.3 Background on Membrane Technology

Membrane technology is a competitive alternative to conventional separation processes. Membrane filtration and separation is a fast emerging field of separation and was not considered a technically feasible method of separation 25 years ago (Mulder, 1991). As outlined by Li and Chen (Li & Chen, 2005b) the major advantages of membrane separation compared to other conventional methods such as bubble columns, and trayed columns include: (a) Operational flexibility, (b) Economics, (c) Linear scale-up, and (d) Easier prediction of the membrane performance. The size reduction and higher energy efficiency of membrane processes compared to other conventional separation processes are well studied for many separation problems in literature (Bhide, Voskericyan, & Stern, 1998; Feron & Jansen, 1995; Kumar, Hogendoorn, Feron, & Versteeg, 2002; Yan et al., 2007). Separation via membrane technology can be performed continuously. Membranes can be combined with other separation processes in a hybrid system. Membrane properties are variable and depending on the application, they can be tailored for a certain separation problem. The major drawbacks of the membrane technology include: (a) Concentration polarization / membrane fouling, (b) limited membrane lifetime, and (c) generally low selectivity (Mulder, 1991). One of the main disadvantages of the membrane technology is its high manufacturing cost. Membranes can be expensive not only to manufacture but also to maintain. Certain solvents and chemicals can quickly and permanently disintegrate the membrane structure due to the chemical reaction between the solvent and membrane material. Consequently, an appropriate selection of the membrane material can improve the purity of the final product and the economics of the process significantly.

2.3.1 Membrane definition

Wankat (Wankat, 2006) defined the membrane as “a physical barrier between two fluids (feed side and product side) that selectively allows certain components of the feed fluid to pass”. The term selective is the inherent feature of any membrane process. Figure 2.5 shows a schematic of a membrane process (Stanojević, Lazarević, & Radić, 2003).

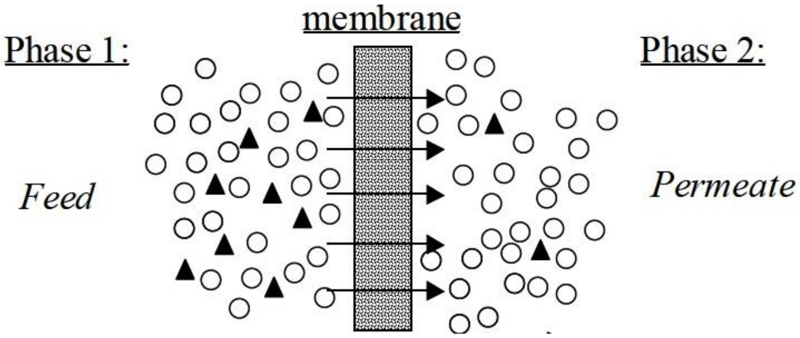

Figure 2.5. Schematic of membrane separation process (Stanojević et al., 2003)

Membranes exist in many forms, structures and materials. They could be natural or synthetic. The synthetic membranes are widely used in industry and they can be classified as symmetric and asymmetric. Commercial membranes are made from polymers, metals and ceramics. Baker (R. Baker, 2012) classified the membrane types into three categories: (a) Metal membranes, (b) Polymeric membranes, and (c) Ceramic and zeolite membranes. Membranes implemented in most of commercial applications are polymeric (solution-diffusion) membranes (Meindersma & Kuczynski, 1996; Puri, 1996).

2.3.2 Membrane flux and selectivity

The performance of any membrane process is determined by two parameters; membrane selectivity and flux. Flux is defined as the volume flowing through the membrane per unit area and time. Higher permeability leads to smaller membrane surface area required for a separation process and this, in turn, leads to a more economical process. An ideal membrane needs to have a high flux for the permeate and low flux for the retentate.

Selectivity is the ability of a membrane to separate a mixture and thus affect the purity of the permeate and retentate streams. The selectivity of a membrane can be defined by one of two parameters; the retention (R) or the separation factor (α) (Mulder, 1991). R is usually used for dilute aqueous mixtures consisting of a solute and a solvent. The retention (R) is given by

$$R = \frac{C_P - C_f}{C_p} = 1 - \frac{C_f}{C_P} \qquad \text{Eqn (1)}$$

where Cf is the solute concentration in the feed and Cp is the solute concentration in the permeate (Mulder, 1991). For the gas mixtures and liquid mixtures, selectivity is usually defined as the separation factor (α). For a binary mixture of A and B, $\alpha_{A/B}$ is given by Equation (2) as

$$\alpha_{A/B} = \frac{y_A/y_B}{X_A/X_B} \qquad \text{Eqn (2)}$$

where y_A and y_B are the concentration of components A and B in the permeate and X_A and X_B are the concentration of the components in the feed (Mulder, 1991).

2.3.3 Transport through dense membranes

As mentioned earlier, membranes have the ability to transport one component of a mixture more readily compared to other components available in that mixture. The differences in chemical / physical properties of different species in the feed stream and different interactions between the membrane material and the permeating components result in different rates of transport and hence the separation of the components. For a specific gas molecule, diffusivity and solubility are intrinsic properties of the membrane material. Transport through the membrane occurs as a result of driving force that exists on the two sides of the membrane (feed side and the permeate side). The relationship between the flux, J, and the driving force is given by

$$J = -D\frac{dX}{dx} \qquad \text{Eqn (3)}$$

where D is the diffusion coefficient (Fick's law) and dX/dx is the driving force perpendicular to the transport barrier. Depending on the membrane separation process, the nature of the driving force may vary. For gas separation membranes, the driving force is the difference in partial pressure of the transferring species across the membrane. For Reverse Osmosis (RO), the driving force is the pressure difference minus the osmotic pressure difference across the membrane. Table 2.5 summarizes the driving forces for different membrane processes.

Table 2.5.Membrane processes and driving forces (Mulder, 1991).

Membrane Process	Phase 1	Phase 2	Driving Force
Microfiltration	L	L	ΔP
Ultrafiltration	L	L	ΔP
Hyperfiltration	L	L	ΔP
Piezodialysis	L	L	ΔP
Gas separation	G	G	ΔP
Dialysis	L	L	ΔC
Osmosis	L	L	ΔC
Pervaporation	L	G	ΔP
Electrodialysis	L	L	ΔE
Thermo-osmosis	L	L	ΔT/ ΔP
Membrane distillation	L	L	ΔT/ ΔP

Note: L=liquid, G=gas, ΔP=pressure difference, ΔT=temperature difference, ΔC=concentration difference, ΔE=electrical potential difference

Two models are widely used to describe the permeation through the membranes. The first is called solution-diffusion model in which different species in the mixture dissolve in the membrane material and then diffuse through the membrane. A separation is achieved as a result of differences between the solubility and diffusivity of different constituents of the mixture (Wijmans & Baker, 1995). The second model is pore-flow in which permeants are separated by pressure-driven convective flow through tiny pores. Separation is achieved because one of the components of the mixture is excluded from some of the pores in which the other component is moving (Wijmans & Baker, 1995). Currently, solution-diffusion is the dominating model for modeling of many membrane processes such as gas permeation, pervaporation, reverse osmosis and dialysis.

Wankat (Wankat, 2006) defined the flux of permeate through the membrane as

$$\text{Flux} = \frac{\text{Transfer Rate}}{\text{Transfer Area}} = \frac{\text{Permeability}}{\text{Separation Thickness}}(\text{Driving Force}) \qquad \text{Eqn (4)}$$

Membrane permeability is the product of the solubility of the gas in the membrane and the diffusivity of the gas in the membrane and is given by

$$P_a = H_a . D_{m,a} \qquad \text{Eqn (5)}$$

where, P_a is the permeability, H_a is the solubility parameter similar to Henry's coefficient and $D_{m,a}$ is the diffusivity. Diffusivity and solubility greatly depends on the size of the molecules. As the size increases, the diffusion coefficient decreases. However, the capability of the component to be absorbed on the membrane surface and then diffuse through the membrane increases. For molecules with a smaller collision diameter, the values for diffusion coefficient are quite large with quite small solubility constants values. However, larger molecules like CO_2, have smaller diffusion coefficient values and large solubility constants values.

In addition to the permeant's properties, the type of the membrane material (polymers in most cases) and the state of the polymer (glassy vs. rubbery) determines the diffusivity and solubility of different components in the membrane. In glassy polymers, the selectivity is basically derived from the molecular dimension difference of the molecules and thus different diffusion rates through the polymer (mobility selectivity) where smaller molecules diffuses faster and favored to be selectively removed. In rubbery polymers, selectivity is derived from the difference of condensability of the molecules, where larger molecules are more likely to dissolve and diffuse through the membrane. For instance, almost all industrial gas separation membranes are glassy polymers because in rubbery polymers, the segmental motions of the chains are not rigid enough to allow a desirable separation of the gas mixture and unless the solubility difference of the gas mixture compounds in the polymer matrix is significant (as in vapors/gases separation), rubbery polymers are not promising candidates for gas-separation membranes.

It is quite evident that a judicious choice of membrane material can significantly influence the separation efficiency and economy. In the next section of this chapter a short review of the membrane types and materials will be given.

2.3.4 Membranes: types and materials

The selection of a membrane material depends on the application of the membrane and the nature of the feed stream. While a certain type of membrane material achieves a desirable level of separation for a gas or liquid mixture, the same membrane may totally fail the task of separation for another application or mixture. Mulder (Mulder, 1991) classified the polymeric membranes into porous and dense nonporous membranes. Table 2.6 shows the type of membrane used for different membrane processes (Perry, Green, & Maloney, 2008).

Table 2.6. Membrane separation Process for Porous/Nonporous membranes

Process Name	Applied Driving Force	Type of Membrane
Pervaporation	Vapor Pressure	Nonporous
Vapor Permeation	Vapor Pressure	Nonporous
Gas Permeation	Partial pressure difference	Nonporous
Reverse Osmosis	Pressure difference	Nonporous
Dialysis	Concentration difference	Nonporous or Microporous
Electrodialysis	Electric Potential difference	Nonporous or Microporous
Microfiltration	Pressure difference	Porous
Ultrafiltration	Pressure difference	Porous

2.3.4.1 Porous membranes

Porous membranes are usually used in microfiltration and ultrafiltration. They contain fixed pores in the range of 0.1-10μm for microfiltration and of 2-100 nm for ultrafiltration (Mulder, 1991). For this type of membrane, selectivity is derived by the dimensions of the pores and the effect of membrane material on absorption, and chemical integrity of the membrane while in use. Fouling and chemical/thermal resistance is the most important factors for selecting this type of membrane material. Table 2.7 summarizes the most common polymers used for microfiltration and ultrafiltration membranes (Mulder, 1991).

Table 2.7 Polymers for microfiltration and ultrafiltration membranes (Mulder, 1991).

Microfiltration membranes	Ultrafiltration membranes
Polycarbonate	Polysulfone/poly (ether sulfone)
Poly(vinylidene-fluoride)	Polyacrylonitrile
Polytetrafluoroethylene (PTFE)	Cellulose esters
Polypropylene (PP)	Polyimide/poly (ether imide)
Polyamide	Polyamide (aliphatic)
Cellulose-esters	Poly (vinylidene fluoride)
Polysulfone	---
Poly (ether-imide)	---

For the microfiltration membranes, polycarbonate is the most common polymer due to its mechanical stability. Hydrophobic polymers such as polytetrafluoroethylene (PTFE), Polyvinylidene fluoride (PVDF) and polypropylene (PP) are commonly used due to their excellent thermal and chemical stability. Despite the great thermal and chemical resistance of such hydrophobic membranes, hydrophilic membranes are gaining more attention. This is mainly because such polymers have reduced adsorption tendencies (Mulder, 1991). The best example of these types of polymers is cellulose and its derivatives. Cellulose and its derivatives are very common membrane materials not only for microfiltration and ultrafiltration membranes but also for other membrane processes such as hyperfiltration, gas separation and dialysis. In fact, cellulose acetate is the most common membrane material for gas separation membranes (Nunes & Peinemann, 2006) because of its crystalline structure which makes it a glassy polymer.

Ultrafiltration membranes pores are in range of nanometer size. Phase inversion is usually used to create such small pores. Polysulfones (PSf) and poly(ether sulfones) (PES) are the basic materials for ultrafiltration membranes (Mulder, 1991). These polymers have very good thermal and chemical stability. Polyimdes and polyacrylonitriles are also used as ultrafiltration membrane materials.

2.3.4.2 Nonporous membranes

Nonporous membranes are used in gas separation and pervaporation. In order to combine the high selectivity of a dense membrane with the high permeation rate of thin porous membranes, nonporous membranes are usually made in form of composite membranes. Unlike the porous membranes, nonporous membranes performance (selectivity and permeation rate) greatly depends on the intrinsic properties of the polymer used in membrane fabrication.

Both permeability and selectivity affect the economy of membrane separation significantly. Substantial amount of research has been done to modify the chemical and physical structure of the membranes for improved permeability and selectivity. It is well established that polarity and steric characteristics of the polymer backbone affect the basic properties of the membrane such as structural regularity, packing density, fractional free volume and rigidity of the polymer chain which in turn significantly influence the permeation properties of the membrane. Many researchers have investigated the structure-property relationship in glassy polymers such as polyimides (Coleman & Koros, 1990; B. Freeman, Yampolskii, & Pinnau, 2006; Hu, Xu, & Coleman, 2007; Nunes & Peinemann, 2006; Stern, Mi, Yamamoto, & Clair, 1989), poly[1-(trimethylsilyl)-1-propyne] (PTMSP) (Jia & Baker, 1998; Kelman et al., 2008) and polycarbonates (Chern, Sheu, Jia, Stannett, & Hopfenberg, 1987; Hellums, Koros, Husk, & Paul, 1991; Muruganandam & Paul, 1987; Percec, 1987; Story & Koros, 1992) and rubbery polymers such as polydimethylsiloxane(PDMS) (Coleman & Koros, 1990; Kesting et al., 1990; Kim, Koros, Husk, & O'brien, 1988). Comprehensive reviews on relationship between membrane materials and permeation properties of gases have been published by Koros and Fleming

(Koros & Fleming, 1993), Pixton and Paul (Pixton & Paul, 1994) and Stern (Alexander Stern, 1994).

2.3.4.3 Industrial applications of membranes

Commercial applications of membranes can be categorized in four distinct groups: (1) Gas separation, (2) Liquid separation, (3) Membrane reactors, and (4) Membrane contactors.

The first industrial application of gas separation membranes was to separate hydrogen from ammonia-plant purge-gas by Monsanto company (Henis & Tripodi, 1980). After that, many other companies such as Cynara, Separex, Dow and Air Liquide developed membranes for many industrial gas separation applications. Baker (R. W. Baker, 2002) predicted the market of gas separation membranes in 2020 to be five times of that of year 2000. Current gas separation membranes cover the supply of pure enriched gases such as He, N_2 and O_2 from air, acid gas removal from natural gas, the separation of H_2 in the petrochemical and chemical industries, natural gas dehydration, air dehydration, and hydrocarbons recovery from process streams. One of the rapidly emerging fields of membrane-based gas separation is to separate olefin/paraffin gases. Many scholars studied and outlined the advantages of the application of membranes for the separation of olefin/paraffin gases (Eldridge, 1993; Ilinitch, Semin, Chertova, & Zamaraev, 1992; Park, Won, & Kang, 2001). Comprehensive reviews on the application of gas separation membranes are available in literature (R. Baker, 2012; Mulder, 1991; Spillman, 1989; Toshima, 1992).

Membranes can be used for certain liquid/liquid separation problems in a process called pervaporation. In this process, a liquid mixture enters the feed side of the membrane and the permeate is removed as a vapor. Pervaporation is generally used for separating liquids with close boiling points or azeotropic mixtures. The first industrial pervaporation system was installed by Gesellschaft fur Trenntechnik Gmbh, Germany (GFT) in 1982 for separating water from alcohol by polyvinyl alcohol (PVOH) composite membranes. Currently, pervaporation membranes are widely used in petrochemical industries for variety of applications such as removal of volatile organic compounds from water and aromatic/aliphatic separation. Pervaporation membranes are also used for removing the toxic phenolic (Han, Ferreira, & Livingston, 2001) and aromatic compounds (Dastgir, Ferreira, Peeva, & Livingston, 2004; Dastgir, Peeva, & Livingston, 2005; Han, Puech, Law, Steinke, & Livingston, 2002; Lebo, Zajicek, Huckins, Petty, & Peterman, 1992) from the waste effluent of industrial units.

Membrane reactors are another emerging application of membranes. Membrane reactor is a generic name for reactors that are coupled with membranous walls. The membrane usually removes one of the products and thus shifts the reaction toward products and increases the reaction conversion. Initial applications of membrane reactors involved gas/vapor phase reactions by using the inorganic microporous or mesoporous membranes such as alumina or zirconia. In most cases, membrane reactors also perform the product purification as well (Mulder, 1991). Membrane reactors cover a wide range of applications such as pervaporation and vapor permeation for esterification reactions (Okamoto et al., 1992; Okamoto, Semoto, Tanaka, & Kita, 1991; Zhu, Minet, & Tsotsis, 1996), dehydrogenation (Collins et al., 1996; Itoh, 1987; Kikuchi, 1995) and many other processes.

A membrane contactor is a device that provides an interface between two components such as two liquids or two gases or a liquid and a gas without the dispersion of the phases within each other. The membrane facilitates the mass transfer between the phases. Gabelman and Hwang (Gabelman & Hwang, 1999) outlined the major advantages of the membrane contactors as: absence of emulsions, no flooding at high flow rates, no unloading at low flow rates, no density difference between fluids required and very high interfacial area compared to conventional dispersed phase contactors (30 times more than the gas absorbers and 500 times more than liquid/liquid extraction columns). Membrane contactor technology has applications in wastewater treatment (Pankhania, Stephenson, & Semmens, 1994; Prasad & Sirkar, 1987), pharmaceuticals (Prasad & Sirkar, 1990; Prasad & Sirkar, 1989), semiconductor manufacturing (Wikol, Kobayashi, & Hardwick, 1998), Liquid/liquid extraction (Basu & Sirkar, 1991; Cooney & Poufos, 1987) and so forth (Gabelman & Hwang, 1999; Stanojević et al., 2003).

2.3.5 Membrane approach in this work

While many previous investigators have studied the use of membranes or solvents to separate CO_2 from flue gas, this work evaluates a hybrid approach. In a conventional CO_2 or acid gas removal plant, the regeneration of the solvent is carried out via the steam regeneration (chemical solvents) and pressure swing (physical solvents) techniques. In this work, conventional stripping columns are replaced by a membrane module where the pre-saturated solvent is brought into contact with the membrane.

The overall objective of this study is to research the applicability of polymeric membrane contactors for CO_2 regeneration. Theoretical predictions and experiments were carried out by analyzing the characteristics of membranes suitable for this application. CO_2 regeneration efficiency was studied with varied process parameters. The specific objectives of this project included:

- Design, construct and validate a continuous lab-scale test system to measure membrane performance.
- Assess the capability of a range of porous membrane contactors and composite polymeric membranes to regenerate chemical and physical solvents for CO_2 capture.
- Characterize suitable membrane materials for the CO_2 stripping application.
- Determine an appropriate operation window for this process. Study and optimize the CO_2 regeneration efficiency with a parametric study of operating temperatures and pressures, feed solution flow rates, and sweep gas flow rates.
- Investigate how mass transfer is affected by different chemical compositions and structures of membranes, such as membrane hydrophilicity and hydrophobicity, as well as membrane pore size.

3 Experimental Methods

3.1 Chemical solvent system overview

This system consists of a CO_2 absorption tank, a feed delivery pump, an inline heating system and a membrane separation unit that houses a polymeric membrane (see detailed description in Appendix). N_2 sweep gas is used for permeate removal. CO_2 is pre-loaded to the solvent by mass flow controlled (Brooks 9400) flow from gas cylinder (Praxair) until saturated. In the stripping process, the CO_2 saturated solution was pumped from the solvent tank to a heater to achieve a desired temperature and then delivered to the membrane cell for separation and the stripped retentate solution flowed back to the tank. This small amount of retentate lean solution was diluted by the large volume solution in the tank in terms of both temperature and CO_2 saturation level. Meanwhile, cooling water circulating through cooling coils in the tank took away accumulated heat and maintained low temperature in the absorption tank constantly. A schematic of the system is shown in Figure 3.1.

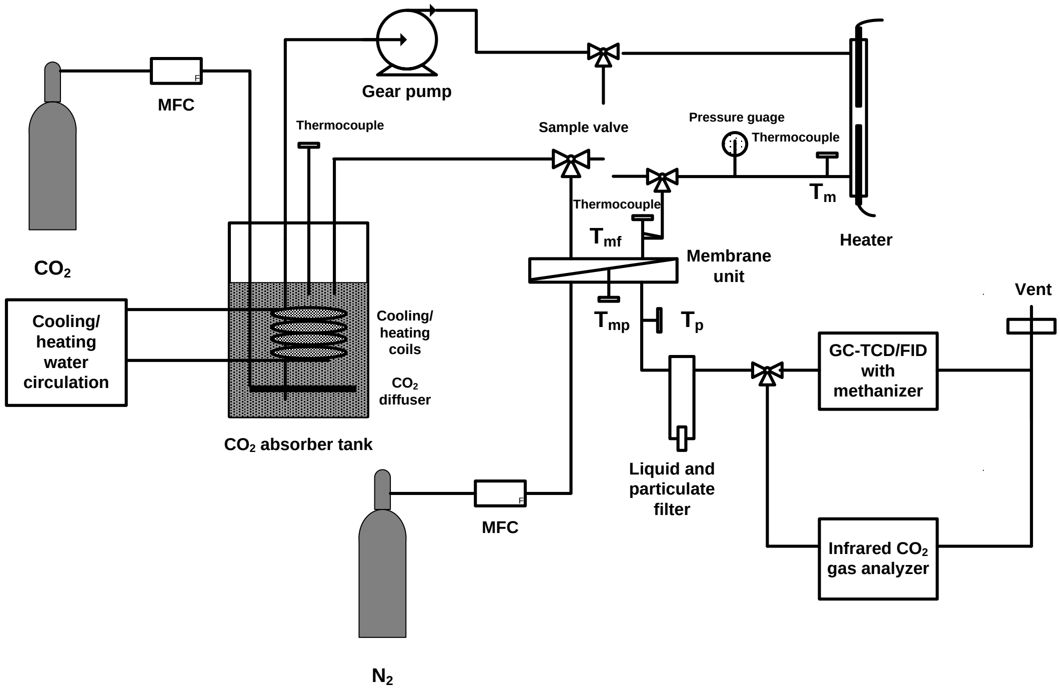

Figure 3.1 Schematic of the membrane evaluation system for chemical solvent regeneration

3.2 Physical solvent system overview

The physical solvent regeneration setup consists of a high pressure absorber vessel for saturating the solvent with CO_2 and the membrane module where CO_2 permeates across the membrane (see detailed description in Appendix). The purpose of this system is to evaluate the ability of membranes to recover CO_2 from the solvent, and these initial studies focused on using pure CO_2, rather than a simulated syngas. The schematic of the experimental setup is shown in Figure 3.2. Initially, the absorber is charged up with solvent. The absorber is equipped with a relief valve on top for safety purposes and degasing the solvent at the end of the experiments via the pressure letdown technique. During the solvent saturation process, this relief valve is kept open initially for a couple of minutes to push the air out of the absorber. The absorber is equipped with a home-made cooling water coil to control the absorber temperature. The absorber pressure and temperature are measured and recorded continuously. Solvent recirculates through the membrane module and then returns back to the absorber. In order to study the effect of feed side pressure and temperature, the feed line pressure and temperature, downstream of the membrane module, are measured and recorded continuously. The feed side flow rate is adjusted using a varying speed pump. The solvent temperature can be controlled using an inline pencil heater coupled with a temperature controller.

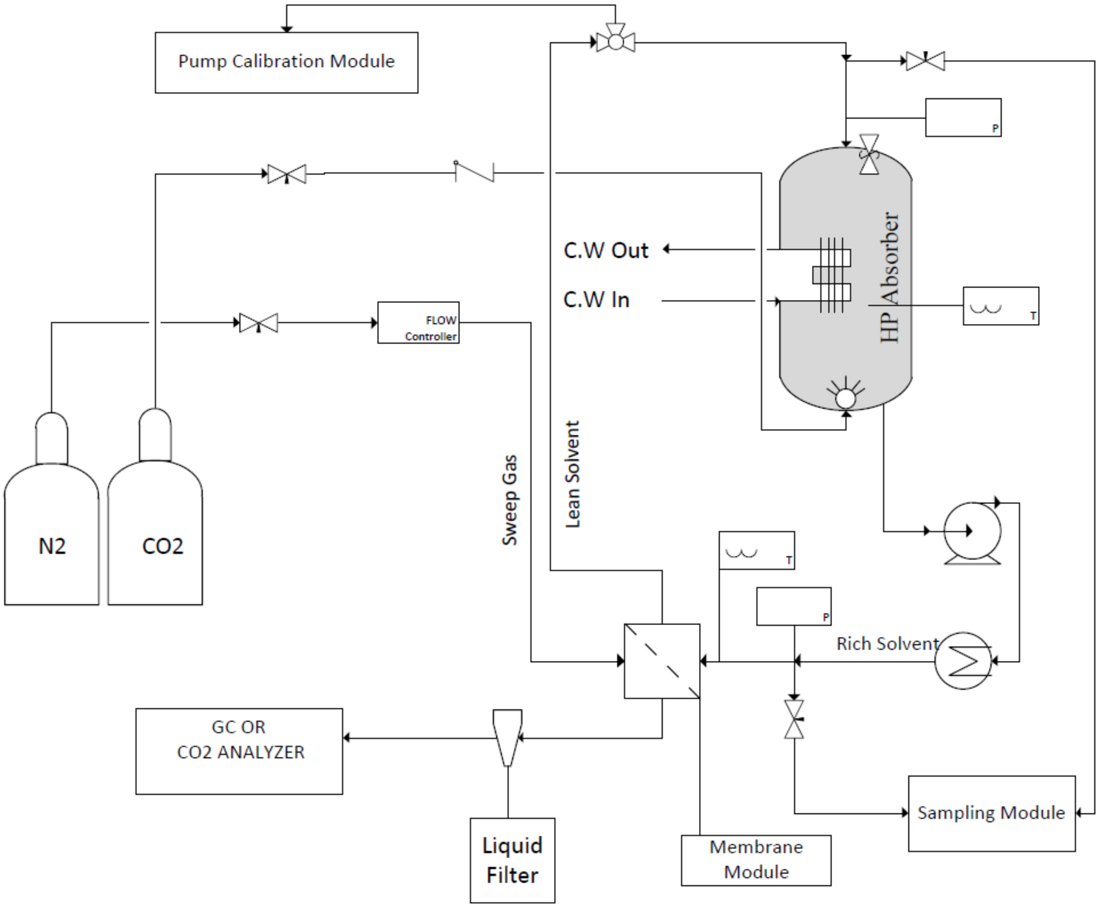

Figure 3.2 Schematic of high pressure permeation system for physical solvent regeneration.

To increase the driving force across the membrane, N_2 is used as a sweep gas. To investigate the effect of sweep gas flow rate, a mass flow controller is used to adjust the N_2 flow rate. To prevent damage to the GC and the CO_2 analyzer and to measure the solvent permeation (or leakage) through the membrane and thus calculating the selectivity, the sweep gas is filtered using a Parker coalescing filter from Cole-Parmer.

Knowing the exact solvent delivery to the membrane module is critical to calculate the percentage recovery of the solvent by the membrane.

In order to better understand the required time to saturate the solvent with CO_2 and evaluate the capacity of the membrane in regenerating the solvent, it is necessary to measure the concentration of CO_2 in the solvent at different operating conditions. This is achieved by taking the solvent samples downstream and upstream of the membrane module and measuring the CO_2 concentration in the sampling modules.

3.2.1 Pump calibration module

In order to confirm the readings of the flow controller and to calibrate the pump delivery flow rate versus the speed of the motor, an apparatus has been designed and incorporated into the system. The schematic of the calibration module is shown in Figure 3.3.

The calibration system includes a collecting vessel which is pressurized with CO_2 from the same CO_2 line that is used to load the absorber. Once the valve on the CO_2 line that goes to the collecting vessel is opened, both the collecting vessel and the absorber will have the same pressure. The collecting vessel is equipped with a pressure gauge to ensure that both of the collecting vessel and the absorber are at the same pressure. After pressurizing the collecting vessel, it is isolated from the CO_2 line by closing the valve. Following that, for a specific period of time (30 seconds), the solvent flow is diverted from the main solvent line to the collecting vessel by using the three-way valve. Next, the collecting vessel is depressurized using the relief valve mounted on top of the collecting vessel. Finally, the valve installed on bottom of the collecting vessel is opened and the volume of the collected solvent is measured with a graduated cylinder. The collecting vessel and the absorber are both mounted on the rack at the same elevation from the pump centerline. Since the delivery pressure and the elevation of both the absorber and the collecting vessel are exactly the same, the delivery flow rate to the collecting vessel should be exactly the same as the delivery flow rate to the absorber and thus the flow meter readings can be calibrated using this module.

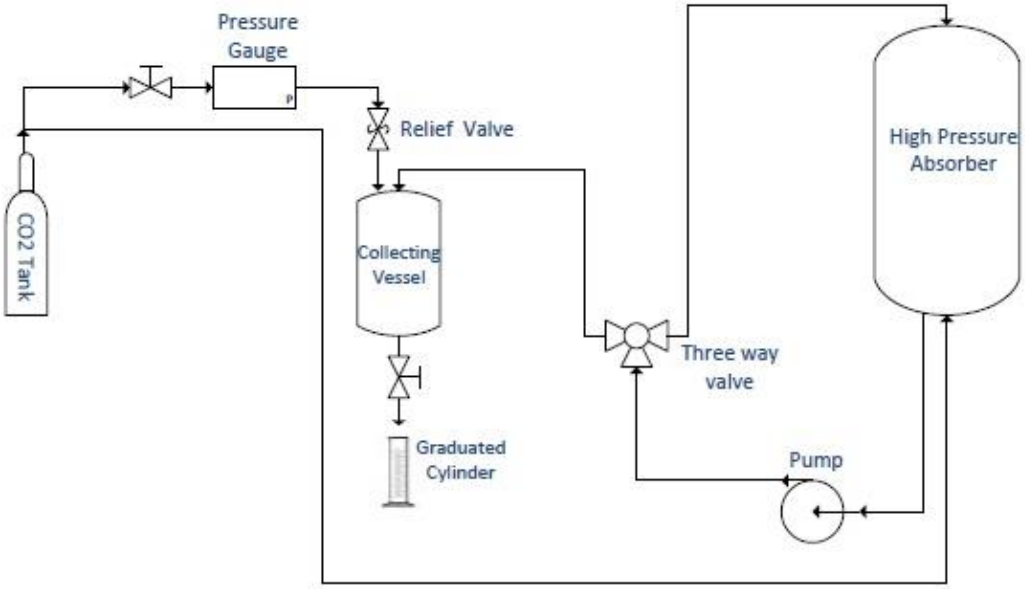

Figure 3.3 Pump calibration apparatus. A flow meter (not shown) was located just downstream of the three-way valve.

3.3 CO_2 measurement in the sweep gas

3.3.1 CO_2 analyzer

Low concentration CO_2 (≤ 2%) in the reference N_2 was continuously monitored and recorded in-situ by a non-dispersive infrared (NDIR) CO_2 analyzer (Li-COR 820). The photograph of the analyzer, software program on computer and the inside schematic are shown in Figure 3.4. With fixed optical bench length and other parameters, the concentration of absorbing species should have a linear relationship with absorbance according to Beer-Lambert law.

More specifically for CO_2, chemical bonds of CO_2 molecules have vibrational frequencies that are excited by photon energy of IR light. By setting frequencies to target CO_2 molecule bonding energy, the amount of radiation absorbed by CO_2 bonds is measured, which can be equated to the quantity of CO_2 in the flow by comparing to the source radiation. Commercially available calibrated cylinders of low concentration CO_2 in N_2 gas (Praxair) were used for concentration verification.

538.4 ppm

Cell Temperature (°C): 50.2

Cell Pressure (kPa): 97.6

Status
Heater: ON
Pressure Comp.: ON
Alarms: OFF
Filter: 2 sec
Span: 2000 ppm
Path Length: 14 cm

Figure 3.4 Non-dispersive infrared (NDIR) CO_2 analyzer.

3.3.2 Gas Chromatography

The CO_2 concentration in the dry gas (≥2%) was determined by an Agilent 7850A gas chromatograph equipped with both a thermal conductivity detector (TCD) and a flame ionization detector (FID) with a methanizer. GC is probably the most common and widely used analytical instruments in industry and laboratory. Separation of gas and/or liquid components in a sample can be achieved through GC, and then the presence and quantity of each component can be identified by the appropriate detector equipped with GC. A GC and a non-dispersive infrared (NDIR) CO_2 analyzer can be coupled either in series or in parallel to provide complete range of gas phase CO_2 analysis.

3.3.2.1 GC detector selection

Many detection systems are available to be coupled with gas chromatography for accurate and fast analysis, the flame ionization detector (FID) and thermal conductivity detector (TCD) are the most common ones being used. The FID has quick response and good sensitivity, however, CO_2 is one of the very few gases to which almost no response can be acquired. The TCD is the most universal detector, as it can detect a wide variety of compounds due to their own different thermal conductivities, and is relatively simple, inexpensive, robust and easy to use.

In this study, a TCD detector and a FID detector with a methanizer were coupled in sequence for the detection and determination of CO_2. The methanizer is usually packed with a nickel catalyst powder. During analysis, the methanizer is heated to 375°C (for Agilent). When the column effluent mixes with the FID hydrogen supply and passes through the methanizer, CO and CO_2 are converted to methane without changing their retention times. The methane can then be detected by FID, thus enabling the detection of low ppm and ppb levels of these gases. The detection limit for CO_2 with helium as the carrier gas with a TCD can reach about 100 ppm with appropriate GC conditions. The methanizer and FID can do a far better job for low level detection and should only be used for measuring less than 100 ppm of CO or CO_2. Higher concentrations of CO or CO_2 cannot be accurately measured by the FID and methanizer as it may exceed the maximum reducing capability of the methanizer.

The TCD consists of four current carrying tungsten-rhenium filaments connected in a Wheatstone bridge circuit, encased in an isothermal aluminum box with thermal insulation. Each filament has the carrier gas passing over it at precisely controlled temperature, pressure and flow rate. The TCD operates on the principle that each gas has a unique thermal conductivity; a gas with a high thermal conductivity is capable of conducting more heat away from the filament than that with low thermal conductivity.

Some optimal parameters being tested and found for the best performance of TCD detector included TCD detector temperature and TCD cell temperature. To gain maximum sensitivity to CO_2, it was recommended to run the TCD at maximum allowable current for the detector temperature. But the increased load on the filaments also increased background noise, instability and the heat up period of the detector. This was significant for trace analyses if the background noise due to operating parameters was large and comparable to the analyte response. On the other hand, condensation of high boiling point components on the filaments is possible when operating at low temperatures. With the detector at just 100°C, it is possible for water and traces of MEA vapor to condense. Detector temperature was set at 200°C to exceed boiling point of MEA (170°C). Prominent signals and relatively low noise was achieved. and this point is also well below the maximum operating temperature so that it ensured the filament should not be oxidized fast and can be operated in long term.

TCD Cell temperature was set about 20°C higher than column temperature to avoid condensation in the TCD cell and maintain stable atmosphere for the TCD filaments.

3.3.2.2 Column selection

GC column is the most important part that performs the function of separating analytes. This separation process segregates the gas mixture into components for the purpose of identifying and quantifying specific compounds. Under desirable conditions, only one component (carried by the carrier gas) passes over the detector at a retention time.

A packed column is commonly preferred for gas sample over a capillary column as larger volume is preferred for gas analysis. Packed columns are metal tubes, filled with fine particles or packing. Packing properties are chosen specifically for the application to cause separation of the sample components by chemical interaction, physical impediment, or polarity interaction. A packed column exhibits a characteristic retention time for different compounds – small molecules relative to the packing porosity may pass through almost unhindered, while larger molecules usually require much longer to work through the column. Similarly some molecules may interact more with the packing due to polarity or reactive groups and take different time to elute.

Several columns were reported to be suitable for the analysis of CO_2. HP-PLOT Q capillary column was used to analyze natural gas samples on the Agilent GC and gained good separation of different gases. This column is a bonded polystyrene-divinylbenzene (DVB) based column that has been specially developed for the separation of targeted apolar and polar compounds including: hydrocarbon (natural gas, refinery gas, ethylene, propylene, all C1-C3 isomers); CO_2, methane, air/CO, and water. 3" or 6" Silica Gel column was used to analyze room air and showed good performance as reported on the SRI GC manual. Porapak Q is also reported that it is mainly used for hydrocarbon separation but also is able to separate CO_2 from air and water (Wallace, 2006). A 6' length and 1/8" outer diameter stainless steel HayeSep D packed column with mesh 80/100 was proven usable in our lab as HayeSep D polymers offer superior separation characteristics for light gases. It is a high-purity divinylbenzene polymer with 80% highly-crosslinked DVB and combines high surface area with a high operating temperature.

Lowering the column temperature and carrier gas flow rate enhances the performance of a column. Higher temperatures make molecules in the column move and vibrate faster and more randomly in all directions, thus weakening the separation function. Lower carrier gas flow rate provides gas samples more adequate contact time with the column for separation. Helium carrier gas flow rate is preset for the GC at about 40 ml/min. A 45°C isothermal temperature program was employed because this is a relatively low temperature for separation and also high enough to be not affected by surrounding temperature change.

3.3.2.3 Injection method

There are two ways to introduce samples into a GC system: manual injection with a syringe or automatic injection using auto-sampler valves. For manual injection, a syringe needle pierces a rubber or plastic septum and the plunger is depressed. The septum seals around the needle and reseals when the needle is withdrawn.

The Agilent GC was equipped with an automatic injection system of 6-port rotary style gas sampling valves. The gas sample is collected at the load position, and introduced to the GC at injection position. Upon command, an electric motor actuates the valve from flushing to sampling position. The valve channels allow introduction of a certain volume of sample gas (approximately 0.25 ml), but most importantly the volume is precise and injection dynamics are highly repeatable.

Table 3.1 GC setting and analysis parameters.

GC components	Parameters	Specification
Front inlet	Temperature	240 °C
	Pressure	5 psi
	Operation mode	Splitless
	Purge time	0.05 min
	Purge flow	15 mL/min
	Septum purge flow	1 mL/min
	Total flow	59.2 mL/min
Column	Carrier gas	High purity Helium
	Flow rate	43.2 mL/min
	Sample column	Restek 70045(5m×530um) guard column and 80/100 mesh Porapak Q (6 ft×1/8 in×2.1mm SS) in series
	Column pressure	5 psi
	Oven/column temperature	45°C
TCD	Heater	200 °C
	Reference flow	40 mL/min
	Makeup flow	5 mL/min
Methanizer	Temperature	375°C
FID	Heater	315 °C
	H_2 flow	45 mL/min
	Air flow	400 mL/min
	Makeup flow	5 mL/min
	Flame current	0.2 pA

3.3.2.4 Calibration Method

Three calibration methods can be used for quantitative chromatographic analysis: external standard calibration, internal standard calibration, and method of standard addition. External standard calibration method is the most commonly used method. This technique simply compares the detector response between known concentrations of analyte with the response for samples containing unknown concentrations. It works well under the conditions that sample preparation steps are simple and the injection volume precision is good, thus well suited for our application.

Table 3.2 GC column and TCD bake out parameters

GC components	Parameters	Specification
Front inlet	Temperature	240 °C
	Pressure	124 kPag
	Operation mode	Splitless
	Purge time	0.4 min
	Purge flow	15 mL/min
	Septum purge flow	1 mL/min
	Total flow	30 mL/min
Column	Carrier gas	High purity Helium
	Flow rate	30 mL/min
	Sample column	Restek 70045 (5m×530µm) guard column and 80/100 mesh Porapak Q (6 ft×1/8 in×2.1mm SS) in series
	Column pressure	124 kPag
	Oven/column temperature	200°C
	Ramp rate	25°C/min
TCD	Heater	220 °C
	Reference flow	40 mL/min
	Makeup flow	5 mL/min
Methanizer	Temperature	375°C
FID	Heater	350 °C
	H_2 flow	45 mL/min
	Air flow	500 mL/min
	Makeup flow	25 mL/min

Gas mixture sample composition can be determined by the response (peak area or peak height) of each gas component. The higher the percentage of a gas component in a mixture sample, the larger the peak area (higher peak height) shows up in the chromatogram. Then taking into account the different thermal conductivities different gases possess, gas component percentages can be calculated. The GC manual provided thermal conductivity factors of common gases, for example, Air 58, CO_2 34, N_2 57 and so on. But this method can only be used for rough estimation of the gas composition, because the thermal conductivities are subject to change and needs to be confirmed for individual TCD detectors. Thus, calibration should be performed and the results from the

GC-TCD analyses relied solely upon the external calibration standard. In another words, its accuracy entirely depends on the calibration standards. If the standards were not accurate, all measurements derived from the GC would be offset from the true CO_2 concentration.

Table 3.3 Calibration standards and GC response performed in May, 2011.

External Standards			Retention Time		Peak Area		Peak Ratio
Actual CO_2 conc. (%)	CO_2 flow (sccm)	N_2 flow (sccm)	CO_2 (min)	N_2 (min)	CO_2 (a.u.)	N_2 (a.u.)	$CO_2/(N_2+CO_2)$ (%)
0	0	1000	N/A	2.144	N/A	9818	N/A
2	20	980	5.467	2.139	188	14190	2.24
5	50	950	5.444	2.141	829	13780	5.67
10	100	900	5.433	2.142	64	1293	11.36
25	250	750	5.411	2.145	4252	11060	27.77
50	500	500	5.396	2.155	5709	4058	58.45
100	1000	0	5.339	2.163	12850	138	98.90

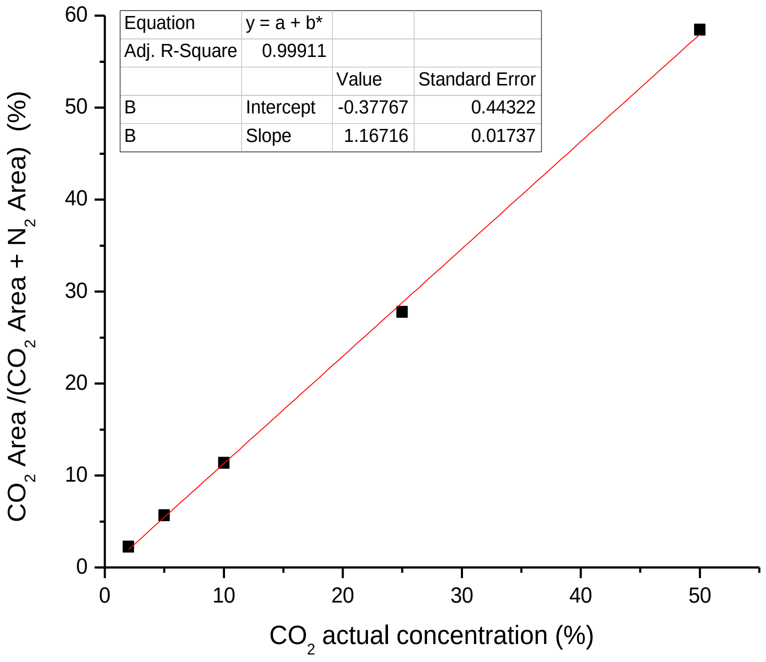

Figure 3.5 Calibration curve generated in May, 2011.

A major concern is whether the thermal conductivity will slowly change over time due to the filament operation at high temperature. Similar calibration runs were performed many times over the project life. Results suggested that the TCD detector responses remained fairly stable over years of usage. Table 3.3 and Table 3.4 showed the peak area ratios for the same standards (2%, 5%, 10%) were almost the same despite being analyzed a year apart. Range selection of the standards is important to determine the calibration curve as shown in Figure 3.5 and Figure 3.6.

Table 3.4 Calibration standards and GC response performed in May, 2012.

External Standards			Retention Time		Peak Area		Peak Ratio
Actual CO_2 conc. (%)	CO_2 flow (sccm)	N_2 flow (sccm)	CO_2 (min)	N_2 (min)	CO_2 (a.u.)	N_2 (a.u.)	$CO_2/(N_2+CO_2)$ (%)
23.1	150	500	5.460	2.153	2984	8388	26.2
15	150	850	5.465	2.149	2536	12630	16.7
10	100	900	5.472	2.147	1687	13300	11.3
5	50	950	5.477	2.145	831	13900	5.6
2	20	980	5.481	2.144	323	14300	2.2
1	10	990	5.478	2.143	5.6	1423	1.0

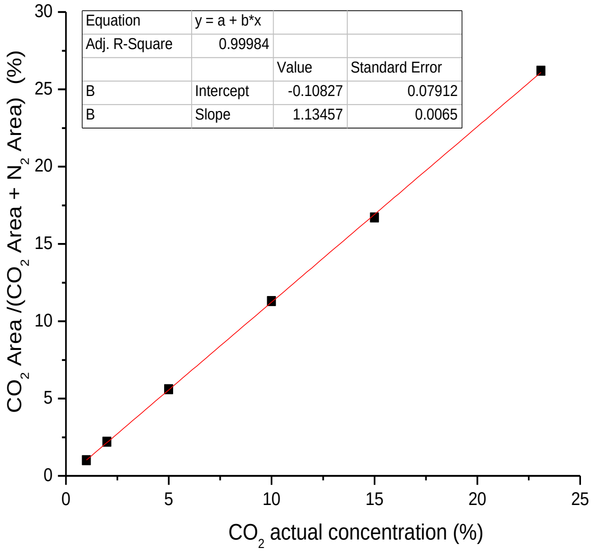

Equation	y = a + b*x		
Adj. R-Square	0.99984		
		Value	Standard Error
B	Intercept	-0.10827	0.07912
B	Slope	1.13457	0.0065

Figure 3.6 Calibration curve generated in May, 2012.

3.4 Validation

3.4.1 Chemical solvent system validation

3.4.1.1 Verification of Absorber Performance

CO_2 absorption was carried out by delivering CO_2 at 500 sccm flow rate to 5L 15 weight % lean aqueous MEA solution at ambient temperature and pressure. Twenty-two solution samples were collected over a 12 hour span. Titration analysis and pH value were taken for these samples. CO_2 loading as a function of absorption time is shown in Figure 3.7.

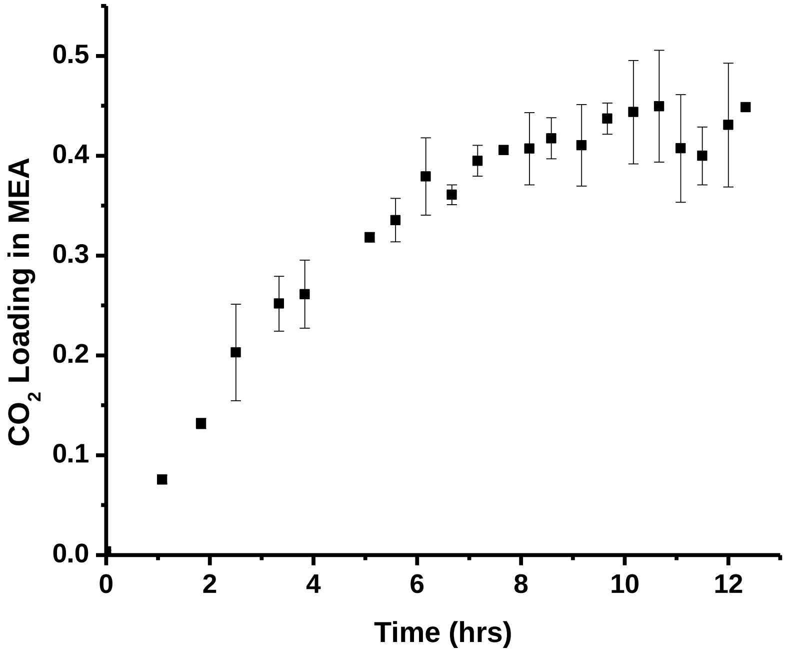

Figure 3.7 CO_2 loading (moles CO_2/moles MEA) versus absorption time.

It can be seen that CO_2 loading gradually increased over time. A mass balance analysis showed that, before saturation, almost all CO_2 was absorbed by the MEA solution due to the fast reaction kinetics. The CO_2 loading became saturated at a loading of about 0.45 moles CO2/moles MEA, which was close to reaction stoichiometric point of 0.5. The large error bars arise from solvent and gas evaporation during sampling as well as from the inherent measurement error in this method. Despite the error, these measurements verified the capability of the absorber. The pH value of these samples was also measured over time (Figure 3.8). CO_2 loading and pH were found to have a fairly linear relationship Y= 12.4 – 10.0X (R^2= 0.98) in Figure 3.9.

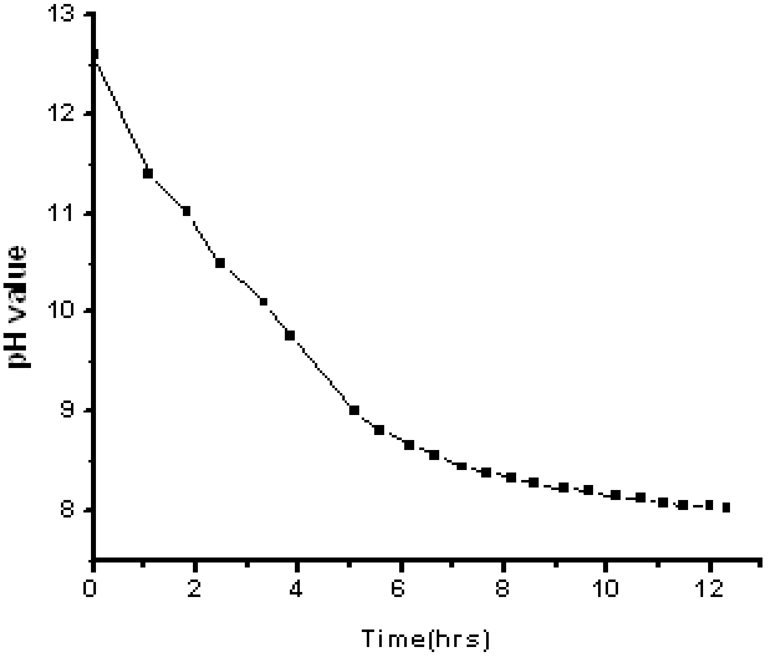

Figure 3.8 15 wt % aqueous MEA pH value vs. CO_2 absorption time.

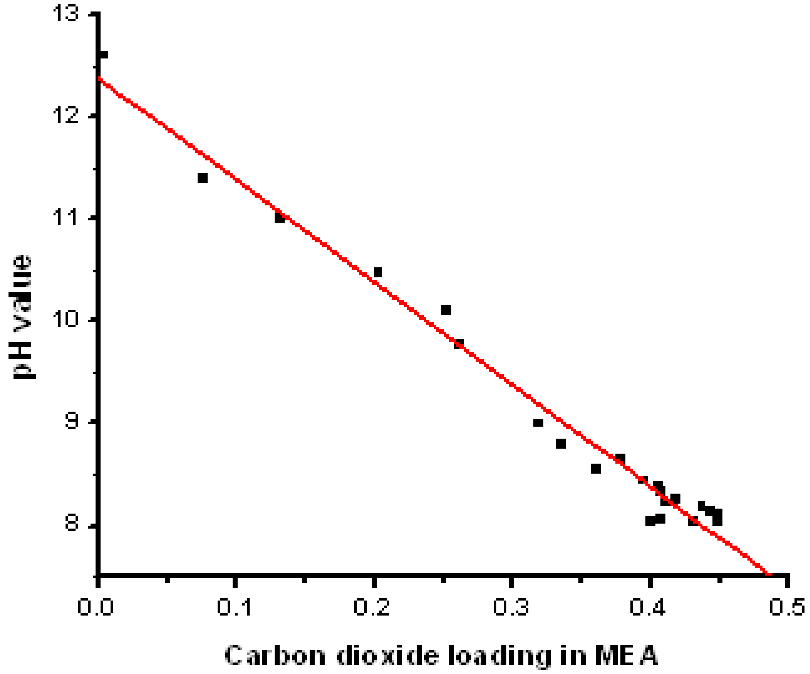

Figure 3.9 pH value vs. CO_2 loading.

3.4.1.2 Verification of Membrane Stripping Performance

Using the apparatus described in Section 3.1, validation experiments were performed using a 0.45 micron porous polypropylene membrane (GE Water & Process Technologies). This membrane was used to strip CO_2 from 6L of saturated 15 wt% aqueous MEA solution. CO_2 concentration in the1000 sccm N_2 sweep gas was monitored under the conditions of solution pumping speed at 120 mL/min and membrane unit temperature at 80 ºC. These conditions were selected for the purposes of verfiying the operation of the experimental setup, with the intention that a full parametric study would later be performed. Temperature and pressure data were recorded by LabView during 10 hours of running.

The CO_2 flux through the membrane was calculated by the following equation and plotted in Figure 3.10. The value 13.8 cm^2 represents the area of the membrane.

$$Flux\ (CO_2) = (CO_2\ ppm\ value)(10^{-4})(Retentate\ flow\ rate\ in\ sccm)\left(\frac{1min}{60sec}\right)(\frac{1}{13.8cm^2})$$

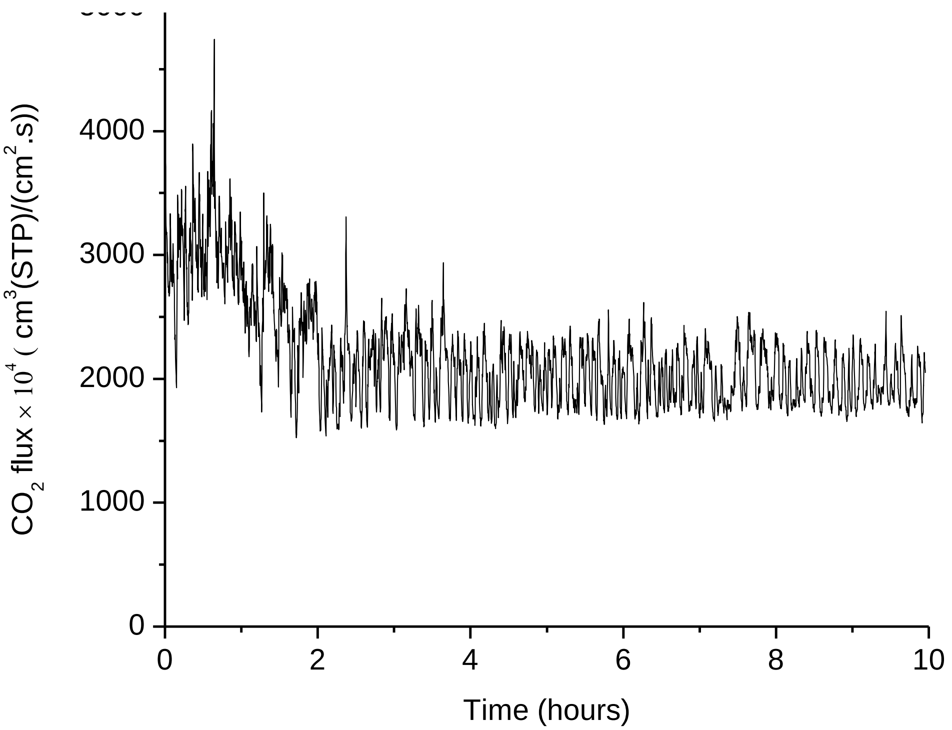

Figure 3.10 CO_2 flux versus stripping time

Nine samples were collected from the absorption tank during this experiment and the pH value was measured (Figure 3.11). The pH value increases over time as the CO_2 is stripped out of the solution. A mass balance calculation showed that it would take about 60 hours to strip all CO_2 out of 6L of fully saturated 15 wt% MEA under the average flux of 0.3 cm^3 (STP)/(cm^2.s) due to the small membrane surface area in this experiment. While this experiment was run for only 10 hours, it nonetheless verifies the ability of the system to strip CO_2 from the MEA solution.

Substantial average CO_2 flux of 0.3 cm^3 (STP)/(cm^2.s) (1.3×10^{-1} mol.m^{-2}.s^{-1}) was detected for 10-hours after steady state was reached. Naim et al. (2012) reported CO_2 stripping flux from diethanolamine solvent achieved by PVDF hollow fiber modules with 5 wt% LiCl (1.6×10^{-2} mol.m^{-2}.s^{-1}). Khaisri et al. (2011) used PTFE hollow fiber membrane module and stripped 3-7 kmol/m^3 CO_2 loaded MEA at 90-100 ºC, measured CO_2

desorption flux ranged from 2×10^{-5} mol.m^{-2}.s^{-1} to 6×10^{-3} mol.m^{-2}.s^{-1} at various process parameters.

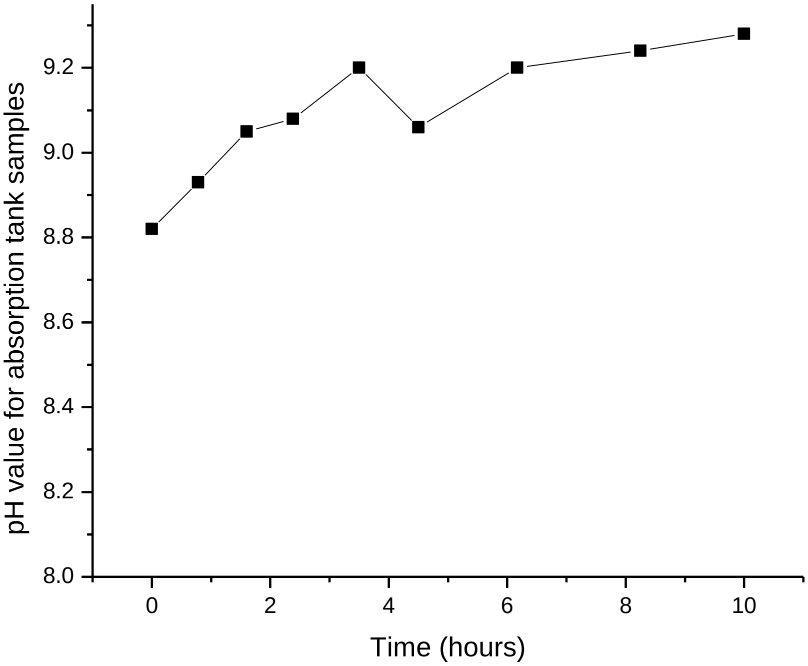

Figure 3.11 pH of the solution in the absorber versus time.

3.4.2 Physical solvent system validation

In order to compare the permeation properties of different membranes, it is imperative to verify the consistency and accuracy of operational parameters measurements. System temperature and pressure is measured and recorded using the pressure transducers, thermocouples and the data logger from National Instruments. The accurate measurement of the solvent flow rate and its CO_2 concentration is also critical to the calculations of the membrane effectiveness in separating the CO_2 from the solvent. In this section, the verifications of various operational parameters will be presented.

3.4.2.1 Pump Calibration

Figure 3.12 shows the pump calibration curves at different system gauge pressures. The calibration curves were generated using the pump calibration module explained in section 3.2.1. As the curves in Figure 3.12 indicate, at a certain pumping speed, solvent flow rate decreases as the pressure of the system increases. The effect of pressure on flow rate drop becomes more pronounced as the motor speed increases. At the lower pumping speeds, solvent flow rate does not significantly change with pressure.

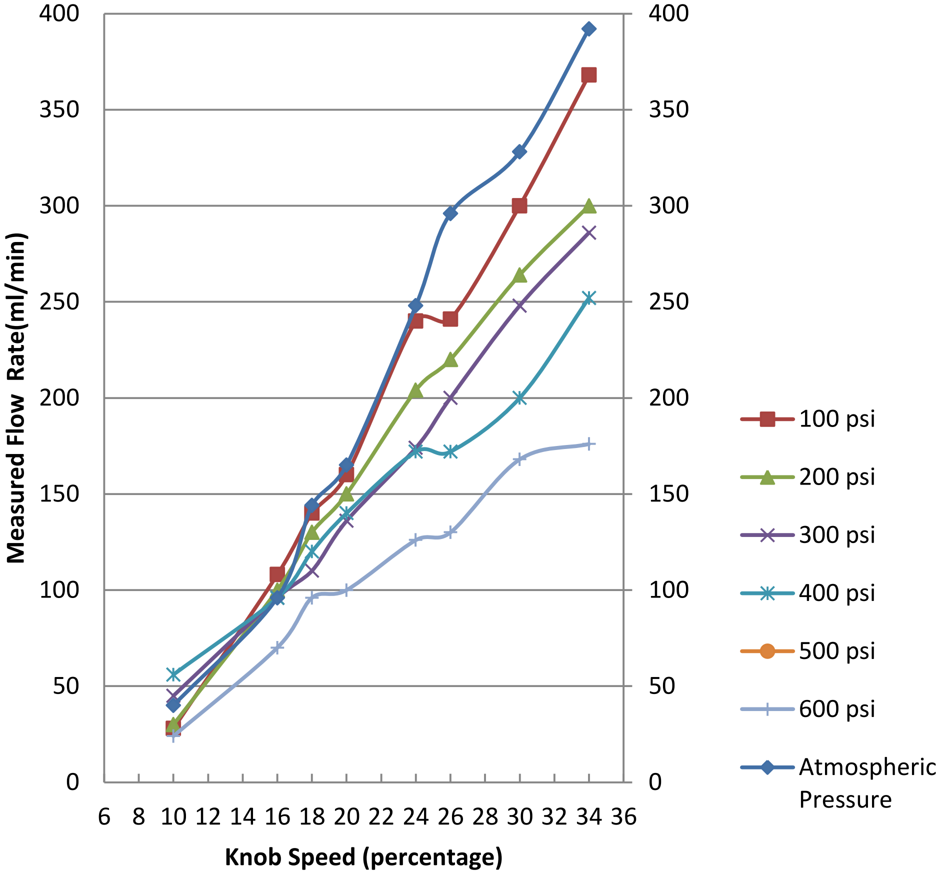

Figure 3.12 Pump calibration curves at different gauge pressures (The horizontal axis represents the percentage of the maximum pump motor speed, 1750 rpm).

Figure 3.13 shows the flow meter readings versus the actual flow rate in the system. These graphs were used to adjust the actual solvent delivery at different pressures using the flow meter readings.

3.4.2.2 Absorber pressure and temperature

Figure 3.14 and Figure 3.15 show the stability of the absorber pressure and temperature with respect to time. The measured pressure (via a pressure transducer) and temperature variations were acceptable for the purpose of the permeation experiments. To study the stability of the pressure in the system, the absorber was pressurized with CO_2 at 2310 kPag (335 psig) and the pressure of the absorber was recorded. The pressure in the absorber remained at an acceptable range of 2310±1 kPag (335±0.2 psig) over a two hour period.

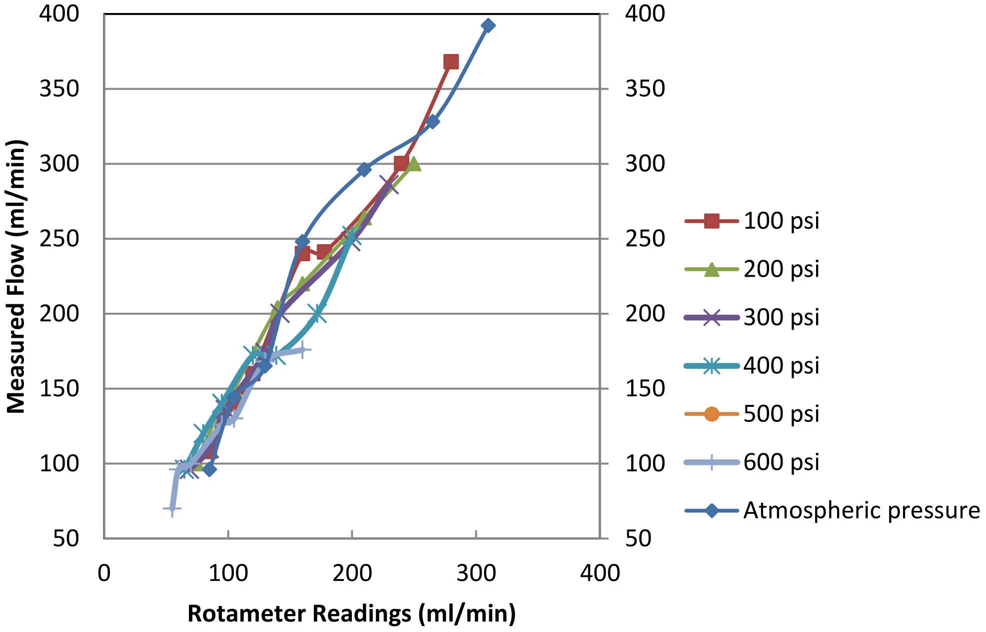

Figure 3.13 Measured solvent flow rate versus the rotameter readings.

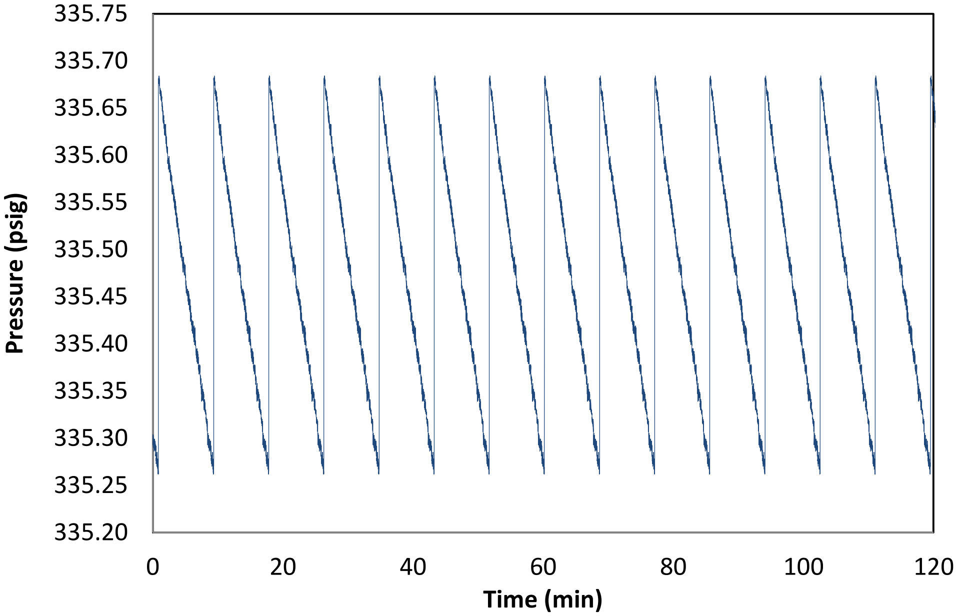

Figure 3.14 Absorber pressure versus time.

Figure 3.15 shows the temperature fluctuations in the absorber. The temperature was measured using a K-type Omega thermocouple mounted on top of the absorber. It is clear that temperature of the system remained at an acceptable range with respect to time. Using the temperature controller and the pencil heaters, the temperature of the solvent line can be adjusted downstream of the membrane module. Using the home-made cooling water coil installed in the absorber, the temperature of the absorber can be controlled within an acceptable range.

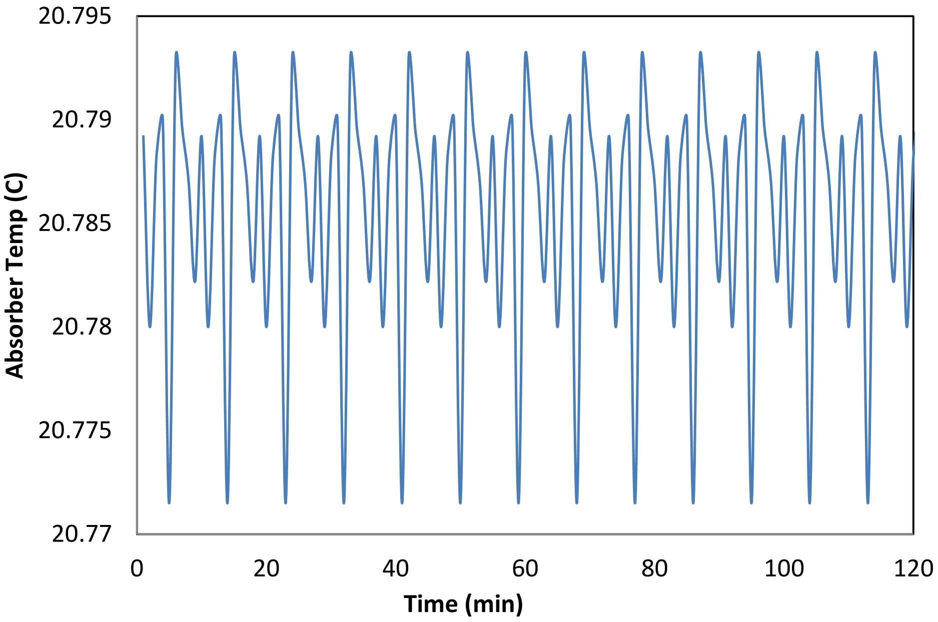

Figure 3.15 Absorber temperature versus time.

3.4.2.3 Verification of the membrane stripping performance

Prior to the screening study, sample runs were carried out with a PVOH-based membrane (PERVAP 1211/2203) and a PDMS-based membrane (PERVATECH). The absorber was pressurized with CO_2 to 2758 kPag (400 psig). Using the pump calibration curves and the pump motor speed controller, the solvent flow rate was set to 120 (mL/min). The sweep gas flow rate was adjusted at 500 (sccm). Figure 3.16 and Figure 3.17 show CO_2 concentration in the sweep gas. The PDMS-based membrane (Figure 3.17) has a significantly higher CO_2 flux compared to the PVOH-based membrane. As mentioned earlier, PDMS has a very high affinity for CO_2 compared to other polymers and this explains the higher CO_2 flux in our permeation experiments.

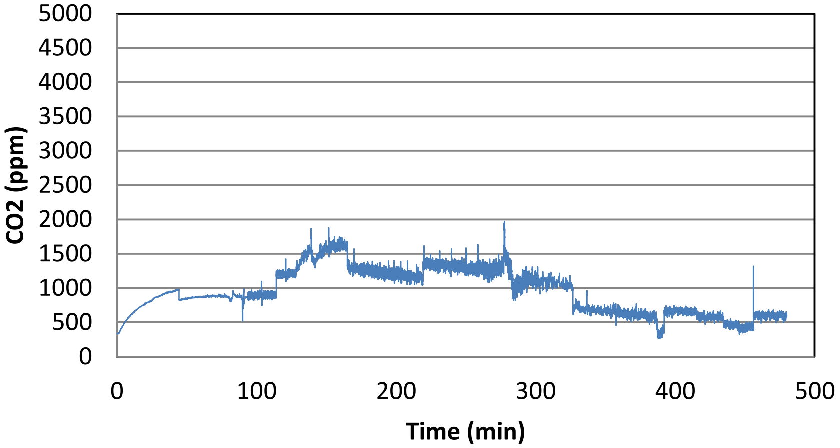

Figure 3.16 CO_2 concentration in the sweep gas. (PERVAP1211, PVOH-based membrane).

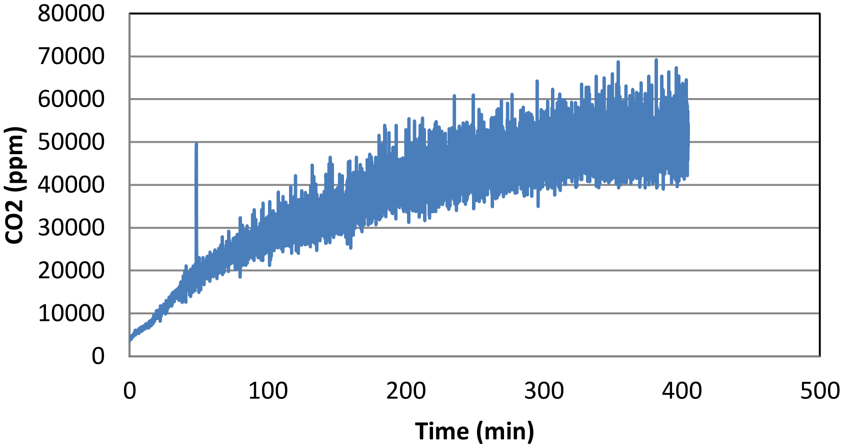

Figure 3.17 CO_2 concentration in the sweep gas, (PERVATECH, PDMS-based membrane).

3.5 Analytical methods

3.5.1 Sorption measurements

One of the major challenges of the membrane processes that prevent the membrane technology from being used commercially is fouling. Fouling may occur due to the blocking of the pores of the membrane or adsorption of the fluid particles on the surface of the membrane. Fouling causes the flux to decline and eventually decreases the performance of the membrane significantly. A comprehensive review on flux decline in membrane processes was given by van den Berg and Smolders (Van Den Berg & Smolders, 1988). The following procedure was used to carry out the sorption experiment:

- Polymeric membranes were cut in the circular shape with the diameter of 47 mm.
- Membrane thickness was measured (average of three points) using a digital micrometer (Fowler IP54, ±0.00001 in) and weighed on a microbalance (Fisher Scientific, ±0.00001g).
- Duplicate polymer samples were immersed in 1L of the solvent in a water bath (Precision Microprocessor, Controlled 280 series Water Bath) at constant temperature of 25 ^{o}C for 20 hours.
- Following that, membranes were removed from the bath and the excessive solvent on the membranes surface were wiped off using dry filter papers.
- The membranes were weighed immediately.
- The weight changes of each membrane sample were recorded in 30 minutes intervals till no detectable change was observed.

Using the criteria developed by Yamaguchi et al, the solubility coefficient, S, was calculated using equation 6.

$$S = \frac{\frac{\Delta W}{\rho 1}}{(\frac{\Delta W}{\rho 1} + \frac{1}{\rho 2})} \qquad \text{Eqn (6)}$$

where ΔW is the weight of liquid dissolved in the membrane (g of solvent/g of dry membrane) and ρ1 and ρ2 are densities of solvent and dry membrane respectively.

3.5.2 Differential Scanning Calorimetry (DSC)

Differential scanning calorimetry (DSC) is a thermo-analytical tool to determine the thermal properties of polymers. It measures the heat flow rate between a sample and an inert reference as a function of time and temperature. For amorphous glass state polymers, the molecular chains begin to move and become rubbery state when the temperature reaches the glass transition temperature, T_g. When temperature continues rising to a point, polymer molecules begin to flow, this temperature is called the viscous flow temperature (T_f). The range between T_g and T_f is known as the rubbery state of polymer. All these changes can be characterized by DSC and expressed by the thermal-mechanical curve of a polymer. Some semi-crystalline polymers exhibit both crystalline and amorphous behavior, such as PE, PP, and PTFE. DSC can characterize both the glass transition temperature (T_g) of amorphous behavior and the melting temperature (T_m) of the crystalline behavior. In this work, a Perkin Elmer 7 Series Diamond DSC was used to analyze the membrane samples. The analysis was performed for both the original and post-experiment samples for each type of membrane. The polymer samples, each approximately 7 mg, were sealed in aluminum pans. For each sample, two thermal scans were conducted. The first scan erased the thermal history of the sample. Only the second scan was used to compare the structural integrity of membrane samples after being exposed to the high pressure solvent stream.

3.5.3 Scanning Electron Microscopy (SEM)

SEM is a microscope that uses a focused beam of high-energy electrons to form an image. The signals from electron-sample interactions give information about the sample morphology, chemical composition, and crystalline structure of the sample. In this work, the surface and cross-section SEM images of the membrane samples were captured using a JEOL SEM (Model No: JSM-7600F). In order to identify any changes of the membrane surface or structure, the original and post experiment membranes images were compared side by side.

3.5.4 Fourier Transform Infrared (FTIR) Analysis

FTIR analysis is employed in our study for qualitative analysis of membrane materials. And with relevant standards, it can be used for quantitative analysis as well. In Infrared (IR) spectroscopy, IR light or IR beam radiation passes through the sample. Some of the photon energy is absorbed by the sample molecules when the wavelength corresponding to the energy difference between levels is reached. And some of the light is transmitted through. Usually, vibrations of chemical bonds that change the dipole moment of the molecules are sensitive to the light wavelength in the Infra-red (IR) region. Different functional groups have their unique characteristic absorption bands, from which the identification of molecules can be recognized. The position of a certain absorption band is specified by its wavenumber ($\bar{\nu}$), which is defined as the inverse of the wavelength (λ) and is preferred to be used because it is in linear relationship with photon energy.

$$\bar{\nu}\ (cm^{-1}) = \frac{1}{\lambda\ (cm)} \qquad \text{Eqn (7)}$$

FTIR can also be used in quantitative analysis under certain conditions by applying the Beer-Lambert Law. Figure 3.18 shows a typical setup for the absorption technique.

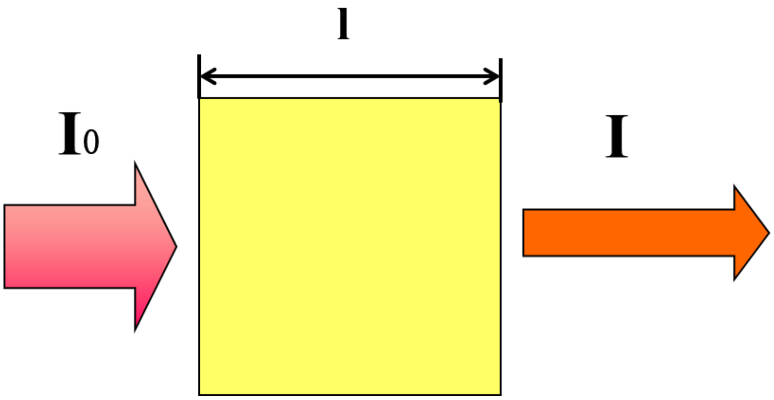

Figure 3.18. Typical experimental direct absorption setup.

A radiation beam passes through a sample, the incoming intensity of the beam is I_0 and the outgoing intensity is I. If the radiant beam is assumed to be monochromatic, The Beer-Lambert law can be written as:

$$A = -\log\left(\frac{I}{I_0}\right) = -a \times l \times c \qquad \text{Eqn (8)}$$

where A is the absorbance, c is the concentration of absorbing species, l is the light pathlength, and a the absorption coefficient or the molar absorptivity of the absorber.

FTIR is generally a useful tool to investigate the structure and chemical changes of a membrane after being used in the process. A Nicolet IR-200 spectrometer (Thermo-Nicolet Corp, Madison, WI) was used to analyze the original and post-experiment membrane samples. Analysis was performed on Thunderdome Swap-Top operation module equipped with ZnSe crystal. All spectra were recorded in the absorbance mode in the wave number range of 400-4000 cm^{-1} with a detection resolution of 16 and 16 scans per sample. OMNIC 6.0 software (Madison, WI.) was used to determine peak positions and intensities. Two replicates of each sample were run to ensure reproducibility of the results. Figure 3.19 shows the FTIR settings used for both the original and the post-experiment membranes.

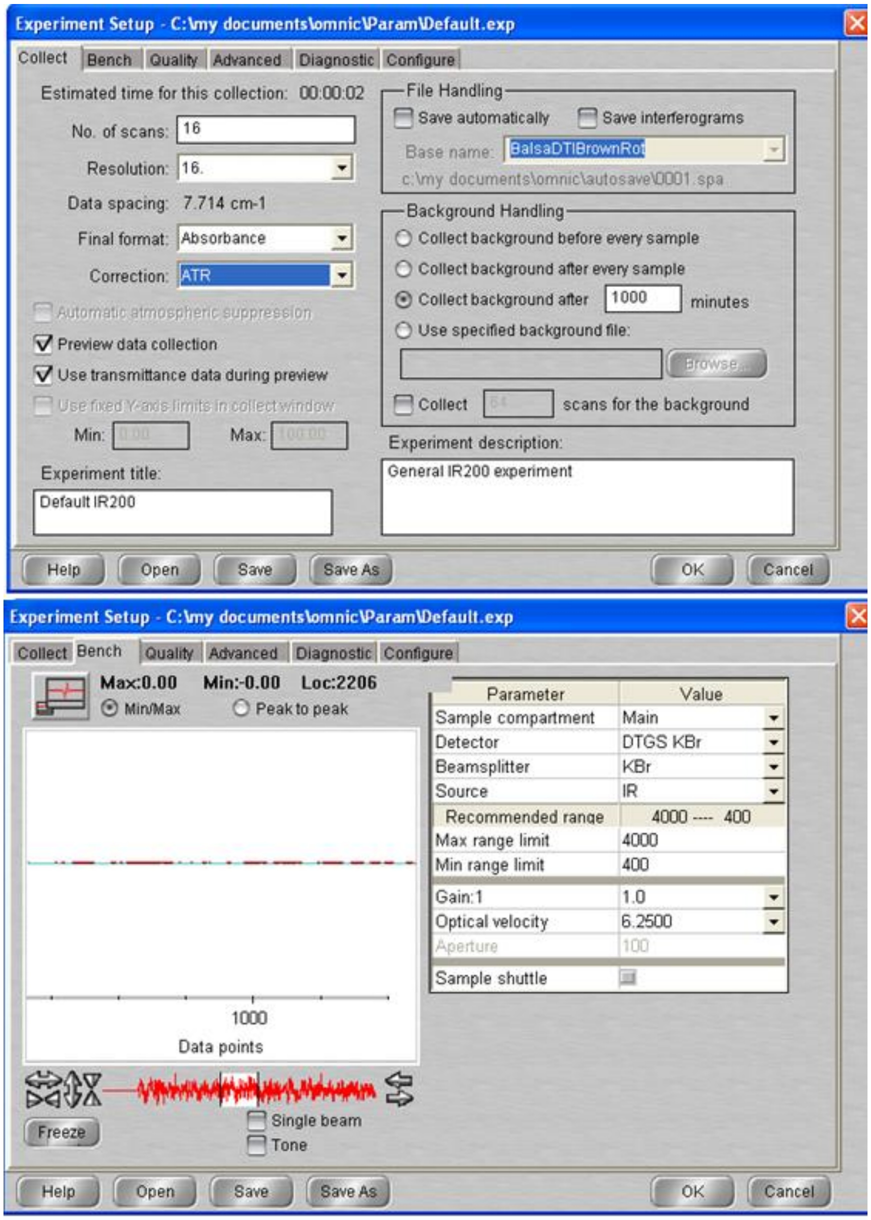
Experiment Setup - C:\my documents\omnic\Param\Default.exp

Estimated time for this collection: 00:00:02

No. of scans: 16

Resolution: 16.

Data spacing: 7.714 cm-1

Final format: Absorbance

Correction: ATR

☐ Automatic atmospheric suppression

☑ Preview data collection

☑ Use transmittance data during preview

☐ Use fixed Y-axis limits in collect window

Min: 0.00 Max: 100.00

Experiment title: Default IR200

File Handling

☐ Save automatically ☐ Save interferograms

Base name: BalsaDTIBrownRot

c:\my documents\omnic\autosave\0001.spa

Background Handling

○ Collect background before every sample

○ Collect background after every sample

● Collect background after 1000 minutes

○ Use specified background file:

☐ Collect 64 scans for the background

Experiment description: General IR200 experiment

Experiment Setup - C:\my documents\omnic\Param\Default.exp

Max:0.00 Min:-0.00 Loc:2206

● Min/Max ○ Peak to peak

Parameter	Value
Sample compartment	Main
Detector	DTGS KBr
Beamsplitter	KBr
Source	IR
Recommended range	4000 ---- 400
Max range limit	4000
Min range limit	400
Gain:1	1.0
Optical velocity	6.2500
Aperture	100
Sample shuttle	☐

☐ Single beam

☐ Tone

Figure 3.19 FTIR settings.

3.5.5 UV-Vis

UV-vis spectroscopy was also used as an alternative technique to show the CO_2 loading and solution changes. Original lean aqueous MEA solution was used as a reference. The fully CO_2 loaded solution or stripped solution samples were analyzed by subtraction of the reference scan, thus only the CO_2 absorption peak (around 270 nm) or solution compositional changes were shown prominently in the spectra. The drawback of this analytical method is that it can only show the differences. Detailed analysis, especially quantitative analysis, is very challenging. UV-vis spectra of CO_2 loaded MEA solution, stripped MEA solution and permeated liquid through the membrane are shown in Figure 3.20. CO_2 absorption peak intensities decreased significantly after 4 hours stripping and confirmed the stripping performance. The permeated liquid through the membrane showed very different composition than the solutions on the retentate side. The differences could be explained from two aspects: one could be due to the majority of the CO_2 being stripped off the permeated liquid; and the other reason could be more water vapor permeated than MEA vapors due to its higher concentration and lower boiling point.

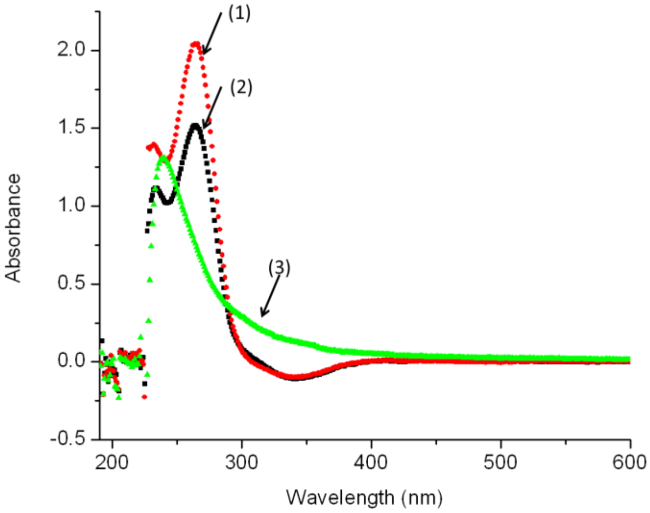

Figure 3.20 UV-vis spectra of (1) full CO_2 loaded aqueous 15 wt% MEA solution; (2) solution after 4 hours of stripping; (3) liquid collected at the coalescing filter during the course of the run. (All with lean aqueous 15 wt% MEA solutions as a reference)

3.5.6 Chittick titration apparatus

The MEA and CO_2 concentrations were checked using a titration method with 2N hydrochloric acid. This titration apparatus was adapted from the Chittick CO_2 analyzer apparatus (Miller et al., 2009). This apparatus allows for the measurement of the MEA solution concentration and the amount of CO_2 absorbed by the amine solution. A schematic of the apparatus is shown in Figure 3.21.

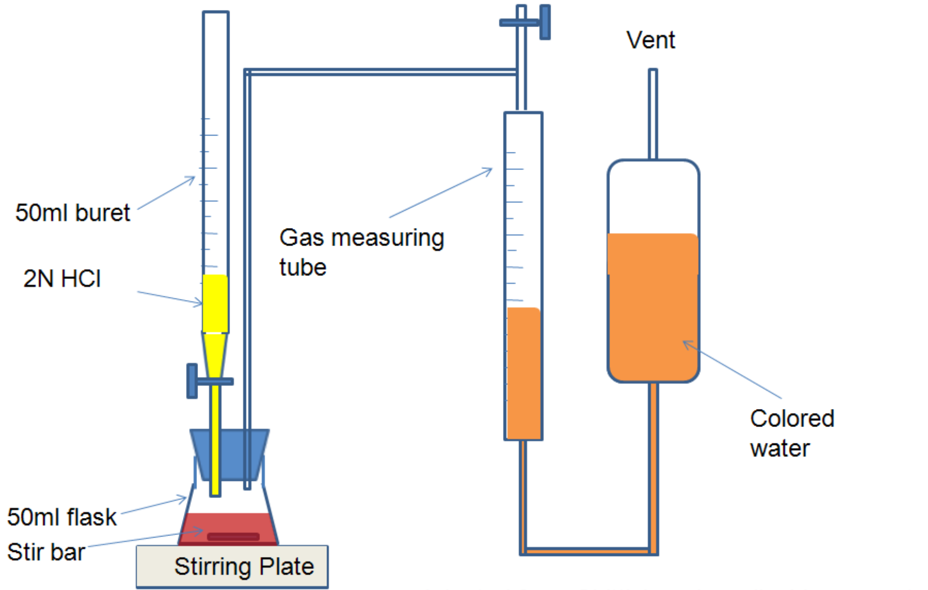

Adapted from Chittick carbon dioxide apparatus

Figure 3.21 MEA and CO_2 titration apparatus.

During titration analysis, a sample of known volume (0.5 mL, 1 mL, or 2 mL), titration indicator and a stir bar were placed in the reaction flask. The flask was then connected and sealed to a graduated gas measuring tube and adjustable leveling bulb reservoir which contains colored water. 2N hydrochloric acid (2 mol/L HCl) was slowly added to the reaction flask using a 50mL titration burette until the titration indicator changed color. The solution was also stirred by a magnetic stir bar to homogenize and help liberate CO_2 from the solution. The consumed HCl was used to calculate the MEA weight fraction of the solution. Figure 3.22 shows a titration plot for a slightly loaded 15 wt % MEA solution. The solution has a sharp pH change from around 7 to 2. This is the endpoint where all the MEA has reacted with HCl and all the CO_2 has been released from the solution. Methyl orange was used as an endpoint indicator, which is often used to titrate weak bases with strong acids. Its color changes from orange-yellow (at pH 4.4) to red (at pH 3.1). CO_2 vapor evolves from the reaction and displaces the fluid in the tube, which allows for the evolved gas to be measured.

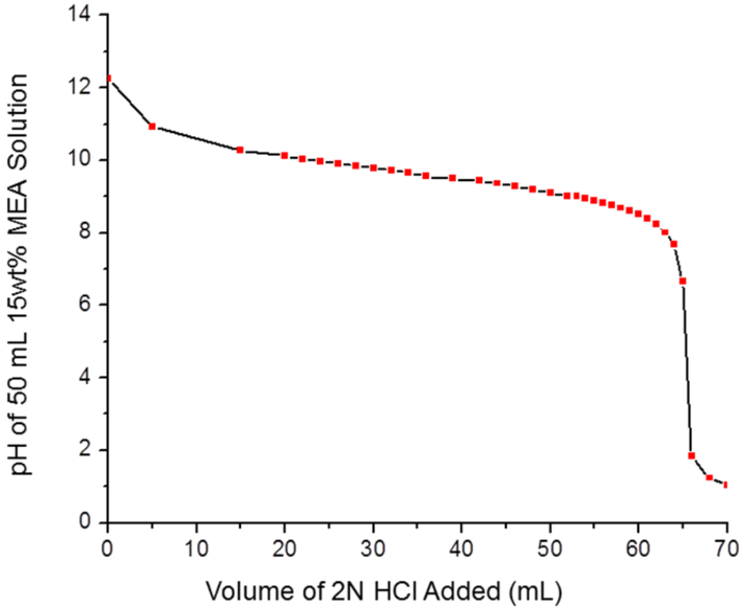

Figure 3.22 Titration plot of lean 15 wt% MEA solution.

The MEA solution concentration can be determined by equation (2.4) (Ji, Miksche, Rimpf, & Farthing, 2009):

$$C_1V_1 = C_2V_2 \qquad \text{Eqn (9)}$$

Where:

C_1 = MEA solution concentration (mol/L)
V_1 = MEA solution sample volume (mL)
C_2 = HCl concentration (M=2 mol/L)
V_2 = Acid volume consumed for titration (mL)

The amount of CO_2 absorbed by the amine solution (defined as moles of CO_2 per mole of amine group) can then be obtained by equation (10) (Ji et al., 2009):

$$\alpha = \frac{moles(CO_2)}{moles(MEA)} = \frac{\left[\frac{(V_{gas} - V_{HCl})(P)(273K)}{(760mmHg)(T)(22.4L/mol)}\right]}{C_1V_1} \qquad \text{Eqn(10)}$$

Where:

α = solution CO_2 loading (mol CO_2/mol MEA)
C1= MEA solution concentration (M = mol/L)
P = barometric pressure (mmHg)
T = room temperature (K)
V1 = MEA solution sample volume (mL)

V_{gas} = volume of displaced solution in the gas measuring tube (mL)
V_{HCl} = volume of HCl titrant (mL)

It should be noted here that the pressure created by liberating CO_2 from MEA in the flask is higher than the atmospheric pressure. It is this pressure difference that drives the colored water displacement in the gas measuring tube. But this pressure difference is relatively small compared to atmospheric pressure (1 atm can lift approximately 10.3 m water), and on the order of 2%, 1% or even less according to the displacement. This pressure difference is neglected to simplify the calculation and the pressure in the system is approximated as the same as atmospheric pressure.

3.5.7 Physical solvent sampling module

In order to calculate the amount of CO_2 recovered from the rich solvent stream by the membrane module and determine the efficiency of the absorber in terms of solvent saturation at different pressures and temperatures, it was necessary to design and develop a method to measure the amount of dissolved CO_2 in the solvent. As discussed earlier, unlike chemical solvents, physical solvents do not react with the solute and they physically dissolve the acid gases, which are then stripped by means of pressure swing techniques or a combination of heat and pressure letdown. The performance of a physical solvent can be predicted by its solubility. The solubility of an individual gas follows the Henry's law—the solubility of a compound in the solvent is directly proportional to its partial pressure in the gas phase. Hence, the capacity of a physical solvent increases with an increase in the partial pressures of sour gases. Since there is no reaction between the solvent and the solute in the case of physical solvents, desorption of the gas from the liquid can be achieved by reducing the pressure. Pressure reduction is used as a mean to measure the concentration of the CO_2 in the solvent stream. The sampling apparatus is shown schematically in Figure 3.23.

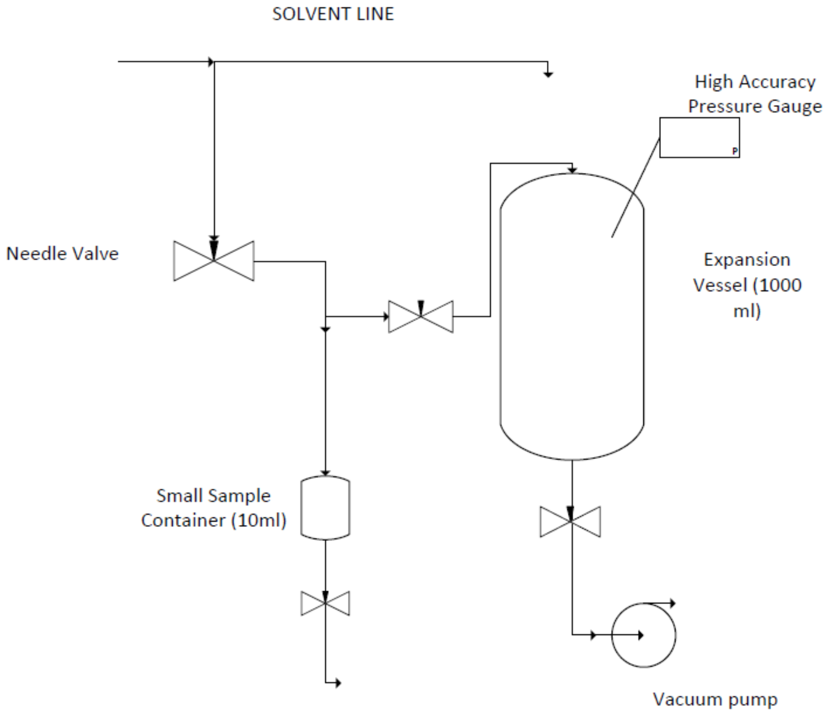

Figure 3.23 Schematic of physical solvent sampling apparatus

The apparatus mainly consists of a small sampling cylinder (10 ml) (purchased from Swagelok, part No: SS-4CD-TW-10) and a 1 liter expansion vessel (purchased through Swagelok, part No: 304L-HDF4-1000) connected to the sampling cylinder. The expansion vessel is equipped with a high accuracy 0.08% pressure gauge from Omega (part No: DPG409-030A). Both the sampling cylinder and the expansion vessel are connected to a 1.1 cfm vacuum/pressure diaphragm pump (purchased from Cole-Parmer, part No: EW-07061-40). Before drawing the sample from the solvent line, the whole sampling module is vacuumed and isolated using the valves. The initial pressure of the expansion vessel is recorded. Following that, using a valve the expansion vessel is isolated from the sampling cylinder and using a metering valve, a few millimeters of the solvent from the solvent line is injected into the sampling cylinder. Next, the valve that blocks the expansion vessel from the sampling cylinder is opened and the desorbed gas from the solvent enters the expansion vessel and increases the pressure in the expansion vessel. Approximately two hours after the sample injection, the final pressure of the expansion vessel is recorded. Following that, the valve at the bottom of the sampling cylinder is opened and the collected solvent is weighed to calculate the number of moles of the solvent using average molecular weight of the solvent. To ensure all solvent collected in the sampling cylinder is drained, the entire sampling module is purged with 50 psi N_2 gas. It was assumed that all the CO_2 content of the solvent desorbs under vacuum condition.

By using: (1) an equation of state such as ideal gas law or Soave-Redlich-Kwong equation of state, (2) the expansion vessel pressure difference before and after the sample injection, and (3) the volume of the sampling system, the number of moles of CO_2 desorbed (n_{CO2}) from the solvent sample is given by equations 11 and 12

$$n_{CO2} = \frac{[P_2(V_T - V_S) - P_1 V_T]}{RT} \qquad \text{Eqn (11)}$$

$$X_{CO2} = \frac{n_{CO2}}{n_{CO2} + \frac{m_s}{M_n}} \qquad \text{Eqn (12)}$$

where:
R: Universal Gas Constant ($cm^3.psi.g\ mol^{-1}.K^{-1}$)
T: Temperature (K)
P_1: Sampling module pressure after evacuation (psi)
P_2: Sampling module final Pressure after sample injection (psi)
V_T: Sampling module total volume (cm^3)
V_S: Sample volume (cm^3)
m_S: Sample weight (gr)
M_n: Average molecular weight of the solvent (g)
X_{CO2}: mole fraction of CO_2

The absorber was pressurized to the desired pressure and the pump was turned on. Solvent samples were drawn into the sampling module at different time periods after the absorber pressurization. The measured CO_2 mole fractions in Selexol at different pressures are shown in Figure 3.24. Clearly, CO_2 mole fraction increases as the pressure of the system increases. Additionally, the concentration of CO_2 in the solvent reaches a steady state value approximately 2 hours after the absorber pressurization. This is important with respect to the calculations of the permeation properties of the membrane. Only steady state CO_2 concentrations in the sweep gas were considered in the calculations. Tabulated values of the mole fractions with respect to time at different pressures are shown in Table 3.5.

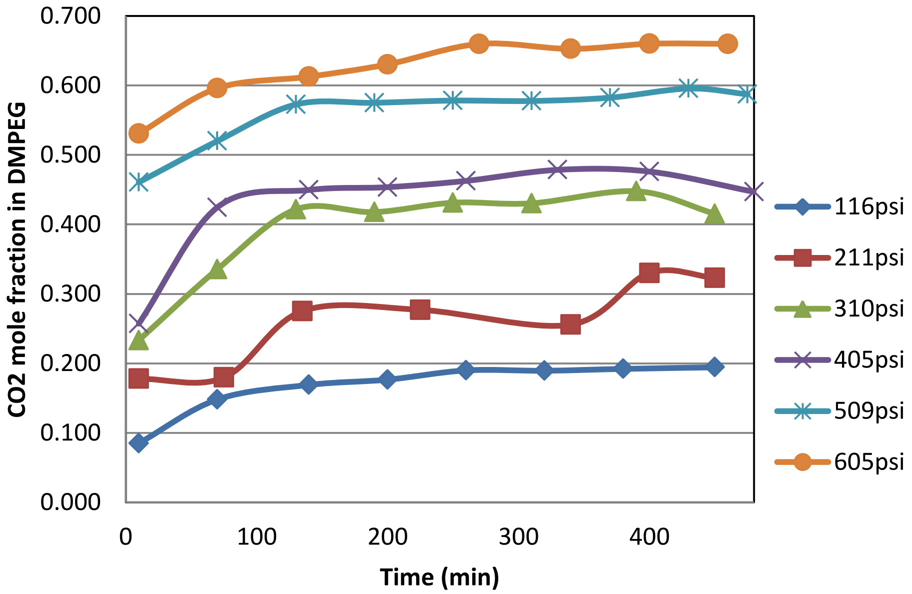

Figure 3.24 CO_2 mole fraction in Selexol at different pressures. All pressures are gauge pressure (psig)

Table 3.6 compares the steady state values of CO_2 mole fraction in the solvent obtained from the sampling module with the literature values (Gainar & Anitescu, 1995). The values from Gainar and Anitescu work were interpolated and reported in Table 3.6. The results are fairly close with the percent average absolute deviation of 5.87%.

Table 3.5 CO_2 mole fraction in DMPEG at different pressures.

Time (min)	Mole Fraction	Time(min)	Mole Fraction
116 (psig)		211 (psig)	
10	0.085	10	0.178
70	0.148	75	0.180
140	0.169	135	0.275
200	0.177	225	0.277
260	0.190	340	0.256
320	0.189	400	0.330
380	0.192	450	0.323
450	0.194		
310 (psig)		405 (psig)	
10	0.233	10	0.257
70	0.335	70	0.425
130	0.422	140	0.450
190	0.418	200	0.454
250	0.431	260	0.463
310	0.430	330	0.479
390	0.448	400	0.476
450	0.415	480	0.447
509 (psig)		605 (psig)	
10	0.461	10	0.531
70	0.520	70	0.596
130	0.573	140	0.613
190	0.575	200	0.630
250	0.578	270	0.660
310	0.578	340	0.653
370	0.582	400	0.660
430	0.596	460	0.660

Table 3.6. Comparison of CO_2 mole fractions in this work with the literature values (Gainar & Anitescu, 1995).

Pressure (psig)	This work	Gainar Work (Interpolated)
116	0.191	0.175
211	0.297	0.28
310	0.431	0.382
405	0.466	0.465
509	0.586	0.547
605	0.658	0.639

4 Results and Discussion

4.1 Chemical Solvents

4.1.1 Membrane screening

The first stage of this study was to screen various materials to assess their potential to be used in this process. Initial membrane candidates consisted of relatively inexpensive and commercially available microfiltration membranes (Table 4.1). PTFE membranes from two different sources with different pore size were included. For membrane performance, both high CO_2 flux and high selectivity over the solvent are favorable. Other operational aspects considered included mechanical strength, chemical and thermal stability of the membranes, and hydrophobicity.

Table 4.1 List of membrane candidates.

Membrane materials	Abbreviation	Pore size (μm)	Thickness (mm)	Sources
Polyethersulfone	PES	0.22	0.16	Millipore
Polyvinylidene Fluoride	PVDF	0.45	0.12	Millipore
Mixed Cellulose Ester	CE	5.0	0.12	Advantec
Polytetrafluoroethylene	PTFE-1	1.2	0.07	Sartorius Stedim
Polyester	PETE	0.4	0.01	GE Water & Process
Laminated Teflon	PTFE-2	0.45	0.12	GE Water & Process
Polypropylene	PP	0.45	0.16	GE Water & Process
Polyamide	PA	0.45	0.12	Sartorius Stedim
Cellulose Acetate	CA	5.0	0.12	Advantec

Porous membrane candidates were each tested under the same conditions. Flow rate of 120 mL/min; heater temperature of 80 ºC; and N_2 sweep gas flow rate at 1000 sccm. The CO_2 concentration in sweep gas was measured every 10 seconds by NDIR. The measurements for 6 hours after steady state reached were used and averaged to calculate the CO_2 permeation flux. Permeated solvent collected by the coalescing filter was also measured to calculate the liquid flux. CO_2 to solvent selectivity was obtained as the ratio of permeated CO_2 flux and permeated liquid flux.

Table 4.2 Porous membranes flux and selectivity

Materials	CO_2 flux ($cm^3/(cm^2.s)$)	Liquid flux ($cm^3/(cm^2.s)$)	Selectivity
PTFE-1	0.80±0.36	7.45×10^{-4}	1074
PTFE-2	0.23±0.02	2.41×10^{-4}	954
PP	0.32±0.03	3.51×10^{-4}	930
PETE	1.56±0.13	2.33×10^{-3}	672

The performance of membrane candidates is shown in Table 4.2. PTFE and PP showed similar performance for both permeation flux and high selectivity. PETE had a significantly higher flux of both CO_2 and liquid but the selectivity toward CO_2 is much lower, which could be due, in part, to its thinner membrane thickness. Mixed cellulose ester membranes, PVDF, polyamide, and cellulose acetate were tested but suffered from excessive liquid leaks, which is likely due to the hydrophilic nature of these materials. It was concluded that these membranes were too easily wetted by the aqueous solvent and are likely to be very hydrophilic for this application. For PES, it was found that the CO_2 flux decreased dramatically over time (Figure 4.1). After taking the membrane out from the system, we found that this membrane had become fouled by a yellowish cake-like deposit. The decrease of CO_2 flux is likely due to the severity of the fouling and the accumulation of the thickness of this layer.

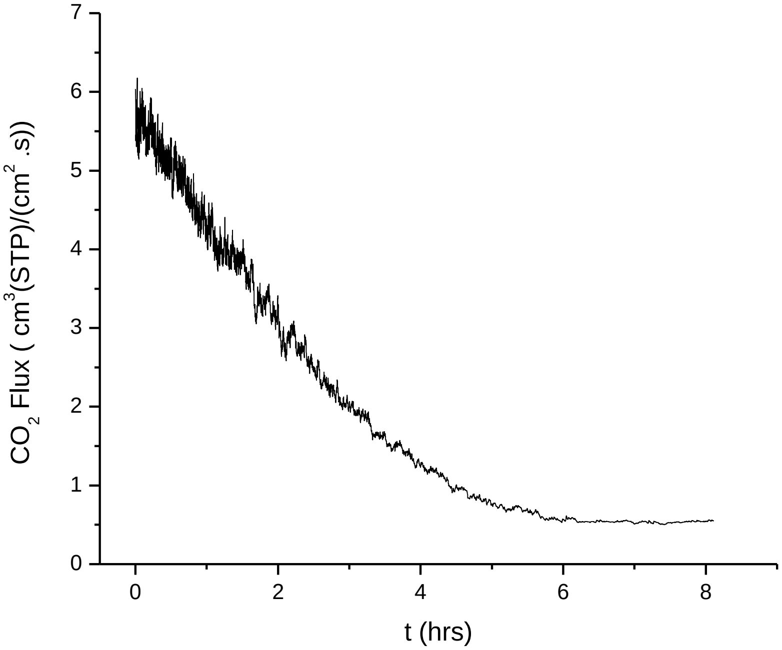

Figure 4.1 CO_2 flux for PES membrane versus stripping time

4.1.2 Porous membrane surface morphology

Membrane surface appearance was observed using an optical microscope. The surface of the membrane before and after testing was observed. No significant surface changes were observed for PP and PTFE using optical microscopy, but some yellowish deposits were found on the polyester membrane surface (picture not shown). This could possibly be precipitated MEA or the by-product of MEA degradation which could not adhere to PP and PTFE surface due to their hydrophobicity or low surface energy.

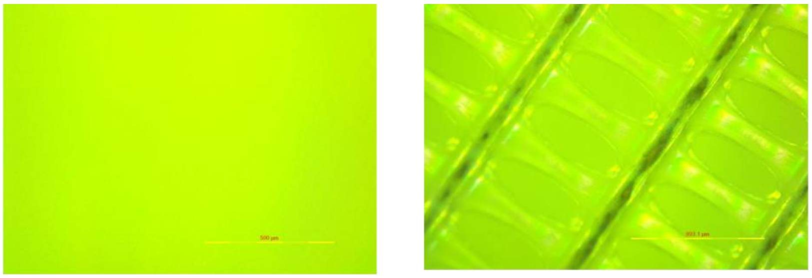

PP membrane before run

PTFE membrane before run

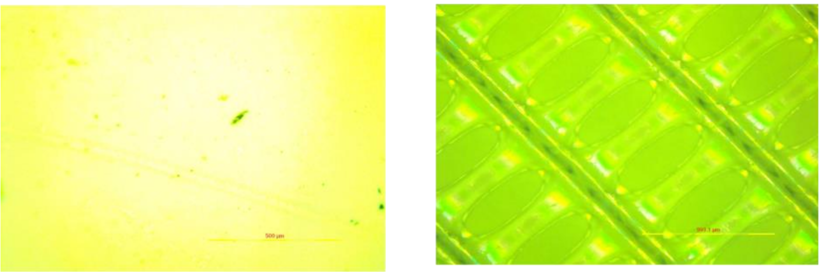

PP membrane after run

PTFE membrane after run

Figure 4.2 PP and PTFE membrane surface before and after run.

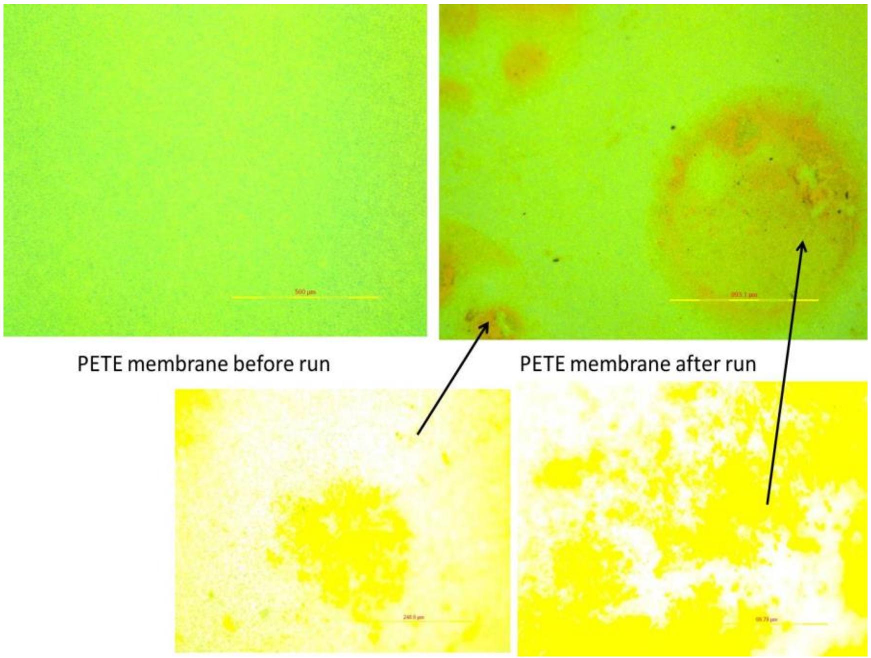

PETE membrane before run

PETE membrane after run

Figure 4.3 PETE membrane surface change before and after run.

4.1.3 Sorption

As previously reported, significant differences were observed in the performance of various membrane materials during porous membrane screening measurements. It was assumed that the hydrophilicity of the material was primarily responsible for these differences, but that chemical incompatibility of some materials to the MEA solution may also play a role. To understand these effects further, sorption experiments were performed to study the absorption of MEA solution into each material, as well as membrane solvent interaction and compatibility. An aqueous solution of 15 wt. % lean MEA was used as solvent. The membrane thickness was measured using a digital micrometer (Fowler IP54, ±0.00001in) and weighed on a microbalance (Fisher Scientific, ±0.00001g). Duplicate fresh samples were measured, then immersed in 2L of solvent and heated in a vented water bath (Precision microprocessor controlled 280 series) at 83°C for 20 hours. Samples were removed from the solvent using tweezers, and then excess solvent was removed by clean dry filter paper (Scientific Products). The membranes were weighed and recorded every 30 minutes until the mass no longer changed. The membrane appearance changed significantly during this experiment (Figure 4.4). The change was likely due to a combination of the strong alkalinity of the MEA and the high temperature.

Table 4.3 Physical properties of membranes before sorption test

Membrane Type	Mass (g)	Thickness (cm)	Volume (cm^3)	Density (g/cm^3)
PES-1	0.0857	0.0164	0.2853	0.3003
PES-2	0.0860	0.0167	0.2901	0.2964
PVDF-1	0.1235	0.0110	0.1917	0.6443
PVDF-2	0.1246	0.0110	0.1917	0.6500
PTFE-1-1	0.0780	0.0072	0.1249	0.6247
PTFE-1-2	0.0793	0.0072	0.1263	0.6277
PETE-1	0.0174	0.0012	0.0205	0.8461
PETE-2	0.0179	0.0011	0.0191	0.9374
PTFE-2-1	0.0767	0.0106	0.1836	0.4177
PTFE-2-2	0.0754	0.0110	0.1902	0.3963
PP-1	0.0433	0.0167	0.2901	0.1493
PP-2	0.0430	0.0171	0.2967	0.1449
PA-1	0.0638	0.0116	0.2012	0.3170
PA-1	0.0617	0.0114	0.1976	0.3123
CA-1	0.0779	0.0120	0.2079	0.3748
CA-2	0.0771	0.0120	0.2049	0.3763

The mass gain of each membrane for around 30 hours was shown (Figure 4.5 Mass change of different membranes after sorption vs. drying time Figure **4.5**). This slow liquid evaporation rate might suggest that the liquid absorbed by the membranes was probably not water alone. The final mass of PVDF, PP, CA and PTFE are close to the original mass. PES and PA had significantly mass gain after sorption, which possibly came from the yellowish deposits from the solution.

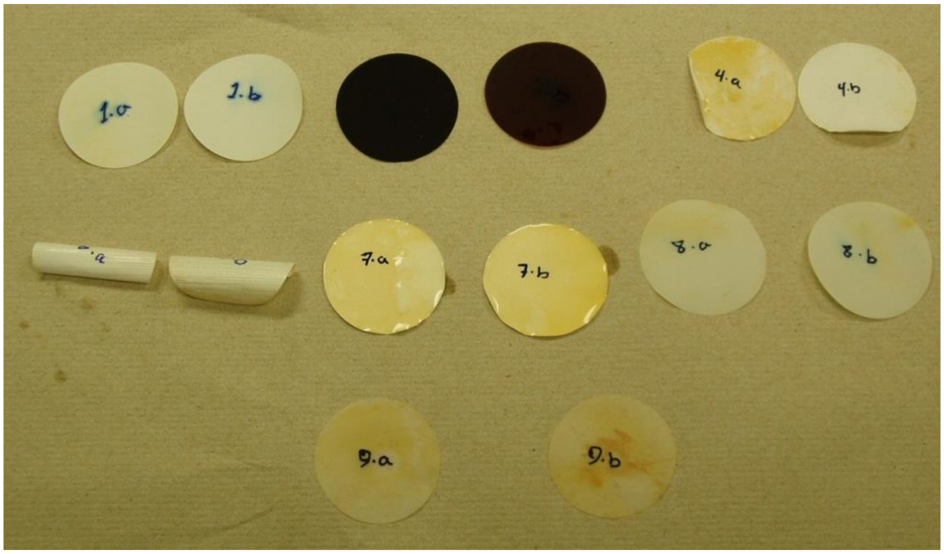

Figure 4.4 Membrane appearance after sorption for 20 hours.

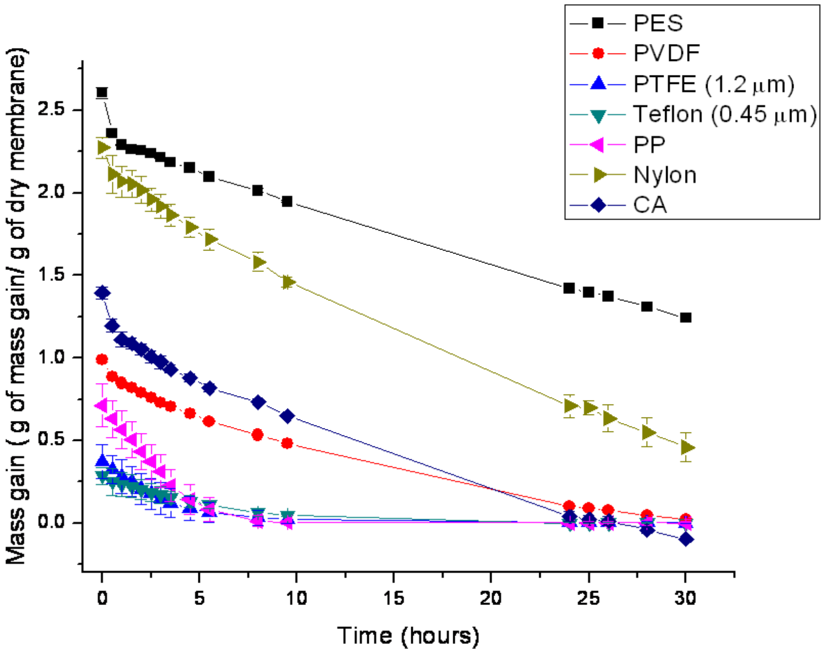

Figure 4.5 Mass change of different membranes after sorption vs. drying time

The mass gained by the membranes is composed of two parts: the non-evaporative deposits on the membrane surface; and solvent swelling of the membrane itself, which does evaporate over time (Figure 4.6). Both of these factors could potentially diminish the membrane performance over time. PP and PTFE were both almost free of deposits and had relatively low swelling, possibly attributed to their low surface energy and high hydrophobicity. PES and PA had a relatively high percentage of non-evaporative mass gain and showed deposit formation and fouling. PA, PVDF, PES and CA showed much higher hydrophilicity than PP and PTFE. For CA, non-evaporative mass gain is negative which may imply cellulose deacetylation in the MEA aqueous solution.

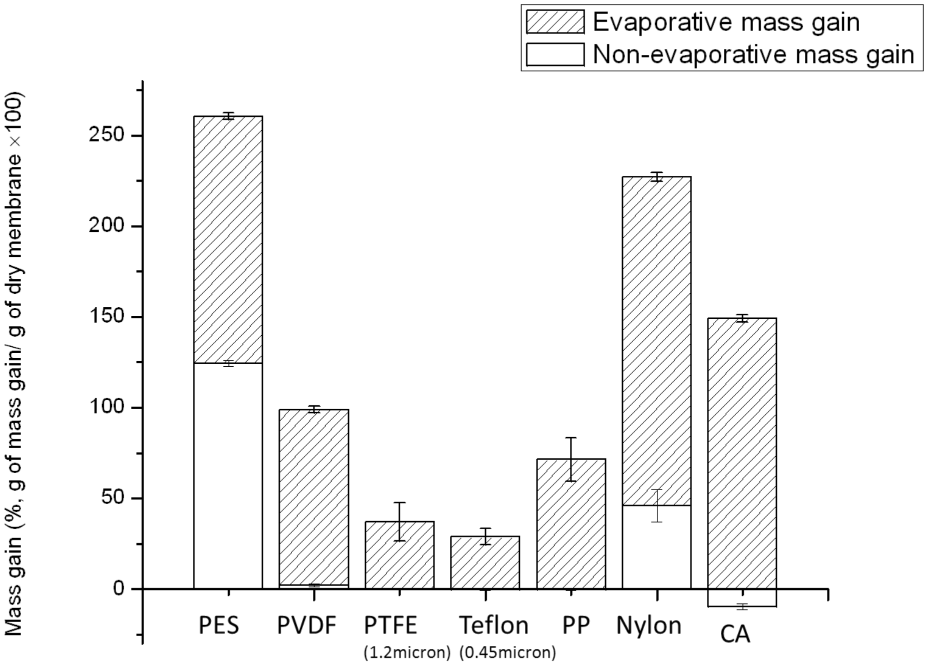

Figure 4.6 Percentage of evaporative and non-evaporative mass gain.

Using equation 6, the calculated values of solubility coefficient for different membranes are shown in Figure 4.7.

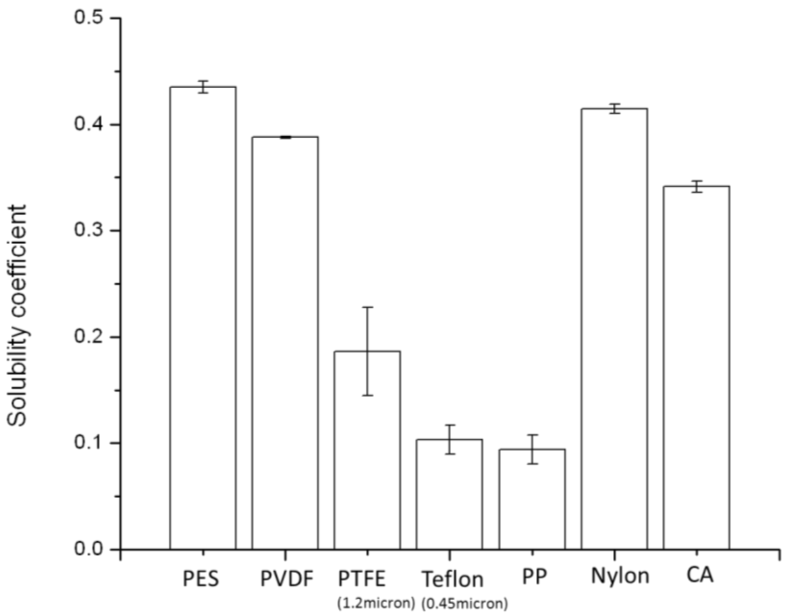

Figure 4.7 Solubility coefficient for different types of membranes

Additional sorption experiments were performed to study the effect of solvent alkalinity on membranes. Because the CO_2 loading of aqueous MEA can significantly affect the pH of the solution, measurements were taken in both lean and loaded solutions. Experiments were performed using a lean 15% aqueous MEA solution (pH=12.5) and a CO_2 loaded 15% aqueous MEA solutions (pH=9.2). A lid was used to prevent significant solvent evaporation.

Samples of each material were first weighed and then placed in the respective solutions at a temperature of 82^oC. After 20 hrs, the membranes were taken out of solution and weighed. Using an OHAUS moisture analyzer the samples were dried by gradually heating to 105^oC and holding it at this temperature until the mass no longer changed. The final weight of each sample was then recorded.

Figure 4.8 is a plot of the mass of each membrane before and after absorption, as well as after drying, for those measurements with a lean MEA solution. Figure 4.9 presents this data as a percentage of the original mass of the membrane. What these data show is that PES, Nylon, PVDF and CA are very hydrophilic, absorbing in some cases 100% or more of their mass in MEA solution. Each of these materials had slight changes in mass after drying, but this was attributed to variability in the mass measurements. Interestingly, PETE completely dissolved in the MEA solution, likely due to hydrolysis of the ester bonds. CA was found to lose considerable mass during the measurement, which could also be due to hydrolysis of the acetate groups in the strong basic solution. As expected, PTFE and PP showed hydrophobic behavior, with only slight mass changes observed after absorption and after drying.

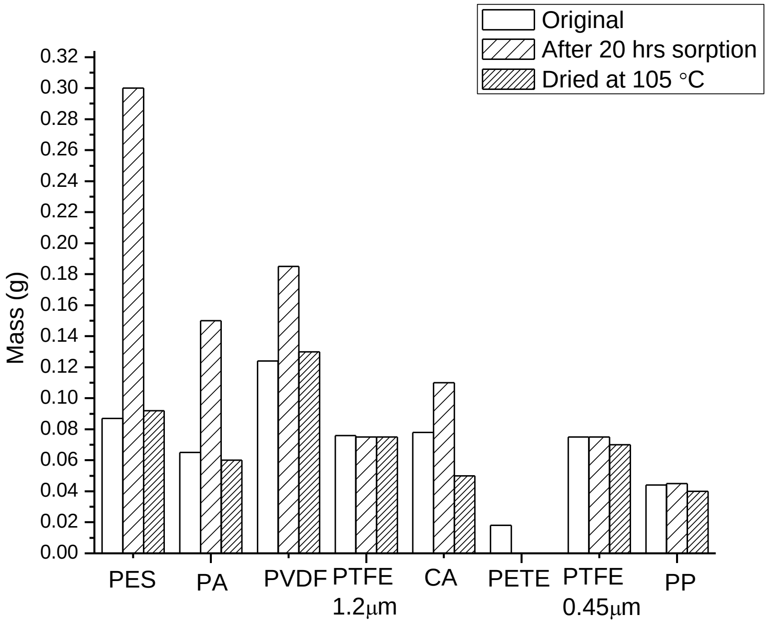

Figure 4.8 Mass comparison for the original membranes, the membranes after absorption in a lean 15% aqueous MEA solution (pH=12.5) at 82°C for 20 hrs, and after drying at 105°C.

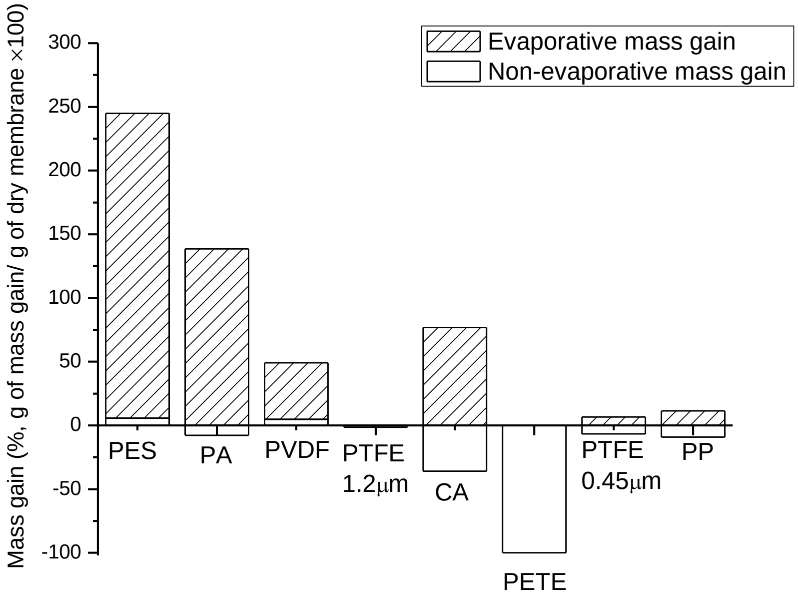

Figure 4.9 Mass change as a function of the original membrane mass, after absorption in lean solution and after drying.

For those measurements in MEA solution loaded with CO_2 (Figure 4.10 and Figure 4.11), the results differed in several ways. First, the amount of solution absorbed by the hydrophilic samples was higher in all cases. For CA, the amount of mass lost was significantly lower. The biggest difference was observed with PETE, which did not dissolve in the solution as it had with lean MEA. The findings for CA and PETE are consistent with the slower rate of hydrolysis at a lower pH. The hydrophobic samples showed essentially the same behavior as with the lean solution. These findings are generally consistent with the membrane screening trials. Hydrophobic materials, in which the solution does not wet the pores of the membrane, perform best. Hydrophilic membranes resulted in excessive wetting and, eventually, an unacceptable rate of leaks. Despite being dissolved in the lean MEA solution, PETE was able to perform well in our membrane screening trials. Since these trials used a fully-saturated MEA solution, hydrolysis was not an issue. However, it could become an issue as the degree of regeneration increases, thereby raising the solution pH.

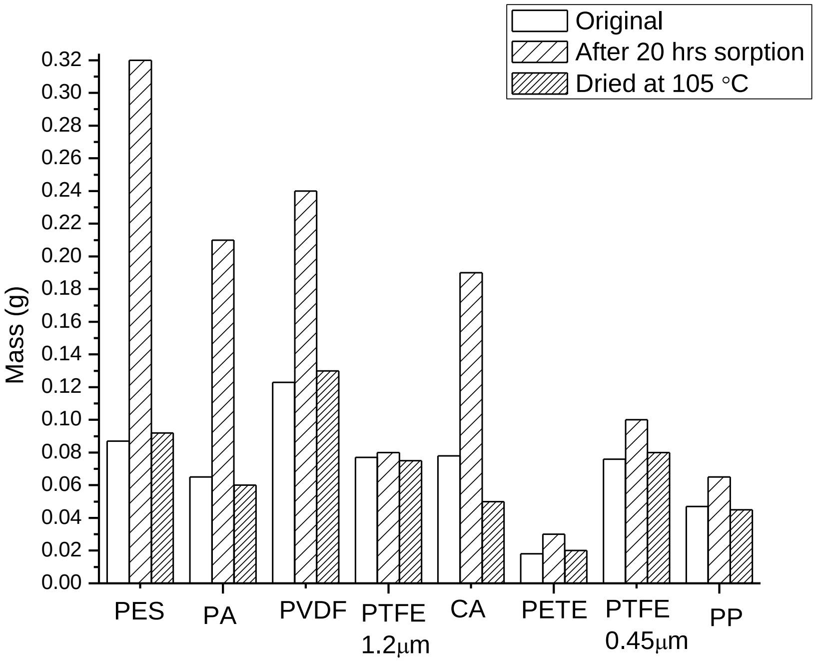

Figure 4.10 Mass comparison for the original membranes, the membranes after absorption in a loaded 15% aqueous MEA solution (pH=9.2) at 82°C for 20 hrs, and after drying at 105°C.

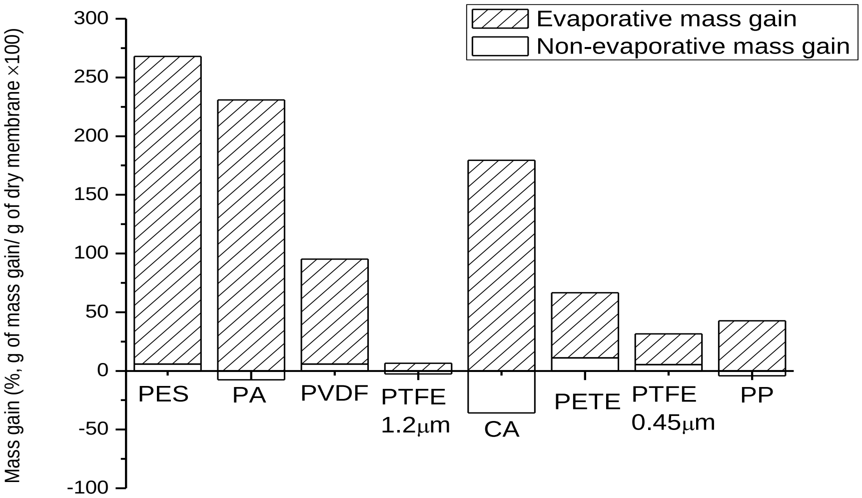

Figure 4.11 Mass change as a function of the original membrane mass, after absorption in loaded solution and after drying.

.

4.1.4 Post-experiment characterization (DSC, FTIR)

4.1.4.1 DSC results

DSC was used to measure the glass transition temperature and melting point of the membranes and characterize the potential structural changes (Figure 4.12). In the cases of PP and PTFE, crystalline peaks were observed, and little change was seen in the melting points after the permeation experiments. Note that differences observed in heat flow (y-axis) are due to sample size differences. A significant change was observed for PETE. It appears that the material becomes more crystalline during the course of the run, as seen by the sharp peak in the DSC curve, due to this semi-crystalline polymer being raised above its glass transition temperature.

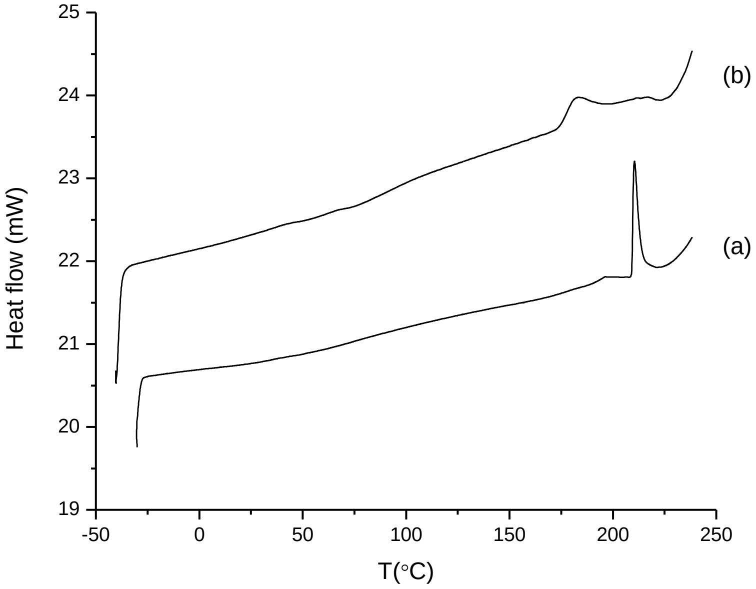
25
24
23
22
21
20
19
-50
0
50
100
150
200
250
Heat flow (mW)
T(°C)
(b)
(a)

(1)

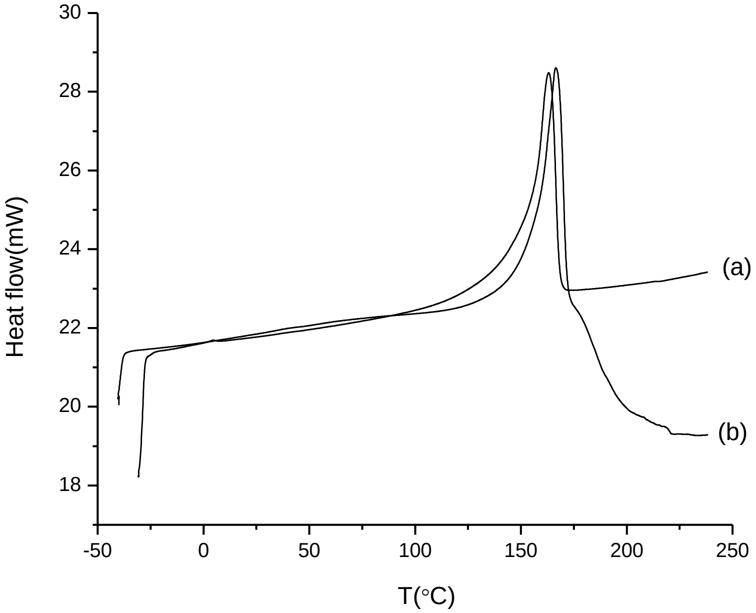
30
28
26
24
22
20
18
-50
0
50
100
150
200
250
Heat flow(mW)
T(°C)
(a)
(b)

(2)

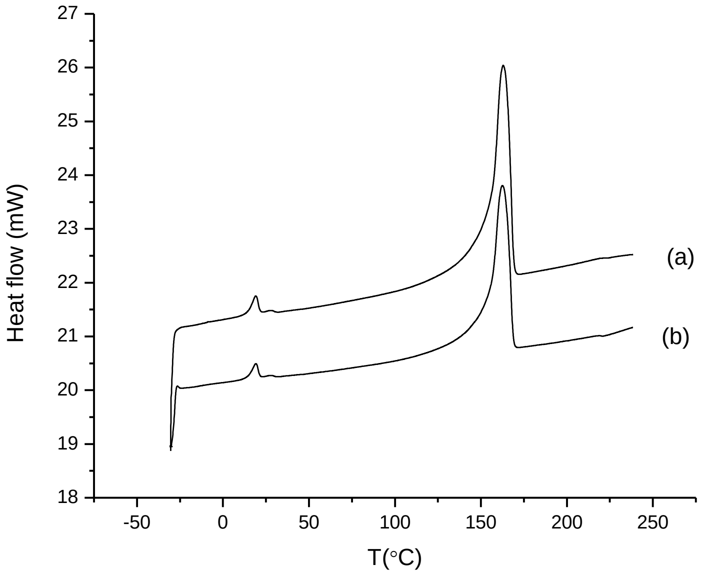

(3)

Figure 4.12 (a) Membrane before experiment; (b) Membrane after experiment (1) DSC results of Polyester, (2) DSC results of PP, (3) DSC results of PTFE

4.1.4.2 FTIR results

FTIR (Thermo Scientific, Nicolet IR 200) was used to characterize the compositional change between the fresh membrane and membrane that was exposed to MEA/CO_2 solution at elevated temperature for stripping runs (Figure 4.13 and Figure 4.14).

The spectra consists of peaks from many sources. The broad peak at 3300 cm^{-1} may come from the OH contribution of water indicating residual water signals (Baudry et al., 2002). CO_2 absorption peaks appear near 2350 cm^{-1} and 670 cm^{-1}. The spectra showed no significant changes in the location of the peaks. This again might suggest that the MEA solvent could be adsorbing onto the membrane surface but no chemical reaction happened between the membrane and the solvent.

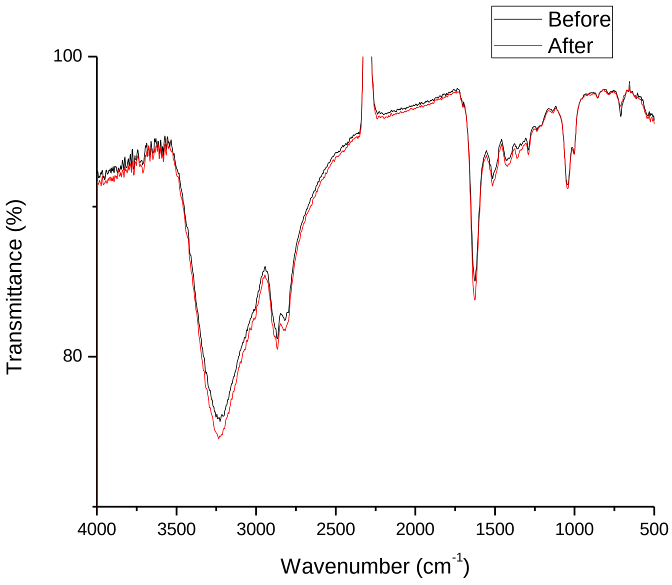

Figure 4.13 FTIR spectrum for PETE membrane before and after run

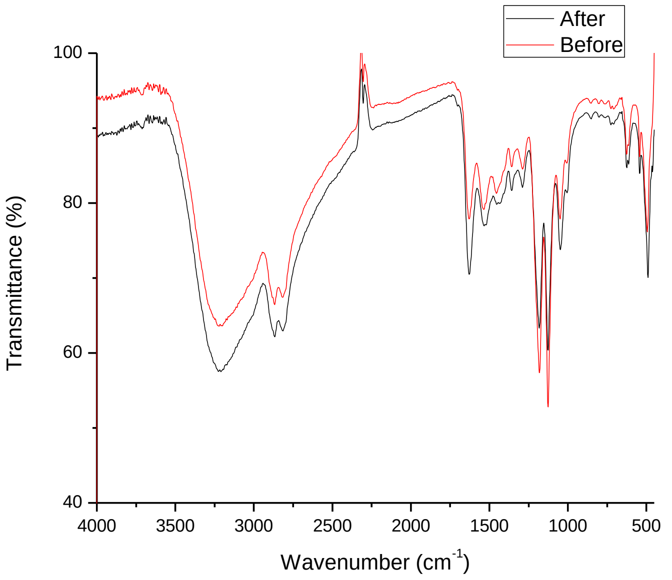

Figure 4.14 FTIR spectrum for PTFE membrane before and after run

4.1.5 Parametric study

A more detailed parametric study was conducted in order to determine the effect of temperature, liquid flow rate, sweep gas flow rate, and liquid pressure. The goal of this work was to understand the parameters affecting the mass transfer rate in this system in order to scale up our results so that they can be compared to a conventional CO_2 absorber-stripper system. For the purposes of this parametric study, we used a PTFE membrane and a 15% MEA aqueous solution.

4.1.5.1 Data analysis method

Other than CO_2 flux and permeated CO_2/liquid selectivity, data obtained from the parametric study were also used to calculate the % CO_2 recovered from the MEA solution. This was determined from the measured CO_2 flow rate in the sweep N_2 gas on the permeate side and the measured saturated CO_2 content in the MEA solution at the retentate side, using the following equation:

$$\% \, regeneration(t) = \frac{\mathrm{CO_2 \text{ content in the sweep gas flow at time t}}}{\mathrm{CO_2 \text{ content in the feed solution at a fixed flow rate}}} \qquad \text{Eqn (13)}$$

For example, for 15 wt% aqueous MEA, the molar concentration of MEA is:

$$\frac{\frac{15\ \mathrm{g}}{61.08\ \mathrm{g/mol}}}{\frac{15\ \mathrm{g}}{997\mathrm{g/L}} + \frac{85\ \mathrm{g}}{1012\ \mathrm{g/L}}} = 2.46\mathrm{mol/L}$$

Here, the MEA molar mass is 61.08 g/mol, the H_2O molar mass is 18.02 g/mol, the density of DI water is 1012 g/L, and the density of MEA 997 g/L. The CO_2 loading of the MEA solution is typically 0.4, as measured by titration analysis. At fixed flow rate of 120 mL/min , the CO_2 flow rate on the feed side is

$$120\,\frac{\mathrm{mL}}{\mathrm{min}} \times 2.46\,\frac{\mathrm{mol}}{\mathrm{L}} \times 10^{-3}\,\frac{\mathrm{L}}{\mathrm{mL}} \times 0.4 \times 22.4\,\frac{\mathrm{L(STP)}}{\mathrm{mol}} \times 10^{3}\,\frac{\mathrm{cm^3}}{\mathrm{L}} = 2645\ \mathrm{cm^3(STP)/min}$$

On the permeate side, if the CO_2 concentration in the 1000 sccm sweep N_2 gas flow was measured at 5000 ppm, the CO_2 flow rate is

$1000\,\frac{\mathrm{cm^3(STP)}}{\mathrm{min}} \times 5000\ \mathrm{ppm} \times \frac{10^{-6}}{\mathrm{ppm}}$=5 $\mathrm{cm^3}$(STP)/min

Therefore, the % CO_2 regeneration in this example is 0.19%. In these experiments, the CO_2 regeneration rate is generally low due to the small lab scale membrane surface area of 13.8 cm^2 (manufacturer specification) provided by a 47 mm diameter circular membrane holder. However, for a typical commercial membrane module, the surface area is several orders of magnitude larger.

4.1.5.2 Effect of temperature

Temperature was expected to have a significant effect on the flux of CO_2 since the maximum loading of CO_2 in MEA decreases with temperature. Also, for membranes in general, an increase in temperature normally leads to increased permeability, though there is normally a decrease in selectivity as well.

A series of experiments was run using porous PTFE membranes to determine the effect of process temperature on the separation of CO_2 from aqueous MEA solution. Two porous PFTE membranes (Sartorius Stedim, 1.2 micron pore size, 47 mm diameter, 0.166±0.020 mm thickness) were mounted in the membrane holder. The aqueous MEA solution (15% wt) was pre-loaded and saturated with CO_2. To check for leaks, the solution was circulated at a speed of 330 mL/min at room temperature. No liquid leakswere observed. The permeation measurements were performed for 8 hours of continuous running at each temperature of room temperature (no heat), 40 ºC, 50 ºC, 60 ºC, 70 ºC, and 80 ºC. Other than varying the temperature, the feed side pumping speed was kept constant at 120mL/min ,the N_2 sweep gas delivery rate was held at 500 sccm, and the CO_2 was delivered to the absorption tank at 300 sccm in the whole process to keep the same CO_2 saturation level.

The CO_2 flux through the membrane (Figure 4.15) showed no significant change up to around 60 ºC. A significant flux increase was seen above 70 ºC. These results matched with previous reported MEA properties by other researchers, who found that aqueous MEA absorption of CO_2 occurs at temperatures up to approximately 60°C (Wallace, 2006). Yeh et. al. (Yeh et al., 2001) reported no significant difference in absorption ability in the range 38-50°C for a 20 weight percent (wt%) aqueous MEA solution. The MEA–CO_2 reaction is exothermic and reversible by supplying heat to the system. The temperature swing absorption/evolution process reverses at approximately 70°C (Wallace, 2006).

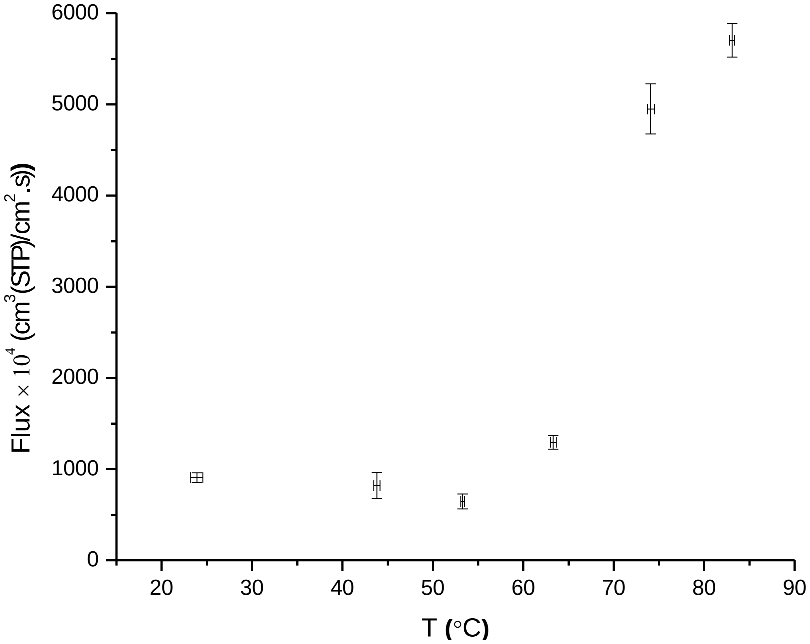

Figure 4.15 CO_2 average flux through the porous PTFE membrane at various temperatures

Once the measurements no longer changing over time, the temperature, pressure and flux were averaged and standard deviations were calculated. It was noticed that the CO_2 flux and pressure variation was much larger than the temperature variation and they both increased significantly as the temperature increased. The variance in both CO_2 flux value and pressure seem to increase with temperature. The pressure increase suggested that the feed solution flow became more turbulent with the temperature rise and the large variability of pressure measurements at high temperature suggested that gas and liquid may co-exist in the system and this situation would likely facilitate this mass transfer process.

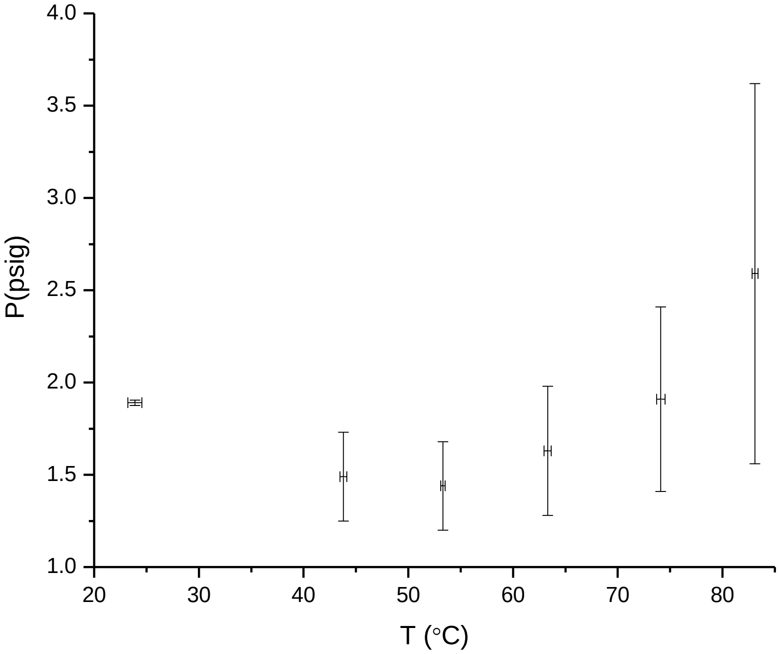

Figure 4.16 Pressure profile at the feed side at various temperatures for PTFE membrane.

Additional experiments were then performed in the temperature range of 70° to 100°C. A trend of improved regeneration was shown (Figure 4.17) as temperature is increased. Note that in this plot and those that follow, the y-axis indicates the % regeneration times a factor of 10^2. This result is expected based on previous results. Further runs at higher temperatures would be needed in order to determine the maximum amount of CO_2 that can be recovered.

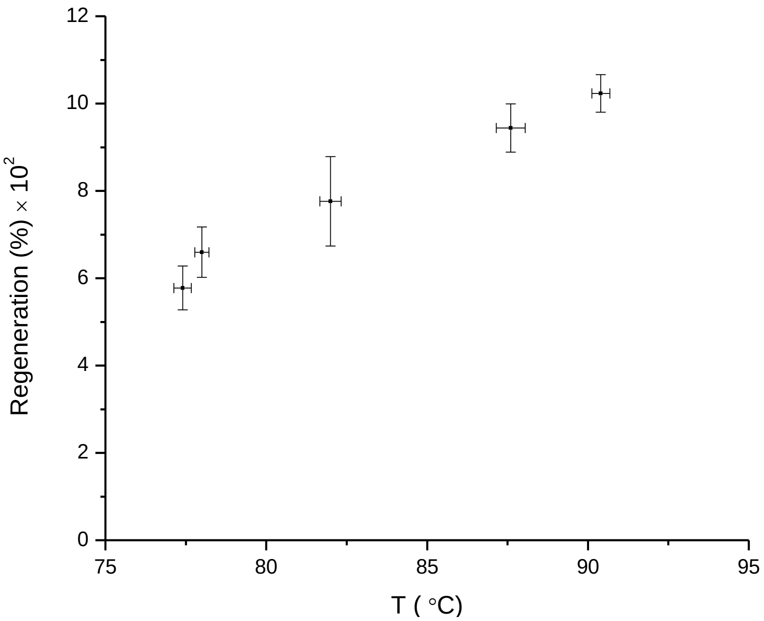

Figure 4.17 CO_2 regeneration as a function of temperature for PTFE membrane

4.1.5.3 Effect of retentate flow rate

A series of experiments was performed to find the appropriate surface to flow rate ratio to maximize CO_2 regeneration yield. The determination of the membrane surface area is essential in membrane module design in order to achieve the best separation performance and reduce the capital size and energy consumption. The results showed that the increase in flow rate on the retentate side (shortened residence time) improved CO_2 flux until a flow rate of around 300mL/min, corresponding to a residence time of close to 0.12 min (Figure 4.18, Figure 4.19). A possible reason for this increase is a thinner liquid boundary layer on the membrane surface resulting from the higher flow rate. This result suggests that an increase in the liquid velocity leads to a decrease in the liquid film mass transfer resistance, which previous studies have shown to be the rate-controlling resistance, accounting for roughly 90% of the total mass transfer resistance of the system (Khaisri, deMontigny, Tontiwachwuthikul, & Jiraratananon, 2009; Khaisri, deMontigny, Tontiwachwuthikul, & Jiraratananon, 2011). The CO_2 flux sharp decrease at

330mL/min flow rate may be related to the membrane wetting caused by the high liquid partial pressure at high retentate flow rate. In terms of the regeneration efficiency, the increase of flow rate decreased it but not at a linear rate. This can be explained as a combined effect of the shortened residence time and improved mass transfer process.

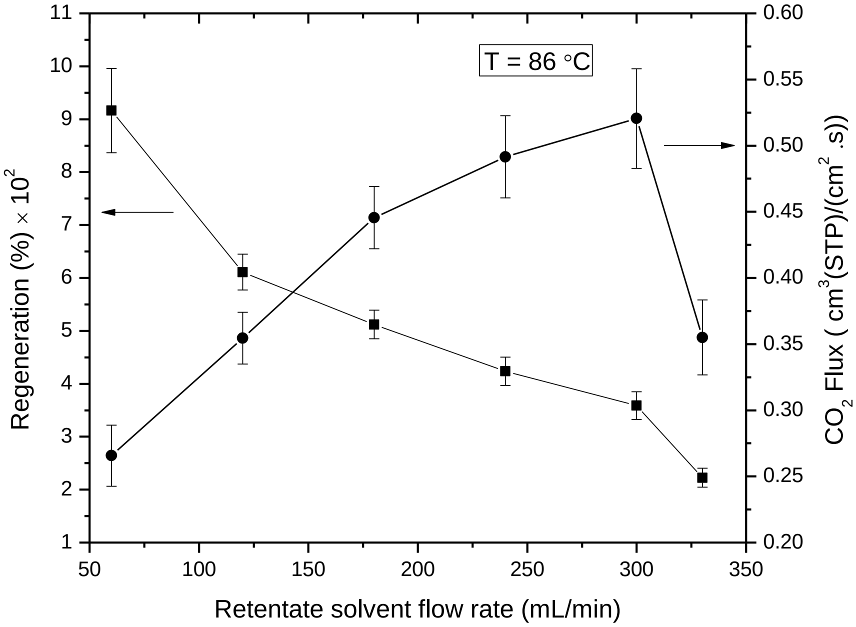

Figure 4.18 CO_2 regeneration as a function of retentate solution flow rate at constant temperature of 86 ºC using a PTFE membrane.

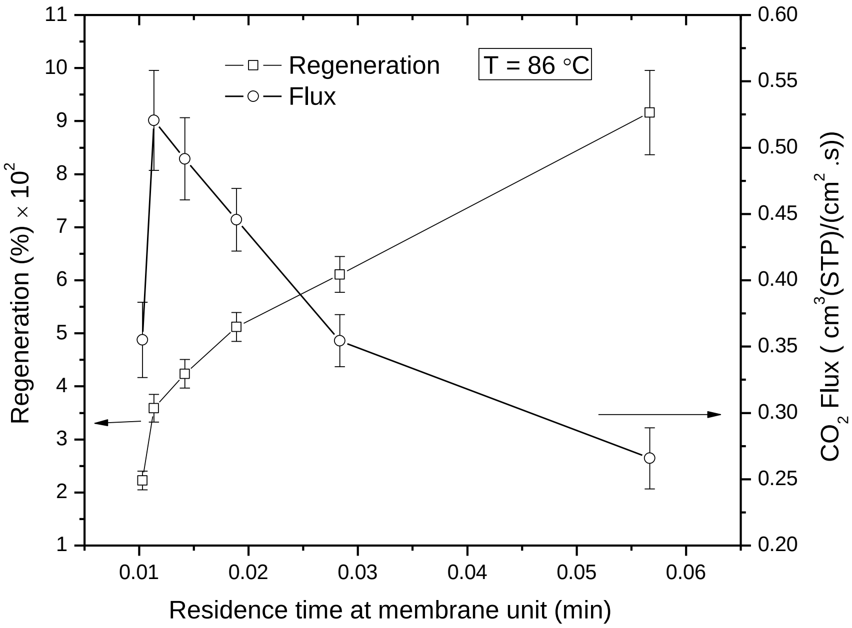

Figure 4.19 CO_2 regeneration as a function of residence time at constant temperature of 86 ºC using a PTFE membrane.

4.1.5.4 Effect of pressure

The pressure on the retentate side of the membrane was controlled by manually closing a needle valve downstream of the membrane module. This valve was adjusted to four different positions: wide open (0 turns), 12 turns, 13 turns, and 14 turns. For reference, the valve can be closed all the way with 14.5 turns. The CO_2 recovery was measured as a function of the pressure at different temperatures (78 ºC, 82 ºC, 88 ºC, 91 ºC).

The results (Figure 4.20) show some interesting points. As can be seen in these graphs, there is considerable fluctuation in the pressure readings. For temperatures above 82 ^oC, the CO_2 recovery generally decreases with increasing pressure and the effect is more pronounced at higher temperatures. This is unexpected for most membrane processes in which the rate of permeation increases with the pressure drop across the membrane. In this system however, the reaction kinetics and liquid film resistance seem to be the dominant factors and so a significant effect of pressure is not seen. Another factor that needs to be considered is the multiphase behavior of the feed solution. Increases in pressure compress the gas phase and potentially increase the liquid layer thickeness, causing more mass transfer resistance.

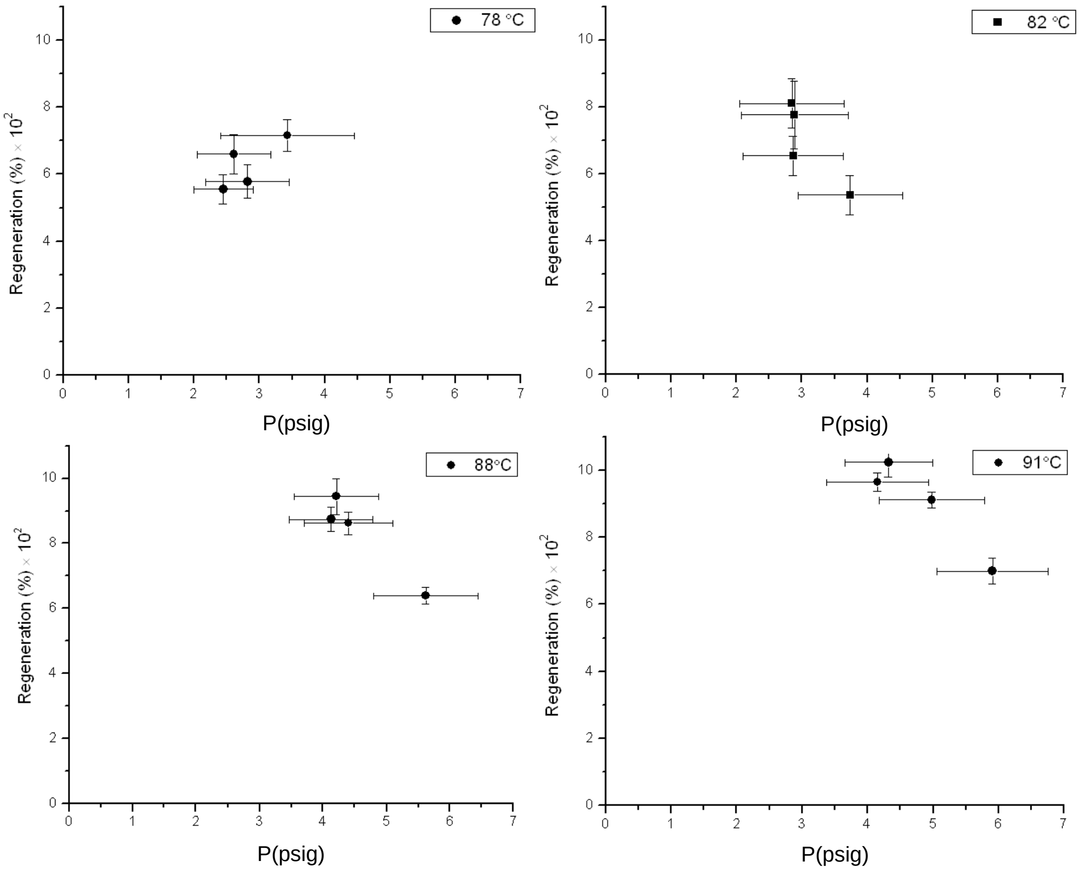

Figure 4.20 CO_2 regeneration as a function of gauge pressure and temperature using a PTFE membrane.

4.1.5.5 Effect of sweep gas rate

Figure 4.21 is a plot of CO_2 recovery vs. the flow rate of the N_2 sweep gas. The function of the sweep gas is to remove permeated CO_2 and maintain a low partial pressure of CO_2 on the permeate side of the membrane. The effect of the sweep gas flow rate on the CO_2 regeneration was investigated at a temperature of 77 ºC and the feed solution flow rate of 180 mL/min. The N_2 sweep gas flow rate was set at 250, 500, 750, and 1000 sccm. The results showed no clear trend as the sweep gas rate is increased. Similar results were obtained at different temperature and flow rate. We can conclude that the sweep gas flow rate does not have a significant effect at these conditions. In other words, the lowest sweep gas rate is sufficient to maintain a low CO_2 partial pressure.

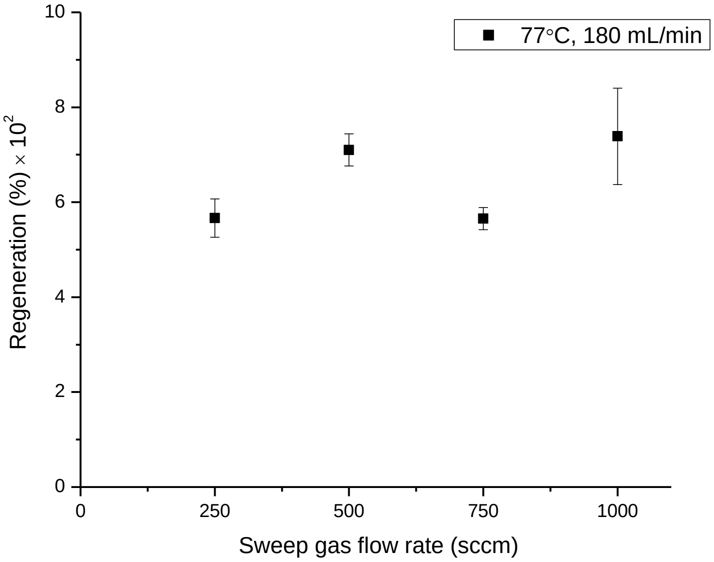

Figure 4.21 Regeneration (%) as a function of N_2 sweep gas flow rate using a PTFE membrane.

4.1.5.6 Screening design of experiment study

A two-level, three-factor full factorial experiment (Table 3.4) was performed to study significant factors and seek optimization of this process. Run order was randomized to eliminate bias. CO_2 flux concentration in the sweep gas stream was recorded for each run after steady state was achieved. All experiments were conducted using a PTFE membrane.

Three factors were studied: 1.solvent temperature at the membrane surface, 2. the retentate solution flow rate, and 3. the permeate side sweep gas rate. The low value of process temperature has to be higher than 70°C to reverse the MEA-CO_2 reaction and release CO_2 gas from solvent. The high value of the process temperature should be lower than the boiling point of water, otherwise a large amount of solvent will be evaporated. For the retentate solution flow rate, it should be high enough to maintain a positive trans-membrane pressure; but excessive high flow rate will shorten the process residence time and lower CO_2 stripping efficiency. The sweep gas rate should be set at a sufficient flowrate to sweep permeated CO_2 and maintain a low CO_2 partial pressure and concentration gradient cross the membrane; but too high of a sweep rate will increase the permeate side pressure, thus lowering the trans-membrane pressure, or even causing reverse permeation. The operation factor values were determined accordingly from preliminary experiments (Table 4.4). The responses of CO_2 permeation flux and selectivity over permeated liquid were analyzed by Minitab software. A Pareto chart and main effects plot for CO_2 permeation flux are shown in Figure 4.22. The vertical red line at a value of 2.306 indicates the critical value from the Student's t distribution for 8 degrees of freedom. Effects above this value are considered to be statistically significant at a confidence level of 95%. It is perhaps not surprising to see that temperature was the only significant factor, as the CO_2-MEA reaction is dominated by reaction.

Table 4.4 Experiment factors and their low and high value

Factors	(-) Low values	(+) High values
Process temperature(°C)	73	92
Solution feed rate (mL/min)	120	180
N_2 sweep gas rate (sccm)	500	1000

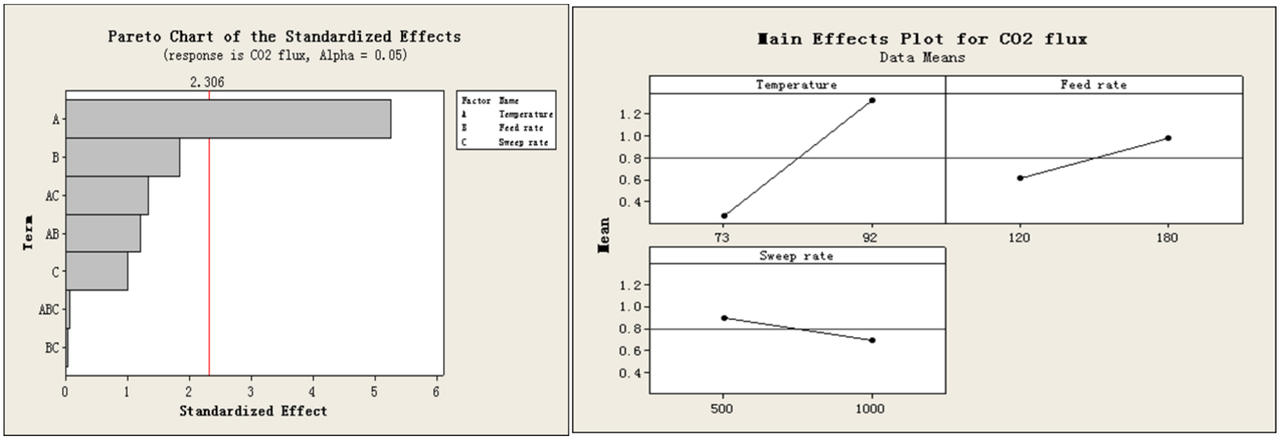

Figure 4.22 Pareto chart and main effects plot for CO_2 permeation flux

A Pareto chart of the effects and main effects plots for selectivity are shown in Figure 4.23. Again, only temperature turned out to be significant. The main effects plots for CO_2 permeation flux and selectivity also showed some interesting features. With temperature increasing, CO_2 permeation flux improved but selectivity decreased. These results suggest a tradeoff between flux and selectivity, which is commonly seen in membranes. The factorial design of experiments results were also consistent with the individual parametric study results.

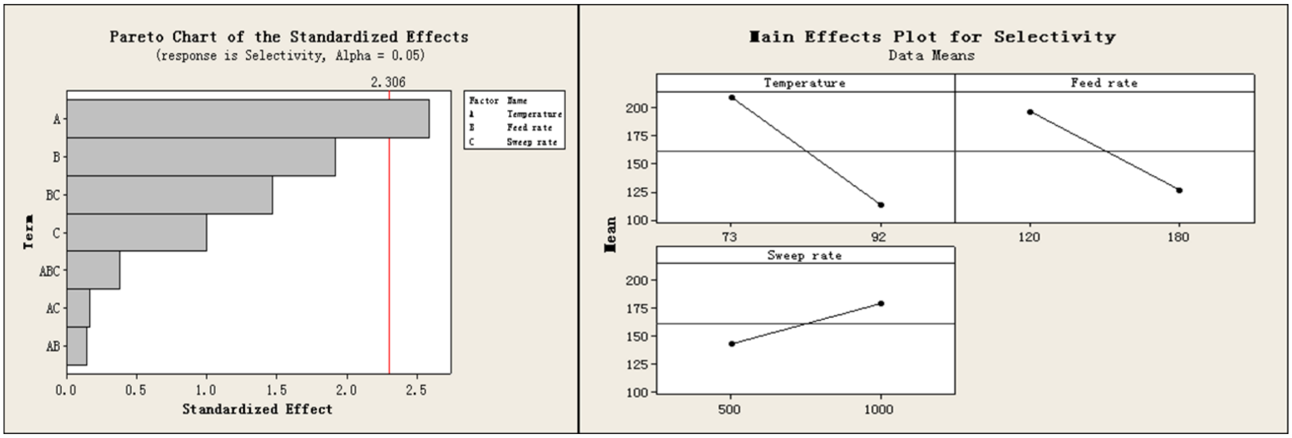

Figure 4.23 Pareto chart and main effects plot for selectivity

4.1.5.7 Membrane mass transfer mechanism study

A mass transfer study was carried out in order to better understand the mechanism of CO_2 and vapor permeation through the membrane and to identify the major mass transfer resistances for this process. The principle of this process is a process similar to but more complex than membrane distillation or pervaporation. This separation process combines simultaneous mass transfer and heat transfer of the feed liquid and gas species through a hydrophobic microporous membrane. In the membrane contactor, a feed solution at elevated temperature is in contact with one side of the membrane and colder sweep gas is in contact with the other side of the membrane. The CO_2 mass transfer process consists of three consecutive steps: 1) CO_2 and solvent gas desorption (physical desorption/chemical reaction) from liquid phase and diffusive transport to the membrane interface; 2) Combined diffusive and convective transport of the gas and vapors through the membrane pores; 3) Gas and the vapor condensation dissociate the membrane on the permeate side of the membrane.

Consequently, the overall mass transfer rates can be expressed in a resistance-in-series model, which are the sum of the mass transfer resistances in the gas and liquid phase and the additional resistances caused by the membrane layer.

In the ideal situation, the micro-porous hydrophobic surface of the membranes only allow the CO_2 gas and the vapor state phases, but not the liquid state, to pass through the membrane pores. The surface tension of liquid solvent helps retain the liquid in the feed side, while the driving force comes from the effective gas/solvent vapor pressure difference produced by the trans-membrane temperature difference and/or concentration difference. What happens in the pores is likely to be explained by the pore-flow model (Kohl & Nielsen, 1997): the liquid phase is restricted by the pores; and the gas and vapor phase evaporates from the interfaces of the liquid and pore openings and travel through the membrane pores. The phase transitions possibly happen in the pore channels as illustrated in Figure 4.24.

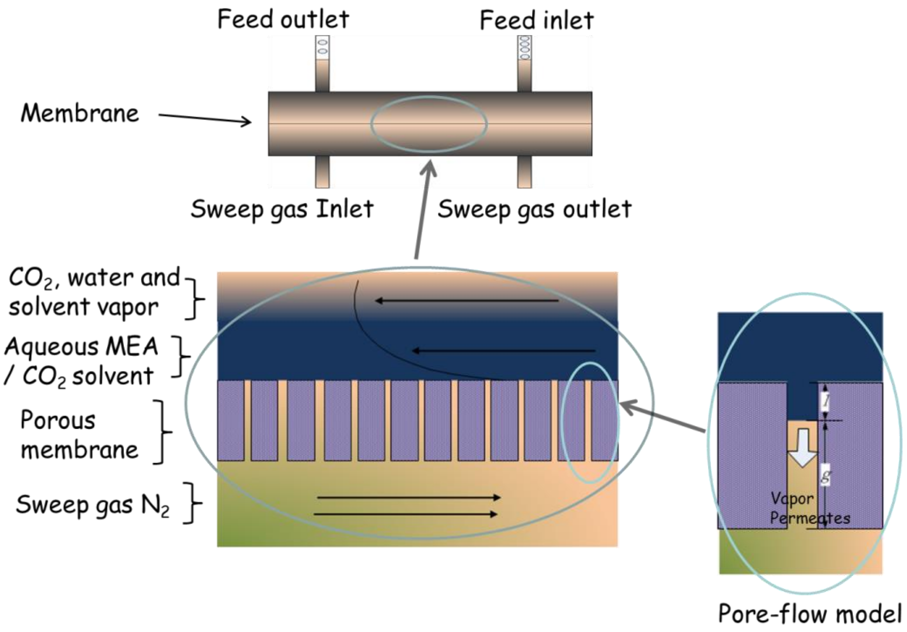

Figure 4.24 CO_2 mass transfer principle through membrane

There are several factors that potentially hinder the mass transfer process and cause energy inefficiency.

1) Uneven temperature distribution and polarization across the membrane surface.
2) Conductive heat loss through the membrane.
3) Laminar boundary layer adjacent to the membrane surface.
4) Liquid or fouling deposits in the pores.

An experiment was carried out in which CO_2 regeneration was measured at steady state using two different orientations of the membrane fixture (Figure 4.25). As expected, CO_2 regeneration was significantly improved by changing to the configuration to one in which the feed solution flowed on the underside of the membrane. This observation underscores the importance of membrane module design for improving the regeneration performance.

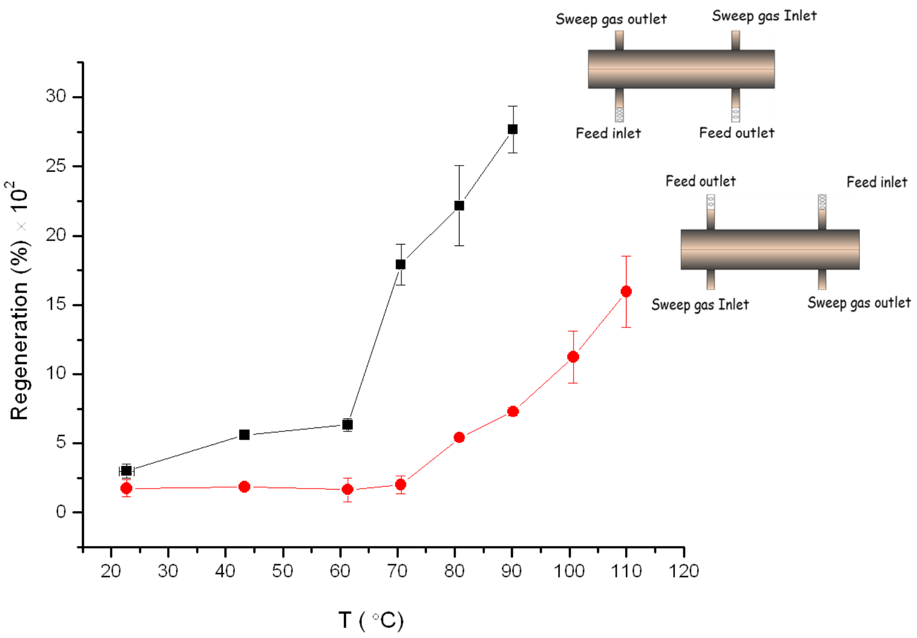

Figure 4.25 Effect of membrane orientation on CO_2 regeneration.

4.1.5.8 Temperature polarization effects

Heat in the membrane unit is transported and dissipated through several major routes. The first route is the transport of the latent heat of evaporation across the membrane; the second route is the heat of reaction that strips the CO_2 by driving the CO_2/MEA reverse reaction; the third route is the convective heat loss through the membrane, together with other conductive heat losses, which leads to energy inefficiency.

This situation is similar to the heat transfer mechanism in membrane distillation (MD). The temperature polarization coefficient (TPC), which is the ratio of useful energy for mass transfer of vapors to the total energy invested in the process, is used in MD and was employed in our study as an indicator of the heat efficiency of our process. TPC is defined as (Lawson & Lloyd, 1997):

$$\mathrm{TPC} = \frac{\mathrm{T_{mf}} - \mathrm{T_{mp}}}{\mathrm{T_f} - \mathrm{T_p}} \qquad \text{Eqn(14)}$$

where T_{mf} is the interfacial feed temperature, T_{mp} is the interfacial permeate temperature, T_f is the bulk feed temperature, and T_p is the bulk permeate temperature. A schematic drawing of temperature polarization effect is shown in Figure 4.26.

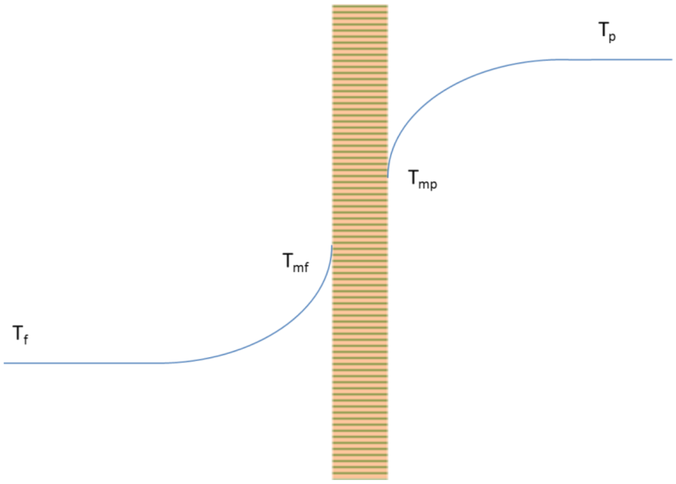

Figure 4.26 Temperature polarization effect

All four of these temperature readings were monitored by thermocouples installed in the system (Figure 3.1) and recorded. Figure 4.26 and Figure 4.28 show that TPC increases at higher temperatures, which agrees with our previous findings that the elevated temperature significantly improves gas and liquid vapor flux through the membrane pores, thus heat flux was also improved across the membrane. Increasing the retentate flow rate from 120 mL/min to 180 mL/min did not significantly change the TPC value. Note that these experiments were performed using the orientation in which the feed solution entered the membrane holder from above.

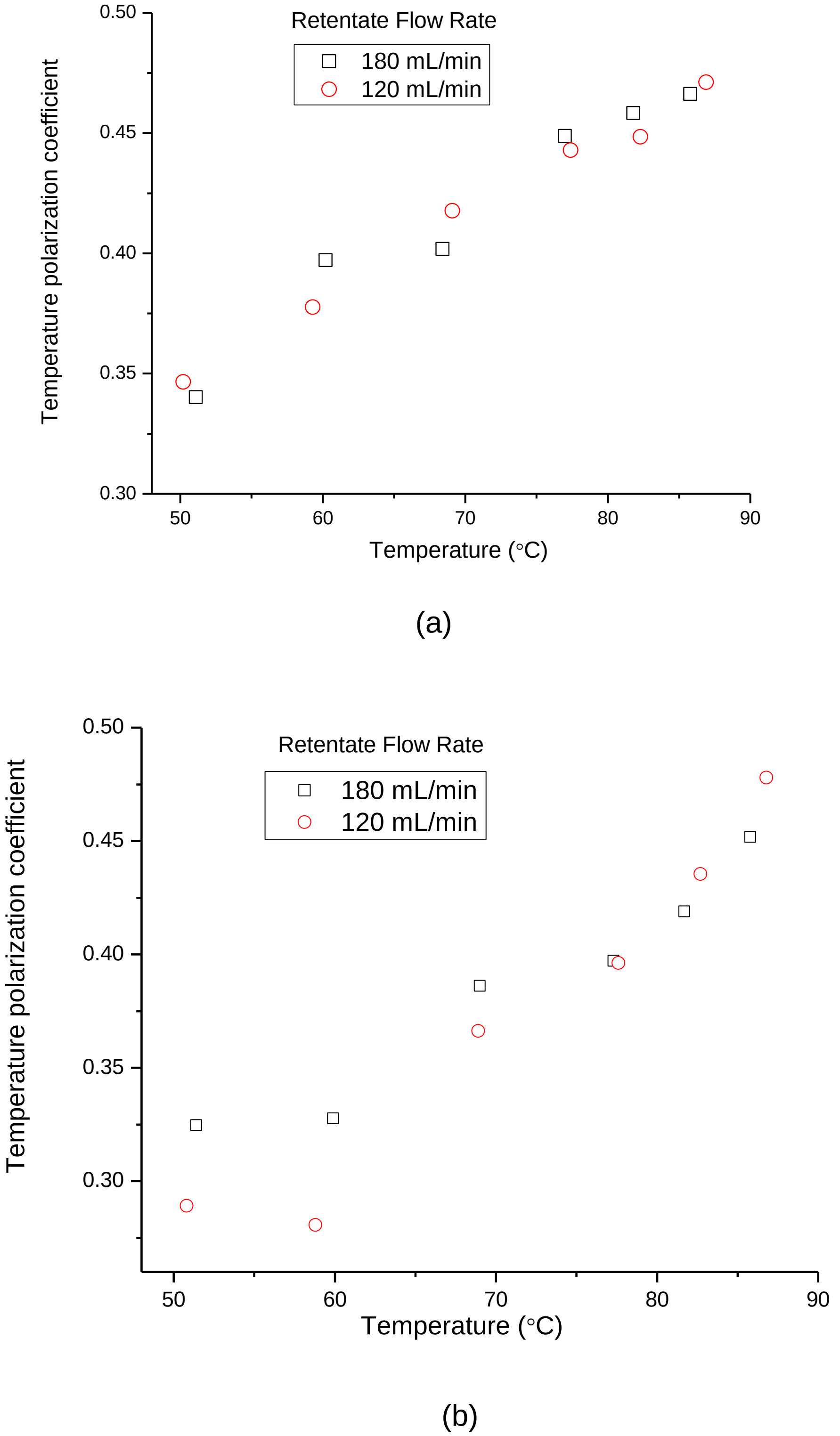

Figure 4.27 Temperature polarization coefficient vs. temperature for PP membrane at different retentate flow rates. (a) sweep gas rate at 1000 sccm; (b) sweep gas rate at 500 sccm.

Figure 4.28 also shows that for a given retentate flow rate, the TPC value was slightly higher at higher sweep gas rates, possibly due to it maintaining a greater temperature gradient. This suggested that the temperature gradient across the membrane could be a major driving force as well for the permeation fluxes, as it is in membrane distillation.

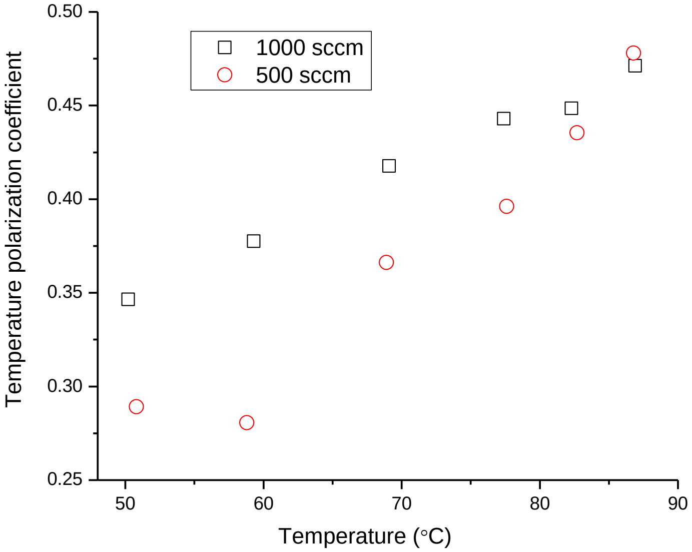

(a)

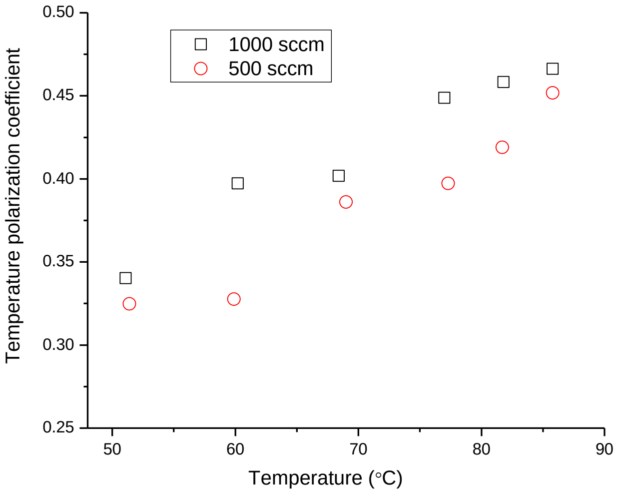

(b)

Figure 4.28 Temperature polarization coefficient vs. temperature for PP membrane at different sweep gas rates. (a) retentate flow rate at 180 mL/min; (b) retentate flow rate at 120 mL/min

With the process temperature above 80 ºC, The TPC measured for our experiment is approaching 0.5, which suggests that roughly half of the heat is used for the mass transfer of CO_2 gas and liquid vapors through the membrane pores. It should be noted here that the TPC value is used to characterize the energy performance of the membrane permeation including CO_2 and liquid vapor and any other permeation components as a whole. The TPC value cannot characterize the energy efficiency performance just for CO_2 alone.

Considering the CO_2 dissociation and liquid evaporation rate is primarily a function of temperature, it is reasonable to assume the CO_2 and vapor evaporation rates depend far more on the interfacial temperature than the bulk temperature. It is reported that most often the TPC varies between 0.2 to 0.9 depending on the membrane module configuration (Cath et. al., 2004). TPC ranged from 0.4 to 0.53 in the laminar regime, to

0.87-0.92 in the turbulent regime (Srisurichan, Jiraratananon, & Fane, 2006). This result also re-confirmed the flow through membrane surface is in the laminar regime.

4.1.5.9 Wetting and Fouling Effects on Mass Transfer

Swelling of membranes, also known as membrane wetting is an important factor on the operability of the membranes. If the liquid absorbent is water or an aqueous solution with inorganic solutes, the liquid has a high surface tension and usually cannot wet common hydrophobic membranes such as PP and PTFE (Lawson & Lloyd, 1997). But the liquid surface tension drops rapidly when a low concentration of the organic compounds is added (Lawson & Lloyd, 1997). With the organic compound concentration exceed a critical point, the contact angle will decrease to less than 90 and the liquid will wet the membrane surface and the pores.

Breakthrough pressure, also known as liquid entry pressure of water (LEPW), is the minimum pressure for the water to overcome the hydrophobic force of the membrane and penetrate the pores. LEPW is a function of the membrane properties, the liquid, and the reaction between them, known as the Laplace (Cantor) equation (Alklaibi & Lior, 2005):

$$LEPW = \frac{2B\gamma_L cos\theta}{r_{max}} \qquad \text{Eqn (15)}$$

where B is a geometric factor determined by pore structure, γ_L is the liquid surface tension, r_{max} is the largest pore size, and θ is the liquid-solid contact angle. It was reported that the LEPW would be 200-400 kPa (29- 58 psi) for 0.2 µm pore size PTFE membranes and 100 kPa (14.5 psi) for 0.45 µm pore size PTFE membranes (Garcia-Payo, Izquierdo-Gil, & Fernandez-Pineda, 2000). If feed solution is flowing at high

Reynolds numbers, the pressure differential can easily be over LEPW, resulting in solvent penetration into pores and slowing down the mass transfer process.

For the application in our system, a positive trans-membrane pressure, feed solution flow at a relatively high Reynolds number, and operation below LEPW are desired. And the most promising solution to meet the desired requirements are probably to choose appropriate membrane materials with high hydrophobicity (low surface energy) and appropriate pore size. Bigger pore size facilitates the mass transfer and smaller pore size provides higher breakthrough pressure.

Based on the mass change measurement of membranes before and after a run, it can be confirmed all the membranes tested experienced the membrane wetting problem, more or less. Detailed data can be found from the mass change study of the membrane sorption study. Many researchers have reported that hydrophobic membranes such as PTFE, PP, and PVDF showed pretty good performance to be free of wetting (Li & Chen, 2005a). That could be the case at low temperatures. But at the elevated temperature, especially approaching the liquid boiling point, the liquid surface tension could be rapidly decreased (Garcia-Payo et al., 2000), and the membrane properties could be changed as well. Another possibility is that the liquid vapor penetrated the pores and could get condensed in the pores to cause wetting. It was observed that wetted membranes gave decreased flux when compared to the fresh membranes flux (Lawson & Lloyd, 1997).

Another possibility (Franco, deMontigny, Kentish, Perera, & Stevens, 2009) reported for the cause of membrane wetting is that the degradation product of MEA reduced the mass transfer rate of CO_2, and furthermore, these degradation acids are believed to adsorb into the PP, altering the surface properties and reducing the hydrophobicity of the membrane. This in turn increases the degree of wetting of the membrane pores. This suggests that membrane wetting and fouling problem may affect each other and deteriorates the membrane performance and long-term stability. The same problem was also revealed on our membranes after stripping CO_2/MEA solvents (Figure 4.29). The MEA could be swelling or adsorbing into the PTFE as well. Figure 4.30 showed the SEM images of PP membranes suggested the similar features from Franco's study.

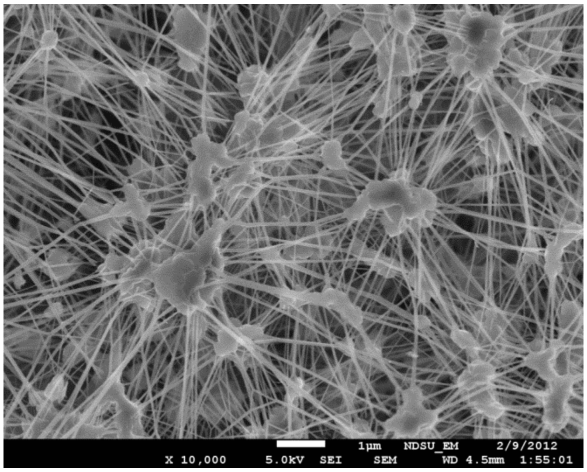

(a)

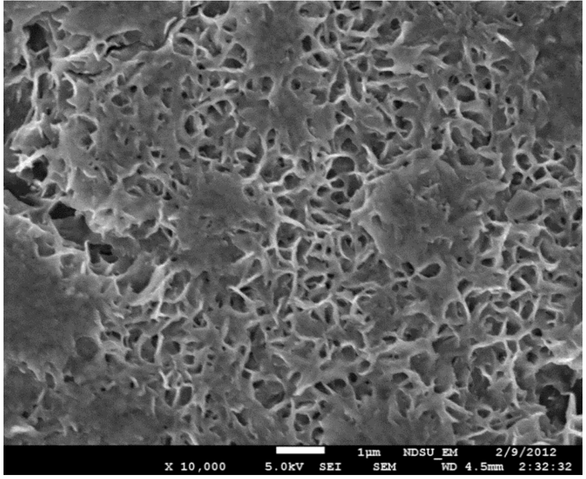

(b)

Figure 4.29 SEM images showing the change in surface morphology of PTFE membrane between fresh PTFE membrane and PTFE membrane that has been used to strip CO_2 from 15 wt% MEA at elevated temperature. (a) fresh membrane at a magnification of 10000x; (b) used membrane.

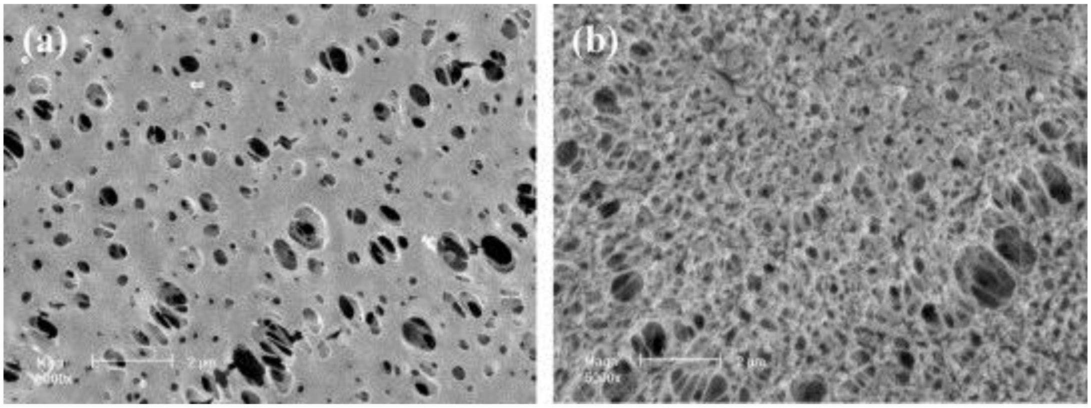

Figure 4.30 SEM images depicting the change in surface morphology of PP membrane between (a) fresh PP membrane and (b) PP membrane that has been exposed to 20 wt% MEA for 25 days at a magnification of 5000x(R. Epps, 1994).

4.1.6 Pore Size study

For this process, porous membrane contactors were chosen because they theoretically provide very little resistance for CO_2 gas transfer while the surface tension reduces the ability of the liquid to pass through the pores. It is important to determine which pore size or what range of pore size can achieve the best performance. However, there is little published literature comparing the performance of membranes with different pore size, and little suggestions can be found about choosing the appropriate pore size. Moreover, no literature has been found to have done similar work studying pore size effect on the CO_2 regeneration process.

4.1.6.1 Theoretical Background

The transport phenomena of gases inside porous membranes can be described by three models: Knudsen diffusion, viscous flow, and molecular diffusion (Phattaranawik, Jiraratananon, & Fane, 2003). The applicability of the models is determined by the comparison of molecular mean free path (λ) and the membrane pore size (d_p), as shown in Figure 4.31. For a single gas system if the mean free path of the gas is much larger than the pore size ($d_p < \lambda$), molecule–wall collisions happen much more often and the gas transport is described by Knudsen diffusion. If the mean free path is much smaller than the membrane pore size ($d_p > 100\lambda$), molecule–molecule collisions become the dominant mass transport mechanism which can be described by viscous flow. When the membrane pore size falls between ($\lambda < d_p < 100\lambda$), both diffusion mechanisms happen in this region. For porous membrane, the gradients of total pressure, concentration, and partial pressure result in viscous flow, molecular diffusion, and Knudsen diffusion, respectively. In our experimental conditions, total pressure is close to atmospheric pressure. Consequently, viscous flow is theoretically omitted. Slip flow (viscous slip) and pressure diffusion can also be neglected. Only diffusion slip contributed from ordinary and Knudsen diffusion exists for the combined mode. Surface diffusion can be ignored due to low molecule–membrane interaction.

For the binary mixture of water vapor and CO_2, the mean free path of water in CO_2 gas (λ_w–CO_2) was evaluated at the average membrane temperature (T_m) as shown in equation 16 (Bird, Stewart, & Lightfoot, 2006):

$$\lambda_{w-CO2} = \frac{k_B T_m}{\pi((\sigma_w + \sigma_{co2})/2)^2 P_T} \frac{1}{\sqrt{1 + (\frac{m_w}{m_{co2}})}} \qquad \text{Eqn (16)}$$

where k_B is the Boltzman constant (1.381×10^{-23} J K^{-1}), P_T is the total pressure (1.013×105 Pa or 1 atm), σ_w and σ_{CO2} are the collision diameters for water vapor (2.641×10^{-10} m) and CO_2 (3.996×10^{-10} m), and m_w and m_{CO2} are the molecular weights of water and CO_2. At the typical process temperature of 80 °C, the mean free path of water in CO_2 gas is 0.12 μm.

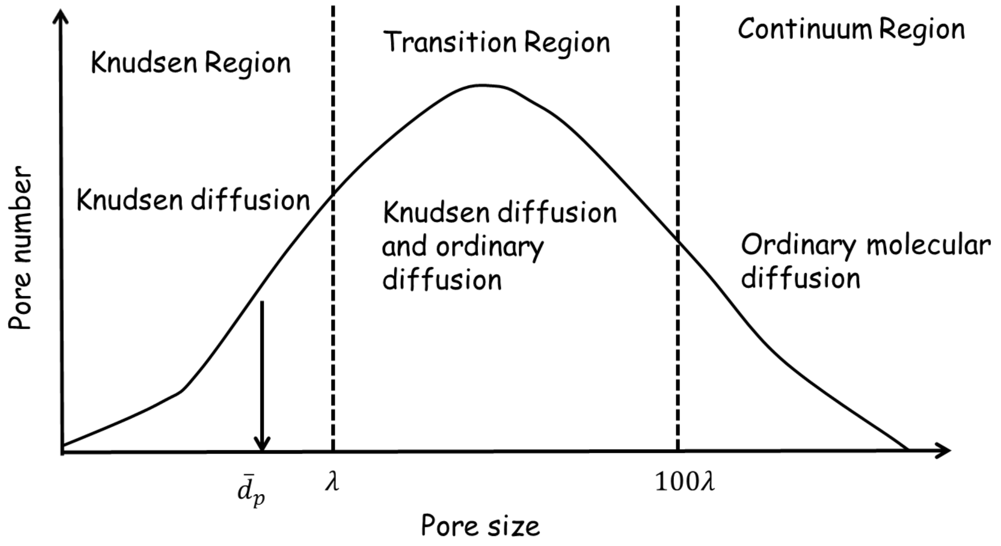

Figure 4.31 The applicability of three porous membrane transport models (Phattaranawik et al., 2003)

4.1.6.2 Membrane Selection and Characterization

Polypropylene (PP) membranes with different pore sizes ranging from 0.1 to 10.0 μm were selected in this study (Table 4-5). Previously, it was roughly estimated that the mean free path of water in CO_2 gas is 0.12 μm. The smallest membrane pore size is close to this mean free path and the largest membrane pore size is close to 100 times of this mean free path. The membrane pore size roughly covered the range from Knudsen region, transition region and continuum region. A total of eight membranes were acquired from two different sources: five membranes from Millipore were supported by a non-woven fabric layer and were designed for microfiltration; three membranes from GE were designed for membrane distillation application. A porosity of 0.35 was provided from manufacture specification by Millipore, and from that, the volume fraction and density of PP fibers can be calculated (0.976 g/cm^3) using Equation 2.3. FTIR (Figure 4.32) and DSC (Figure 4.33) characterization showed that the composition and the structure of these PP membranes are similar. So the same density value was used for all the PP fibers of membranes to calculate membrane porosity (Table 4-5).

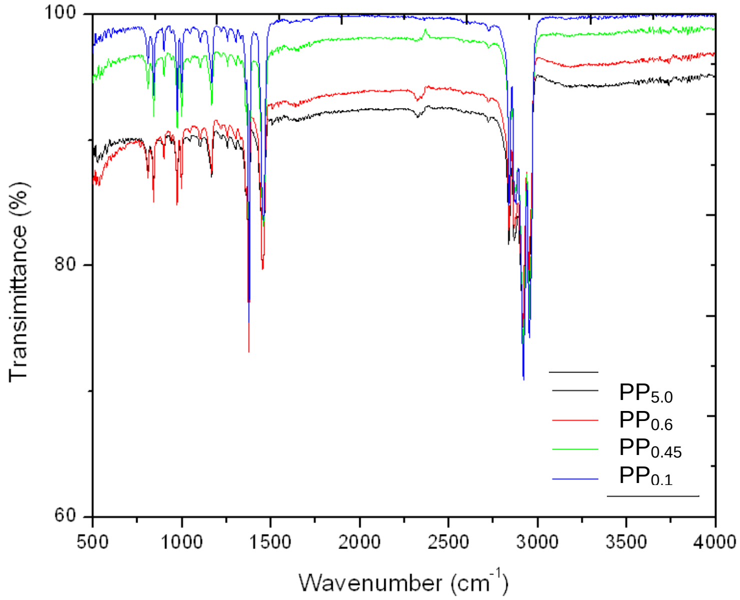

Figure 4.32 FTIR spectra of different membranes.

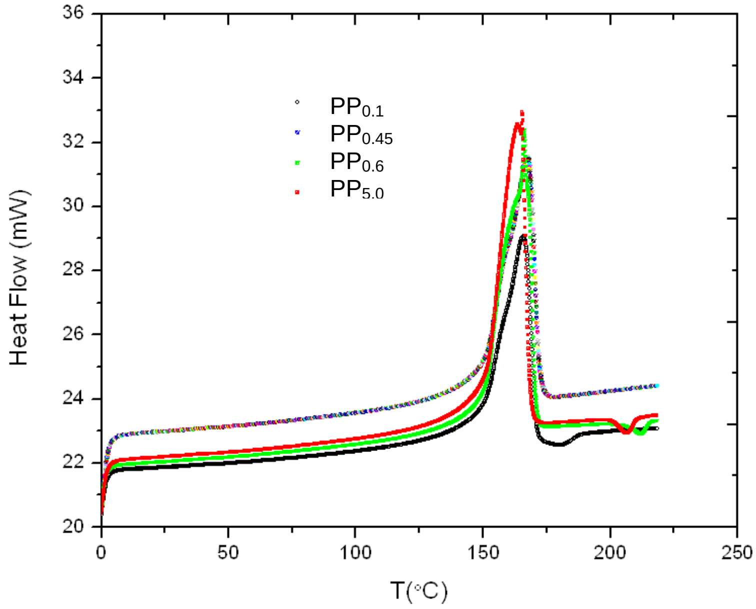

Figure 4.33 DSC spectra of different membranes.

The SEM images of the membrane surfaces (Figure 4.34) clearly show that the structure of GE PP membrane pores are very different from the net-like knot non-woven fiber structures of the Millipore PP membranes.

Table 4-5 Membrane properties (* from manufacturer specification)

Membrane	Nominal pore size (um)	Thickness (mm)	Porosity	Tortuosity	Volume fraction	Provider
$PP_{0.1}$	0.1	0.10	0.76	2.04	0.24	GE
$PP_{0.22}$	0.22	0.17	0.83	1.65	0.17	GE
$PP_{0.45}$	0.45	0.17	0.85	1.55	0.15	GE
$PP_{0.6}$	0.6	0.13	0.35*	7.78	0.65	Millipore
$PP_{1.2}$	1.2	0.13	0.35	7.78	0.65	Millipore
$PP_{2.5}$	2.5	0.13	0.34	8.07	0.66	Millipore
$PP_{5.0}$	5.0	0.10	0.40	6.19	0.59	Millipore
PP_{10}	10.0	0.13	0.59	3.36	0.40	Millipore

GE membranes have more uniformly distributed pores on the surface while the pores of Millipore membranes are relatively not uniformly distributed and have irregular pore shape. It seemed that the smaller Millipore pore size membranes were more compressed than the larger pore non-woven membranes. The observations were consistent with the porosity and tortuosity estimation, as GE membranes appeared to have more straight pores.

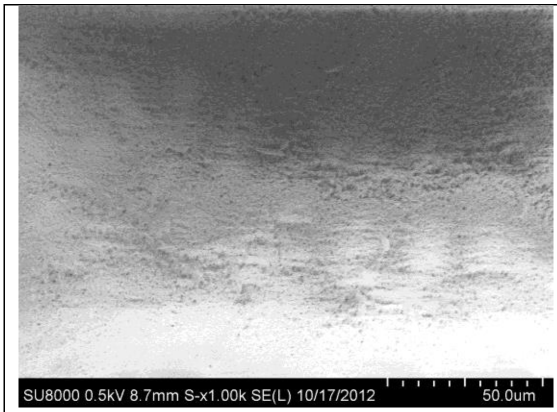

a.GE Membrane surface of $PP_{0.22}$

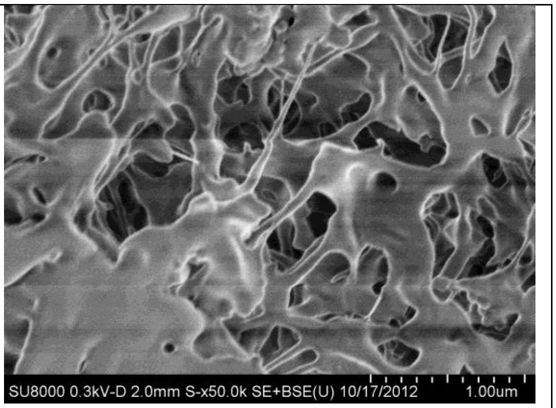

b.GE Pore shape of membrane $PP_{0.22}$

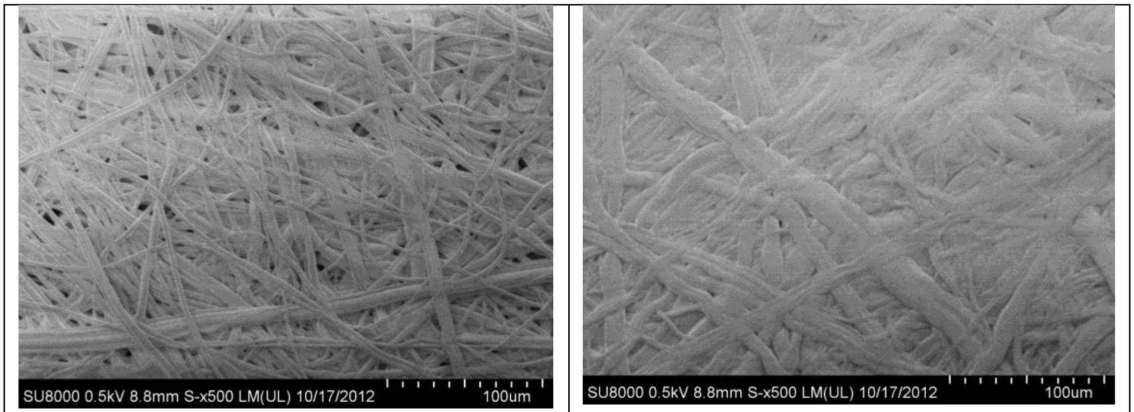

c.Millipore Non-woven fabric surface of membrane $PP_{5.0}$

d.Millipore Non-woven fabric surface of membrane $PP_{1.2}$

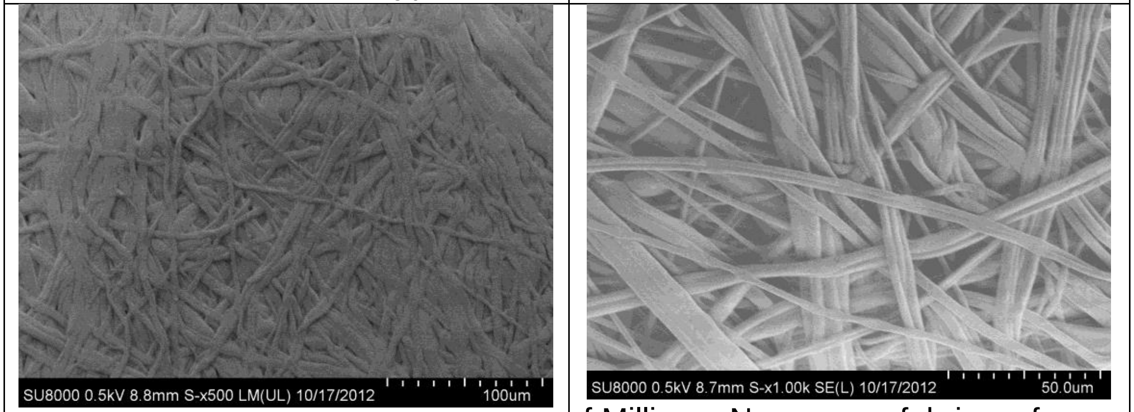

e.Millipore Non-woven fabric surface of membrane $PP_{0.6}$

f.Millipore Non-woven fabric surface of membrane $PP_{5.0}$

Figure 4.34 SEM images of different membrane surface.

These eight membranes with various nominal pore sizes were each studied using a retentate flow rate of 120 mL/min, an N_2 sweep gas rate of 500 sccm, and a temperature of 80 deg C. The results in Table 4-6 show that for these membranes, CO_2 flux showed no significant change from 0.1 µm to 2.5 µm (Figure 4.35). For pore size of 5.0 um and 10.0 um, the CO_2 flux increased dramatically but the liquid flux increased even more, which caused significant loss of selectivity. Membrane $PP_{0.45}$ and $PP_{0.6}$ exhibited significantly better selectivity performance that the rest of the membranes (Figure 4.36). Especially, the $PP_{0.6}$ membrane allowed substantial CO_2 flux and the volume of the permeated liquid and vapors condensate was one magnitude lower than other membranes.

Table 4-6 Flux and selectivity for membranes with different pore size

Nominal pore size (um)	CO_2 flux ($cm^3/(cm^2.s)$)	Liquid flux ($cm^3/(cm^2.s)$)	Selectivity
0.1	0.47±0.06	2.19×10^{-4}	2152
0.22	0.94±0.17	4.25×10^{-4}	2207
0.45	1.02±0.21	2.30×10^{-4}	4420
0.6	0.94±0.18	4.61×10^{-5}	20431
1.2	0.59±0.04	7.30×10^{-4}	802
2.5	0.69±0.45	4.93×10^{-4}	1398
5.0	2.09±0.66	3.44×10^{-3}	608
10.0	6.04±1.43	1.04×10^{-2}	584

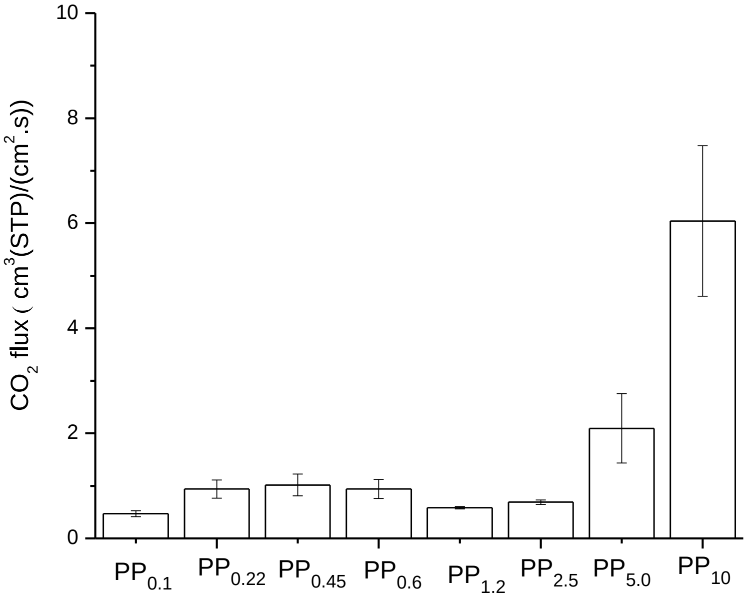

Figure 4.35 CO_2 flux of membranes with different pore size

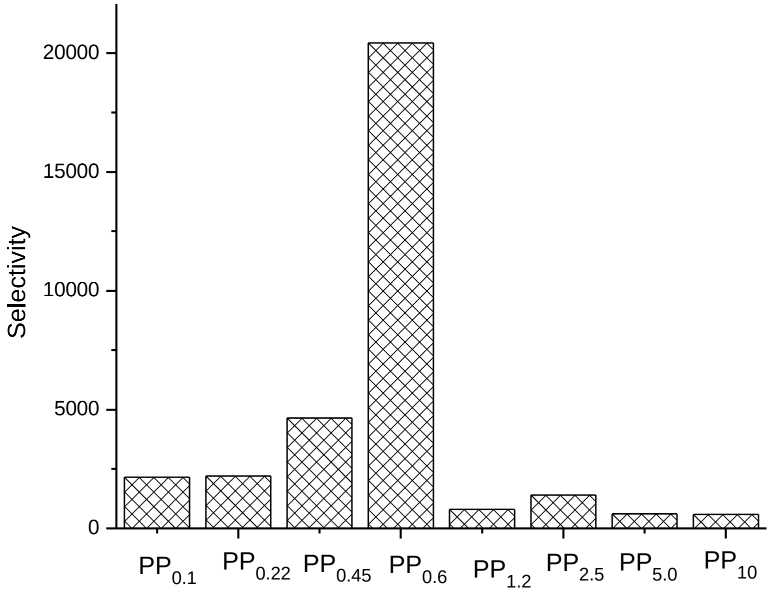

Figure 4.36 Selectivity of membranes with different pore size

Temperatures at the feed side membrane surface, the temperature at permeate side membrane surface, the bulk sweep gas and the TPC are listed in Table 4-7 and TPC was plotted in Figure 4.37. There is no significant difference or apparent trend of TPC as a function of the pore size change. The lower TPC of $PP_{0.6}$ was probably due to the excellent hydrophobicity of this membrane, allowing significantly lower liquid flux through the membrane, thus lowered the bulk permeate temperature and consequently lowed the TPC value.

Table 4-7 Temperature readings and TPC

Nominal pore size (um)	T_{mf} (°C)	T_f (°C)	T_p (°C)	T_{mp} (°C)	TPC
0.1	77.7	81.1	52.5	64.9	0.448
0.22	77.6	81.0	52.9	65.6	0.427
0.45	77.4	81.0	52.3	65.1	0.429
0.6	76.8	80.3	41.8	62.8	0.364
1.2	77.5	81.2	50.6	64.0	0.441
2.5	77.8	81.4	48.7	62.9	0.456
5.0	76.9	79.6	56.9	66.1	0.476
10.0	76.9	80.5	55.0	64.4	0.490

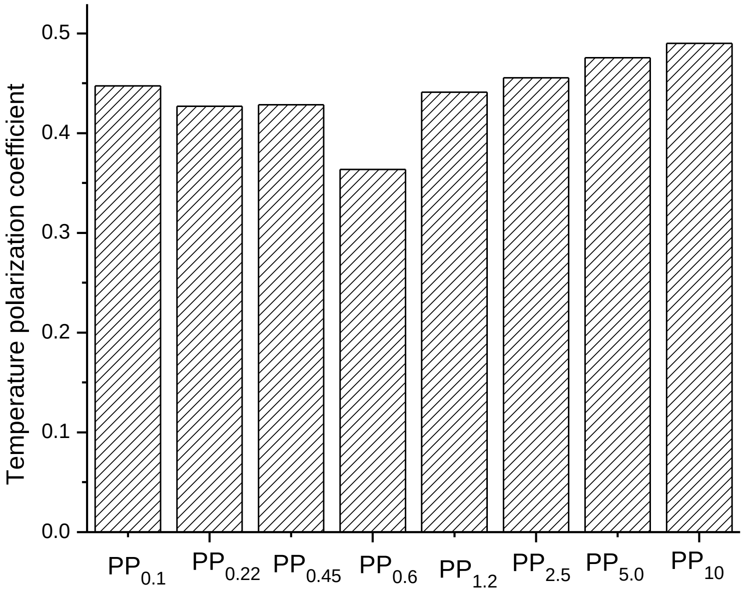

Figure 4.37 TPC of different membranes with different pore size

The membranes were weighed before the experiment and immediately after use. They were then weighed and heated to 105 °C by a moisture analyzer (Table 4-9). Mass comparison was plotted in Figure 4.38. It showed that $PP_{0.1}$, $PP_{0.22}$, $PP_{0.45}$, $PP_{0.6}$ showed excellent hydrophobicity and stayed almost non-wetted. $PP_{1.2}$ and $PP_{2.5}$ became partially wetted in the run. $PP_{5.0}$ and $PP_{10.0}$ were severely wetted. The results again may be attributed to the liquid partial pressure exceeding the breakthrough pressure of the $PP_{5.0}$ and $PP_{10.0}$ membranes. Under the conditions of the same membrane material, liquid solvent, and the same operating parameters, the minimum pressure for the liquid to overcome the hydrophobic force of the membrane and penetrate the pores is inversely proportional to the largest membrane pore size as shown Eqn. 15. The breakthrough pressure values of membranes with different pore size were estimated from this equation and are listed in Table 4-8. Geometric factor B was chosen as 1 (based on literature values) for all membranes; the liquid-solid contact angle θ was estimated to be 105º, a typical value for polypropylene (Erbil, Demirel, Avci, & Mert, 2003); the liquid surface tension γ_L was 73 mN/m from literature (Fu, Xu, Wang, & Chen, 2012); nominal pore size was used as the r_{max} to estimate the breakthrough pressure. Similar results were reported that the breakthrough pressure would be 200-400 kPa (29- 58 psi) for 0.2 µm pore size PTFE membranes and 100 kPa (14.5 psi) for 0.45 µm pore size PTFE membranes (Garcia-Payo et al., 2000) .

Table 4-8 The breakthrough pressure versus membrane pore size

Nominal pore size (µm)	ΔP (Pa)	ΔP (psi)
0.1	35.2×10^4	51
0.22	16.0×10^4	23
0.45	7.8×10^4	11
0.6	5.9×10^4	9
1.2	2.9×10^4	4
2.5	1.4×10^4	2
5.0	0.7×10^4	1
10.0	0.35×10^4	0.5

Table 4-9 The original membrane mass, mass as used and after dried

Nominal pore size (um)	Original mass (g)	Mass as used (g)	Mass after dried (g)	Mass as used (%)	Mass after drying (%)
0.1	0.041	0.040	0.040	97.56	97.56
0.22	0.049	0.050	0.045	102.67	92.40
0.45	0.043	0.045	0.045	104.65	104.65
0.6	0.143	0.150	0.145	104.90	101.40
1.2	0.143	0.155	0.135	108.39	94.41
2.5	0.145	0.160	0.140	110.35	96.55
5.0	0.100	0.140	0.095	140.00	95.00
10.0	0.090	0.180	0.085	200.00	94.44

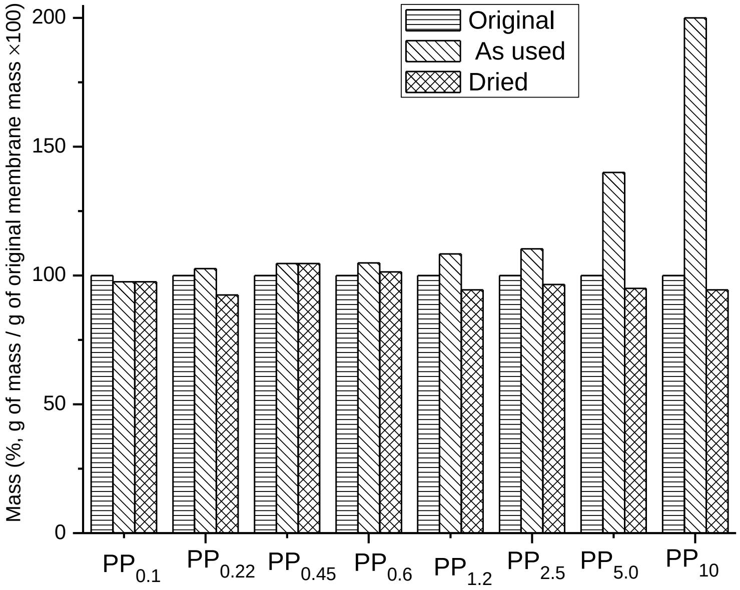

Figure 4.38 Mass comparisons of membranes with different pore size

The membrane mass transfer coefficient (k_M), gas phase mass transfer coefficient (k_G), and liquid phase mass transfer coefficient (k_L) and overall mass transfer coefficient (K_{OL}) were calculated using the theoretical mass transfer model discussed in the appendix for the experimental conditions used above. The results are summarized in Table 3-10.

Table 4-10 Summary of mass transfer coefficients for membranes with different pore size.

Membrane	k_L ($m \cdot s^{-1}$)	k_M ($m \cdot s^{-1}$)	k_G ($m \cdot s^{-1}$)	K_{OL} ($m \cdot s^{-1}$)
$PP_{0.1}$	1.04×10^{-4}	17.8×10^{-3}	2.70×10^{-3}	1.48×10^{-4}
$PP_{0.22}$	1.04×10^{-4}	23.1×10^{-3}	2.70×10^{-3}	1.48×10^{-4}
$PP_{0.45}$	1.04×10^{-4}	34.4×10^{-3}	2.70×10^{-3}	1.49×10^{-4}
$PP_{0.6}$	1.04×10^{-4}	4.04×10^{-3}	2.70×10^{-3}	1.44×10^{-4}
$PP_{1.2}$	1.04×10^{-4}	4.72×10^{-3}	2.70×10^{-3}	1.44×10^{-4}
$PP_{2.5}$	1.04×10^{-4}	4.85×10^{-3}	2.70×10^{-3}	1.45×10^{-4}
$PP_{5.0}$	1.04×10^{-4}	10.1×10^{-3}	2.70×10^{-3}	1.47×10^{-4}
$PP_{10.0}$	1.04×10^{-4}	21.6×10^{-3}	2.70×10^{-3}	1.48×10^{-4}

The data in Table 4-10 were within the range of published values found in the literature. For example, Hoff (Hoff, 2003) reported the membrane mass transfer coefficient (k_M) value of PTFE hollow fiber membrane module with pore size 1-10 µm used in his study for CO_2 capture at 40 °C is 0.03 m/s. Khaisri et al.(Khaisri et al., 2011) reported the mass transfer coefficient analysis results for desorption membrane contactors as: The liquid layer mass transfer coefficient of 1.90×10^{-4} m/s; the membrane mass transfer coefficient of 4.97×10^{-4} m/s; the gas mass transfer coefficient 1.83×10^{-3} m/s to 3.21×10^{-3} m/s due to varying gas velocity; and the overall mass transfer coefficient of 1.84×10^{-4} m/s were reported. Simioni et. al. reported overall mass transfer coefficient range of 1.0×10^{-4} m/s to 2.5×10^{-4} m/s for a temperature range of 60 °C to 100°C using PTFE and other proprietary membranes stripping 30 wt% potassium carbonate. The value of 1.6×10^{-4} m/s was read from the plot for both membranes operating at 80 °C (Simioni, Kentish, & Stevens, 2011), which was comparable to our value regardless of the different solvent, membrane type, operating conditions and slightly different mass transfer calculation method.

Contribution of individual mass transfer resistance to overall resistance of membranes with different pore sizes are listed in Table 4-11 and plotted in Figure 4.39. The majority of mass transfer resistance occurs in the liquid phase layer. It accounted for 90-93% of the overall resistance, which is consistent with our previous mass transfer mechanism study results. Similar results were found in the literature. Khaisri et al. (Khaisri et al., 2009) reported the liquid phase mass transfer resistance was roughly 90% of the overall resistance. This result also agreed with many membrane gas absorption studies for membrane contactors (deMontigny, Tontiwachwuthikul, & Chakma, 2006; Khaisri et al., 2011). Hoff (Hoff, 2003) explained that the diffusivity of CO_2 was approximately 1.8×10^{-5} m^2/s in N_2 gas and 1.3×10^{-9} m^2/s in the liquid (30 wt% aqueous

MEA), which indicated the mass transfer would then be limited by molecular diffusion through a liquid layer with diffusivities 10000 times lower than in the gas. The gas resistance contribution was calculated to be roughly 5-6% of the overall resistance, which was also in agreement of the reported value of roughly 5-10% resistance from the contactor (deMontigny et al., 2006; Khaisri et al., 2011). Our previous parametric study also confirmed that gas velocity was not a significant factor for this process. Membrane resistance contribution was found to be from 0.5% to 4%. Scrutinizing the values, the $PP_{0.1}$, $PP_{0.22}$, and $PP_{0.45}$ (GE) membranes accounted for very little resistance, much smaller than the rest membranes acquired from Millipore. The differences were due to different pore size, porosity and tortuosity values.

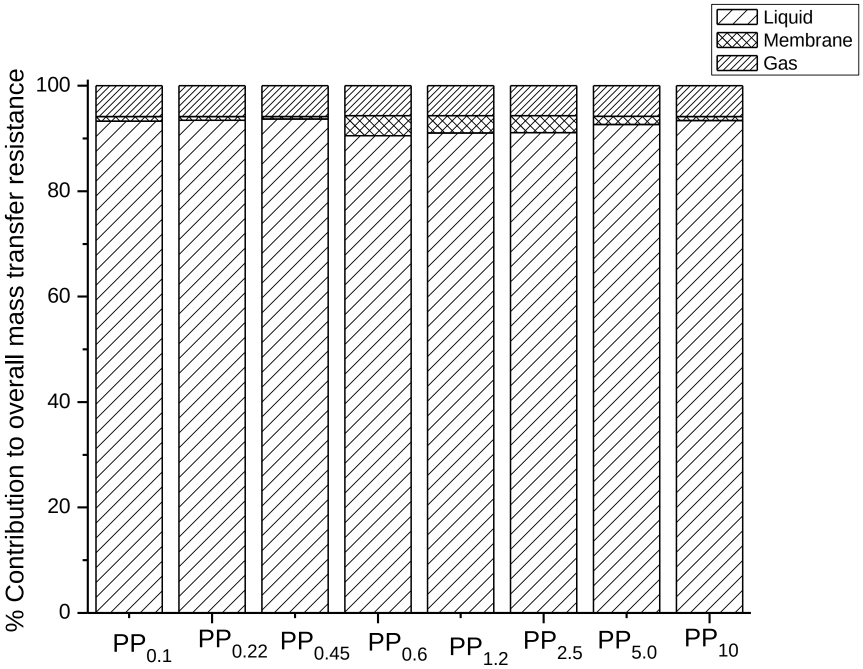

Figure 4.39 Percentage comparison of individual mass transfer resistance to overall resistance for membranes with different pore size

Table 4-11 Summary of percentage of individual resistance to overall resistance for membranes with different pore size.

Membrane	k_L (%)	k_M (%)	k_G (%)
$PP_{0.1}$	93.3	0.9	5.8
$PP_{0.22}$	93.5	0.7	5.8
$PP_{0.45}$	93.7	0.5	5.9
$PP_{0.6}$	90.6	3.8	5.7
$PP_{1.2}$	91.1	3.3	5.7
$PP_{2.5}$	91.1	3.2	5.7
$PP_{5.0}$	92.7	1.5	5.8
$PP_{10.0}$	93.4	0.7	5.8

4.2 Physical Solvents

4.2.1 Commercial membrane screening

Due to the high operating pressure (i.e., consistent with pre-combustion separation of CO2 from syngas) of physical solvent systems, composite polymeric membranes with a dense selective layer on top are assumed to be implemented. Two different types of materials for the dense selective layer were chosen to study their capacity to remove CO_2 from the pre-saturated solvent: (a) PERVAP 1201 and PERVAP 1211 which have poly vinyl alcohol (PVOH)-based selective layer and (b) PERVAP 4060 and PERVATECH which have poly dimethyl siloxane (PDMS)-based selective layer. The structures of these two polymers are given in Figure 4.40.

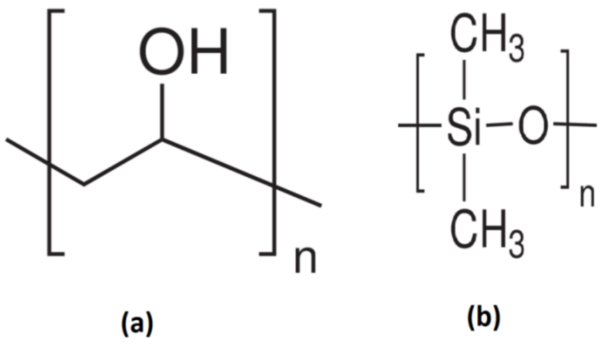

Figure 4.40 (a) PVOH and (b) PDMS structures.

PDMS is an elastomer with the glass transition temperature of -123 ^oC (Mulder, 1991). PDMS is known to have a high permeability for CO_2. The permeability of CO_2 in different polymeric membranes is shown in Table 4.12. It is clear that except for Poly [1-trimethylsilyl-1-propyne] (PTMSP), all other polymeric membranes have significantly lower permeabilities than PDMS for CO_2 (Wankat, 2006; Brunetti et.al, 2010).

Table 4.12. CO_2 permeability in different polymeric membranes (Wankat, 2006).

Membrane	Permeability cm^3 (STP).cm/[cm^2.s.cm Hg]
PTMSP	28,000
PDMS	4550,3240
Natural rubber	99.6, 153, 131
Silicone rubber	2700
Polystyrene	10.0, 12.4, 23.3
Polycarbonate	8.0
Butyl rubber	5.2,5.18
Nylon 6	0.16
Nylon 66	0.17
Poly(4-methyl pentene)	93
Cellulose acetate	7.75

The polymeric membranes used in this work consist of a very thin separation layer (e.g. PDMS or PVOH), a porous support (e.g. polyacrylonitrile) and a mechanical support (e.g. polyester). The schematic of the composite membranes used in this work is shown in Figure 4.41.

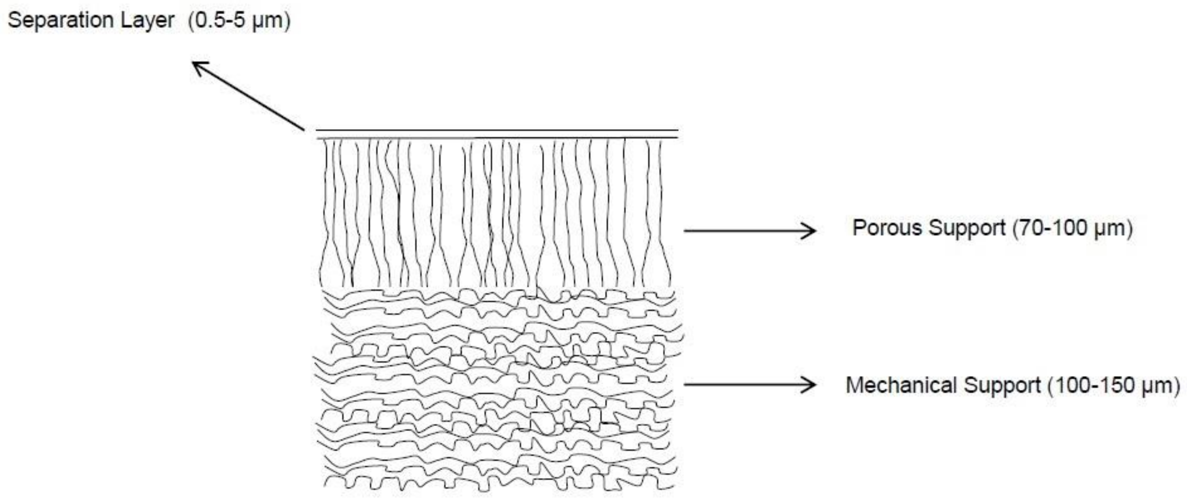

Figure 4.41. Structure of the composite membranes used in this work.

The candidate membranes were each tested in the permeation setup at 400 psig on the feed side and atmospheric pressure on the permeate side. The solvent flow rate was adjusted to 100 (mL/min) and the sweep gas flow rate was 500 (sccm). Absorber temperature was controlled at 17±1 ^{o}C. The permeation properties of the membranes were calculated and shown in Table 4.13.

Table 4.13. Physical solvent regeneration screening study results.

Membrane	PERVAP 4060 (SULZER)	PERVAP 1201 (SULZER)	PERVAP 1211 (SULZER)	PERVATECH
Thickness (mm) as supplied	0.24	0.19	0.19	0.19
Average CO_2 concentration in sweep gas (ppm)	167000 (From GC)	910	952	36475 (From GC)
CO_2 Flux (cm^{3}STP (CO_2)(cm^2)$^{-1}$.S^{-1}	0.14	0.79×10-3	8.26×10-4	32.00×10-3
Solvent Flux (cm^3)(cm^2)$^{-1}$.S^{-1}	3.88×10-5	0	1.80×10-6	9.87×10-5
Selectivity	3608.25	Perm-selective	456.74	320
Percent Recovery	0.79	4.14×10-3	4.69×10-3	0.17

Results of the screening study, along with the CO_2 profiles in the sweep gas, suggest the following preliminary conclusions:

- CO_2 profile in the sweep gas reaches its steady state condition two hours after the absorber pressurization.
- PDMS-based membranes (PERVATECH and PERVAP 4060) show higher CO_2 permeability compared to PVOH based membranes (PERVAP 1211 and PERVAP 1201).
- PEVAP 4060 was chosen as the candidate membrane for further analysis and design of engineering experiments to find the optimum operational conditions due to its high CO_2 flux and selectivity compared to the other membranes.

The term “perm-selective” in Table 4.13 does not necessarily indicate that the membrane is absolutely impermeable to the solvent and only CO_2 can diffuse across the membrane. Rather, it implies no measurable amount of solvent has been collected by the sweep gas filter.

4.2.2 Parametric study

4.2.2.1 Effect of regeneration temperature

As mentioned earlier, unlike chemical solvents, physical solvents do not react with the solute, but rather physically dissolve the acid gases. Consequently, CO_2 absorption/desorption for a physical solvent process is mainly dominated by the pressure of the process. To validate this assumption and to investigate the effect of temperature, solvent stream temperature was raised and the concentration of CO_2 in the sweep gas was measured. CO_2 concentration in the sweep gas for PERVAP 1211 (PVOH based) and PERVAP 4060 (PDMS based) at different temperatures is shown in Figure 4.42. The experiments started at room temperature and then temperature was increased by 20 ^oC for consecutive 2 hours periods. As shown in Figure 4.42, increasing the solvent temperature upstream of the membrane module did not affect the amount of CO_2 liberation. The results of this experiment indicate that increasing the temperature at a constant pressure did not alter the permeation properties of the membranes studied in this work. For both membranes, sweep gas flow rate was set to 500sccm and pressure was constant at 400 psi. For PERVAP 4060 membrane, CO_2 concentration in the sweep gas was measured using the Agilent 7850A GC (CO_2 concentration > 20000 ppm) and for PERVAP 1211, CO_2 concentration was measured using LI-COR 820 Non-Dispersive Infrared CO_2 analyzer (CO_2 concentration < 20000ppm).

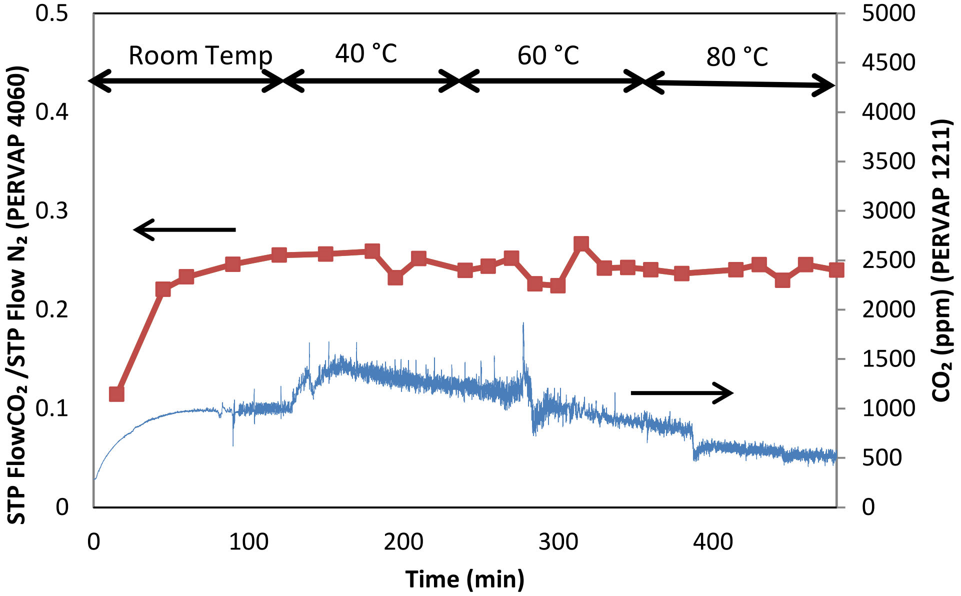

Figure 4.42. Effect of temperature on the rate of CO_2 permeation.

4.2.2.2 Effect of sweep gas flow rate

The primary objective of using the sweep gas is to sweep away the permeated CO_2 and thus maintaining the driving force for CO_2 permeation across the membrane at its maximum possible level. However, considering the size of the membrane chamber and the small amount of CO_2 permeation due to the small membrane area (9.6 cm^2), it was expected that changing the sweep gas flow rate will not affect the CO_2 permeation. To test this hypothesis, PERVAP 4060 membrane was used at two different sweep gas flow rates of 500 and 1000 sccm and CO_2 concentration in the sweep gas was measured using the GC. The profiles of CO_2 permeation rate for the two different sweep gas flow rates are shown in Figure 4.43. Table 4.14 tabulates the calculated flux and solvent rate at average steady-state conditions. It appears that changing the sweep gas flow rate has no significant effect on the rate of CO_2 permeation within the range of the experimental conditions in this study.

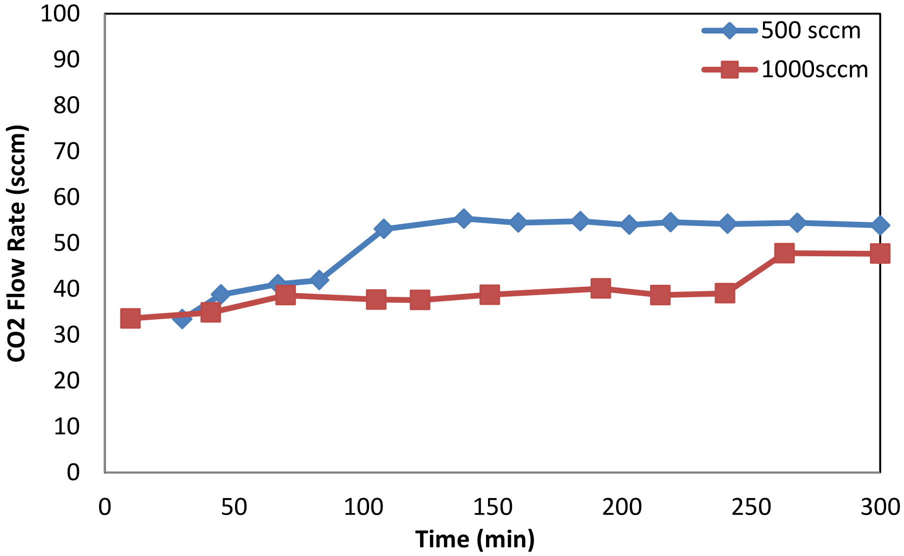

Figure 4.43. CO_2 Permeation rate for two different sweep gas flow rates.

Table 4.14. Effect of Sweep Gas Flow Rate on CO_2 Permeation Rate

Sweep Gas Flow Rate(sccm)	CO_2 Flux ($cm^3STP\ CO_2/cm^2.S$)	Avg Solvent Leak ($mL/cm^2.S$)	% Recovery
500	0.087	3.18×10^{-5}	0.582
1000	0.069	3.47×10^{-5}	0.847

4.2.2.3 Factorial DOE runs

To better understand the effect of system pressure and solvent flow rate on responses such as CO_2 Flux, selectivity and % recovery, a two-factor two-level full factorial design with two replicates and three center points was performed on the PERVAP4060 membrane, which appeared to be the most promising membrane in the screening study. These experiments were conducted at room temperature with a sweep gas rate of 500 sccm. The sweep gas is at atmospheric pressure, so the pressure drop is approximately equal to, and varied along with, the solvent pressure. The summary of the experimental conditions along with the responses are provided in Table 4.15.

Table 4.15. Design of experiment, operating conditions and permeation results.

Solvent Pressure (psi)	Solvent Flow rate (mL)	CO_2 Flux ($cm^3STP\ CO_2/cm^2.s$)	Avg Solvent Leak ($mL/cm^2.sec$)	Selectivity	%Recovery
300	160	0.097	4.10×10^{-5}	2365	0.60
300	80	0.087	3.18×10^{-5}	2741	1.08

600	160	0.442	1.77×10^{-4}	2497	0.9
600	80	0.367	1.67×10^{-4}	2197	1.50
450	120	0.205	4.58×10^{-5}	4470	0.97
300	160	0.095	4.70×10^{-5}	2020	0.59
600	80	0.464	1.93×10^{-4}	2405	1.90
450	120	0.250	9.16×10^{-4}	2733	1.19
450	120	0.356	7.11×10^{-5}	5005	1.69
300	80	0.069	3.47×10^{-5}	1976	0.85
600	160	0.439	2.11×10^{-4}	2080	0.90

A statistical analysis was performed to identify the significant factors for each individual response. To achieve this purpose, the last four columns of Table 4.14 along with the corresponding experimental conditions were imported to Minitab 15 statistical software. The Pareto charts and main effect plots for different responses of each experiment including: (a) CO_2 flux, (b) average solvent leak, (c) selectivity, and (d) % recovery are shown in Figure 4.44 through Figure 4.47, respectively. The vertical red line at a value of 2.447 indicates the critical value from the Student's t distribution for 6 degrees of freedom. Effects above this value are considered to be statistically significant at a confidence level of 95%. Analysis of the Pareto charts in Figure 4.44 clearly indicates the significance of pressure. With respect to CO_2 flux, pressure appears to be strongly significant. As pressure inside the absorber increases, solubility of CO_2 in the solvent stream enhances. Higher pressure difference across the membrane, signifies a higher driving force and thus higher CO_2 flux should be expected. The main effects plot in Figure 4.44 confirms the aforementioned hypothesis. However, solvent flow rate has no significant effect on the CO_2 flux. The immediate conclusion from this observation is that the mass transfer is primarily controlled by the membrane. Increasing the solvent flow rate causes more turbulence inside the membrane chamber, which, in turn, increases the rate of CO_2 diffusion into the boundary layer, adjacent to the membrane surface. However, since the dominant mass transfer resistance exists in the membrane, the rate of CO_2 permeation does not change significantly.

Considering the solvent leak as the response of the experiments, the Pareto chart in Figure 4.45 indicates pressure to be significant. However, solvent flow rate has no effect on the rate of solvent leak through the membrane. As the pressure of the system increases, the liquid on the upper chamber of the membrane module forces itself into the membrane and hence, the solvent leak rate increases. However, increasing the solvent flow rate leads to higher liquid velocity on top of the membrane and no significant changes of the rate of solvent leak occurs.

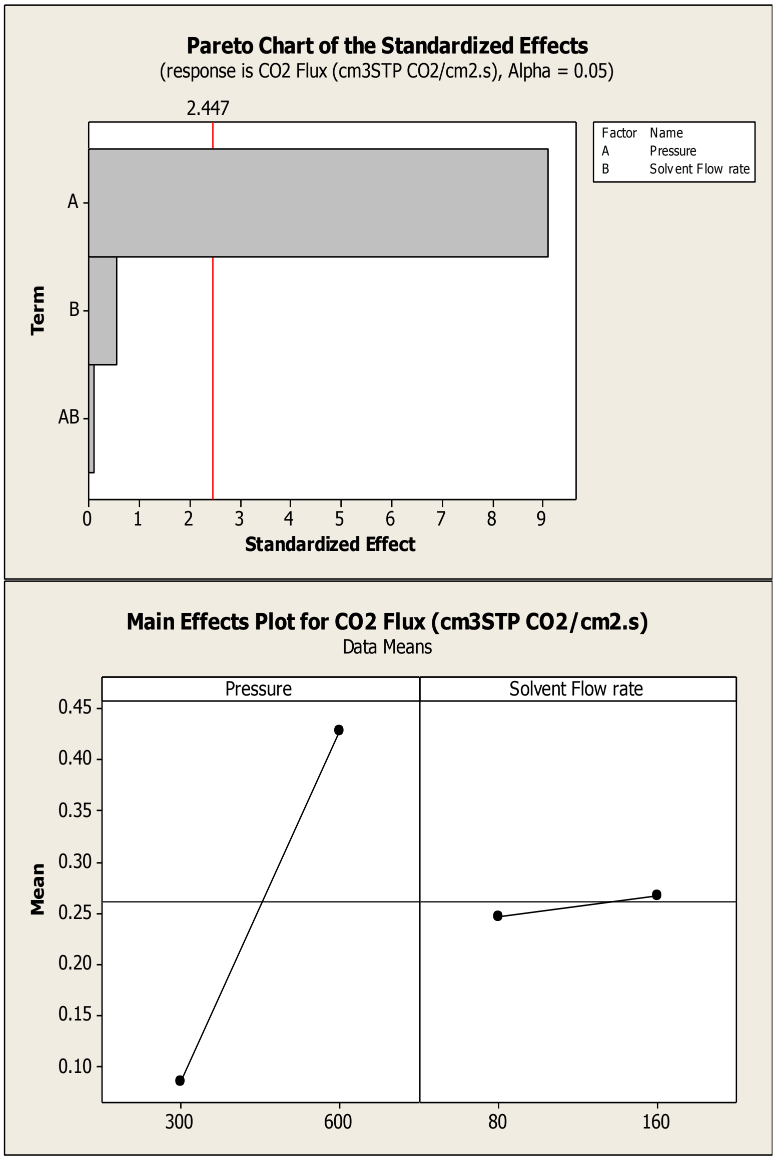

Figure 4.44. Pareto and main effects plots for CO_2 flux.

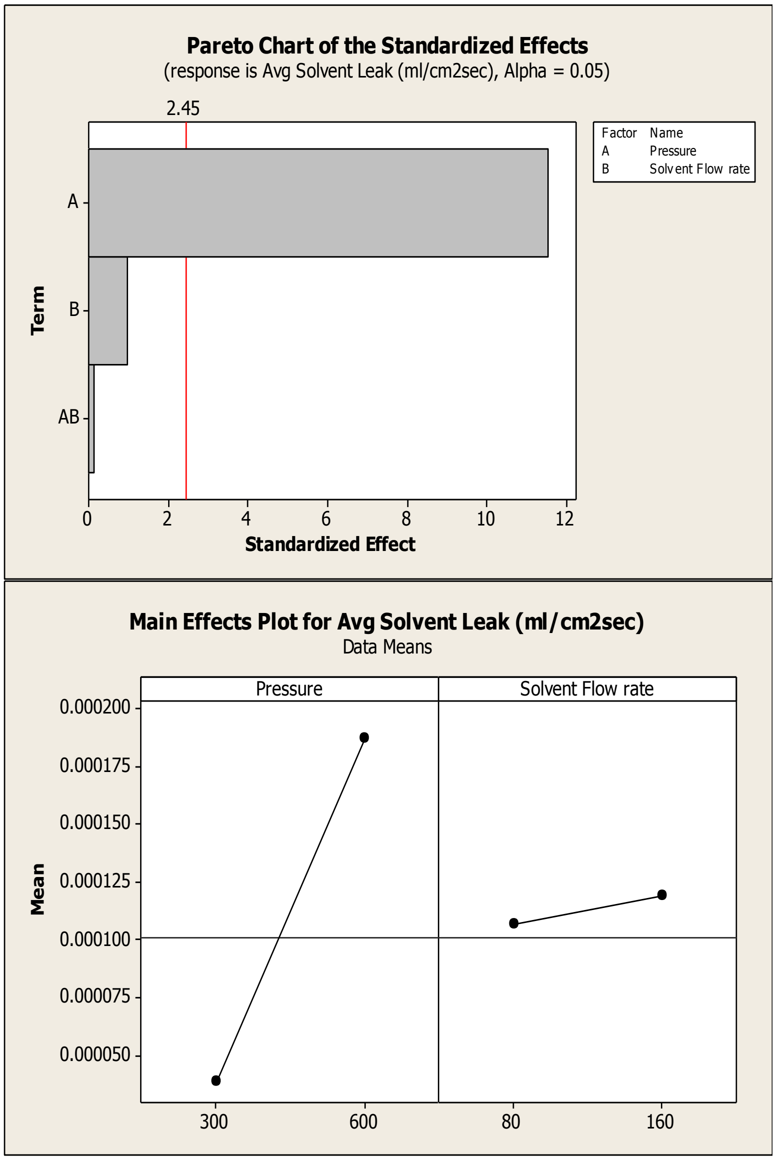

Figure 4.45. Pareto and main effects plots for solvent leak.

Neither the pressure of the system nor the solvent flow rate was found to have a significant effect on the selectivity. (Figure 4.46).

Finally, regarding the percent recovery of the solvent, both the system pressure and solvent flow rate appeared to be significant. At elevated pressures, the mole fraction of CO_2 in the solvent increases and thus a higher driving force for CO_2 permeation exists. As a result of this, percent of recovery increases with pressure as shown by the main effects plot in Figure 4.47. On the other hand, by increasing the solvent flow rate, more CO_2 is introduced to the membrane module. However, the mass transfer resistance through the membrane prevents more CO_2 from being transported. Thus, introducing more CO_2 to the upper chamber and yet a slow mass transport process, being controlled by the membrane, eventually decreases the percent recovery.

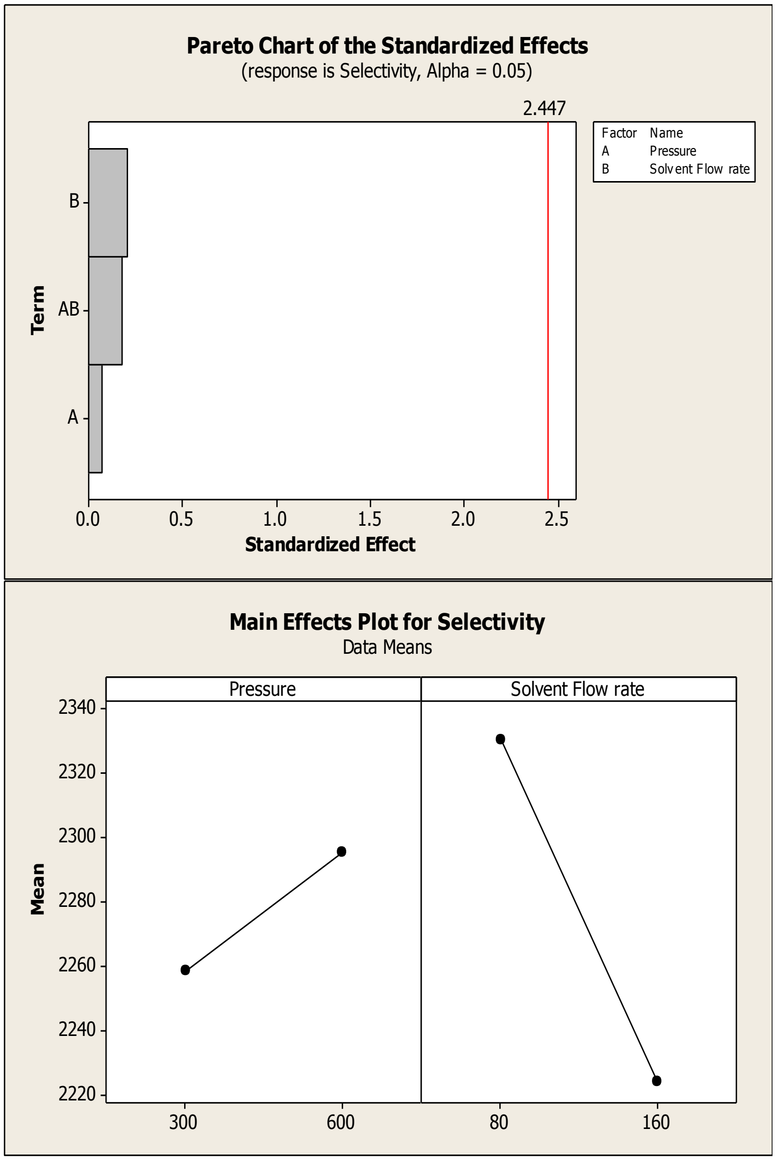

Figure 4.46. Pareto and main effects plots for selectivity.

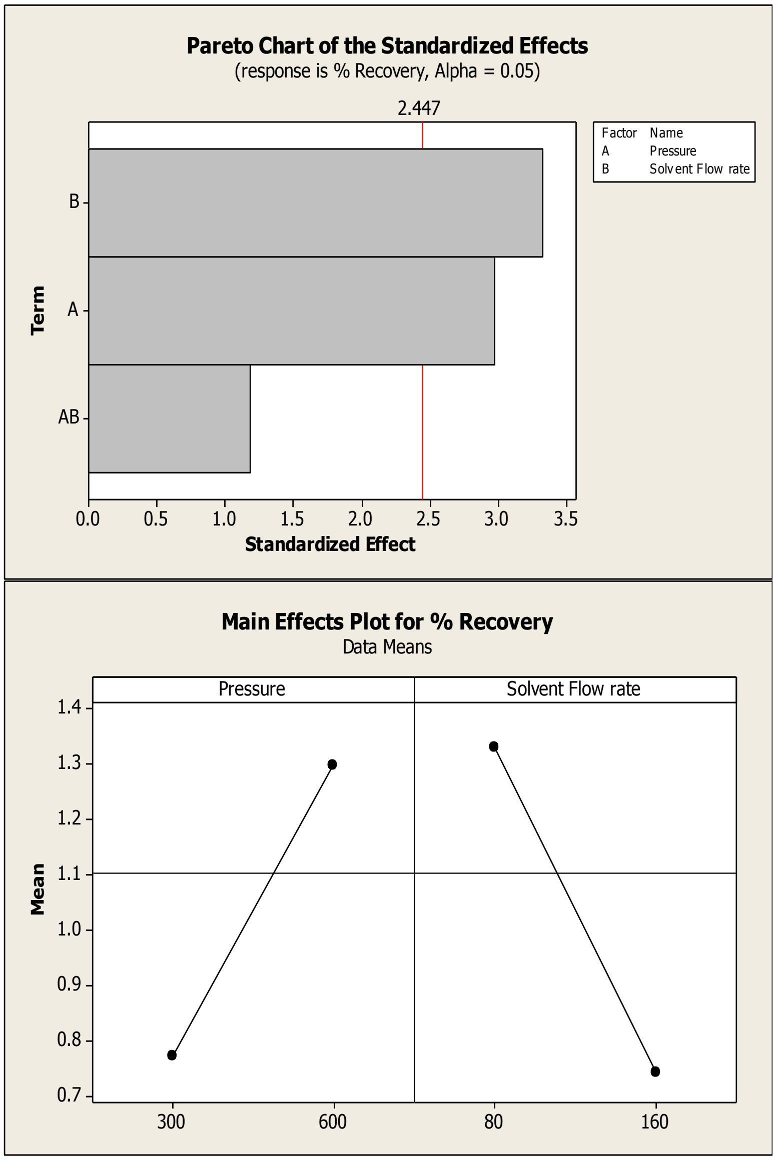

Figure 4.47. Pareto and main effects plots for percent recovery.

4.2.3 Sorption experiment

In order to understand the level of solubility of Selexol in each of the membranes, a series of sorption experiments were conducted. The physical properties of the membranes before the sorption experiment are summarized in Table 4.16.

Table 4.16. Physical properties of the membrane before the sorption experiment.

Membrane	Mass (g)	Thickness (cm)	Volume (cm^3)	Density (g/cm^3)
PERVAP 1201	0.21440	0.020	0.346813	0.62
PERVAP 1211	0.19896	0.018	0.312132	0.64
PERVAP 4060	0.20419	0.021	0.364154	0.56
PERVATECH	0.21845	0.023	0.398835	0.55

Each of the membranes was soaked in Selexol until saturated. They were then removed from the solvent, wiped off, and weighed.

From the initial and final mass, the solubility coefficient for each membrane was calculated (Table 4.17). The high solubility of Selexol in the PERVATECH membrane likely explains the highest rate of solvent flux in Table 4.13.

Table 4.17. Solubility coefficient of composite membranes.

Membrane	Solubility coefficient (S)
PERVAP 1201	0.073
PERVAP 1211	0.050
PERVAP 4060	0.061
PERVATECH	0.37

4.2.4 Post-experiment characterization tests

4.2.4.1 FTIR results

FTIR results for the membranes used in this work are shown in Figure 4.48. For each type of membrane, FTIR was performed for both the original and post-experiment membranes. Comparison of the spectra of the original and post experiment membranes revealed no major differences, with the possible exception of residual Selexol. For reference, a spectrum obtained from the solvent sample is shown in Figure 4.49. It appears that the minor differences in the samples observed at approximately 3000 cm^{-1} could be attributed to the solvent present in the membrane. In general, it seems that there were no significant chemical changes during the course of the approximately 8 hour experiments. However, it is probable that longer contact times may cause chemical degradation of the membrane materials.

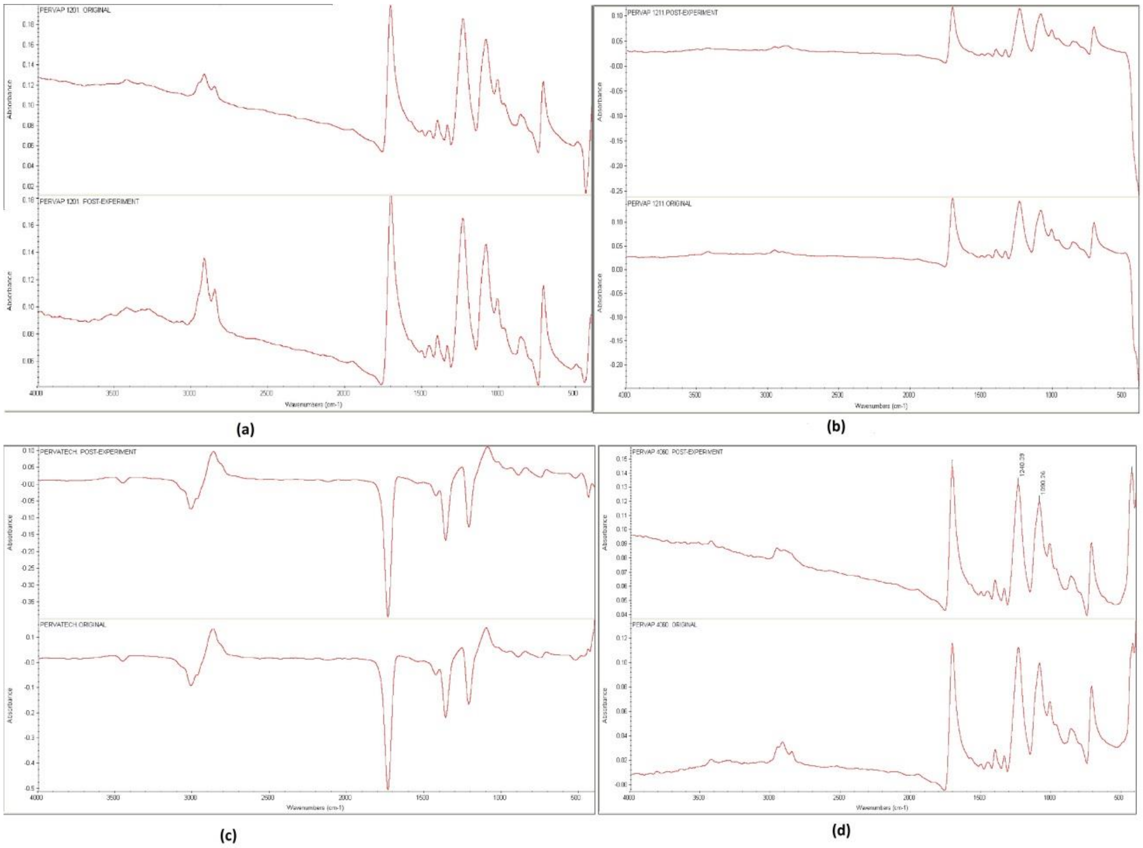

Figure 4.48. FTIR spectra for different membranes: (a) SULZER 1201 (b) SULZER 1211 (c) PERVATECH (d) PERVAP 4060 (For each graph, the upper section shows the post-experiment membrane and lower section shows the original membrane. The x-axis ranges from 4000 down to 500 wavenumbers).

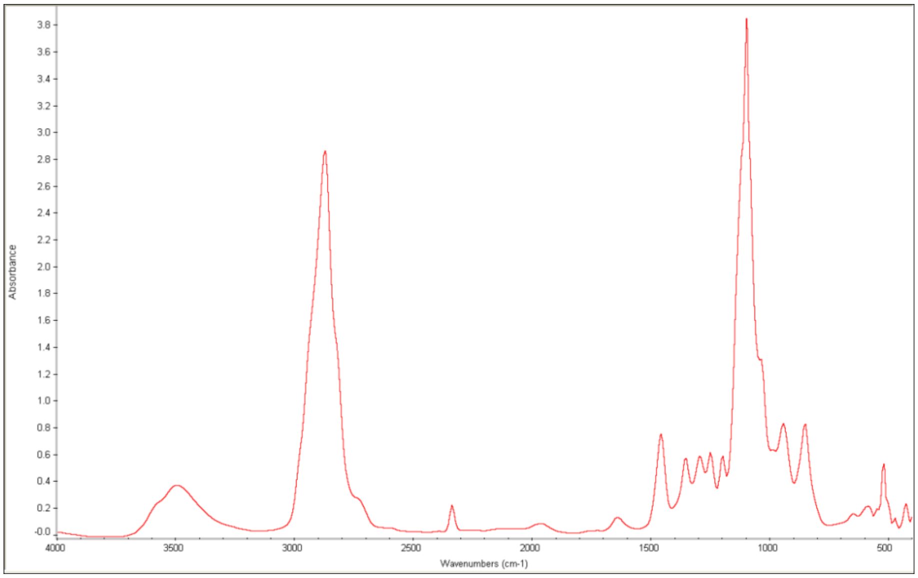

Figure 4.49. FTIR spectrum for the solvent sample.

4.2.4.2 DSC results

Results of the DSC measurements are shown in Figures Figure 4.50 through Figure 4.53. Except for the peaks at the lower temperatures of -80 ^{o}C for the post experiment membranes, no significant structural changes are detectable. The aforementioned peaks could be attributed to residual solvent in the membrane.

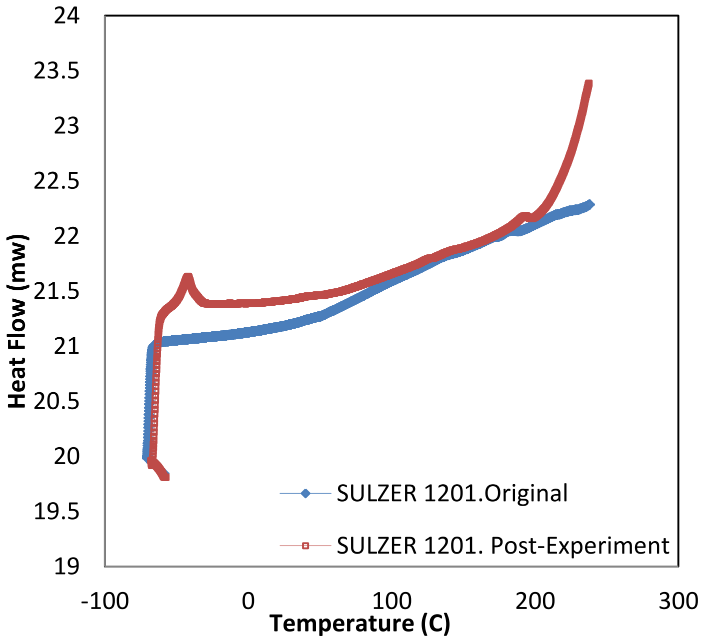

Figure 4.50 DSC results. PERVAP 1201, SULZER.

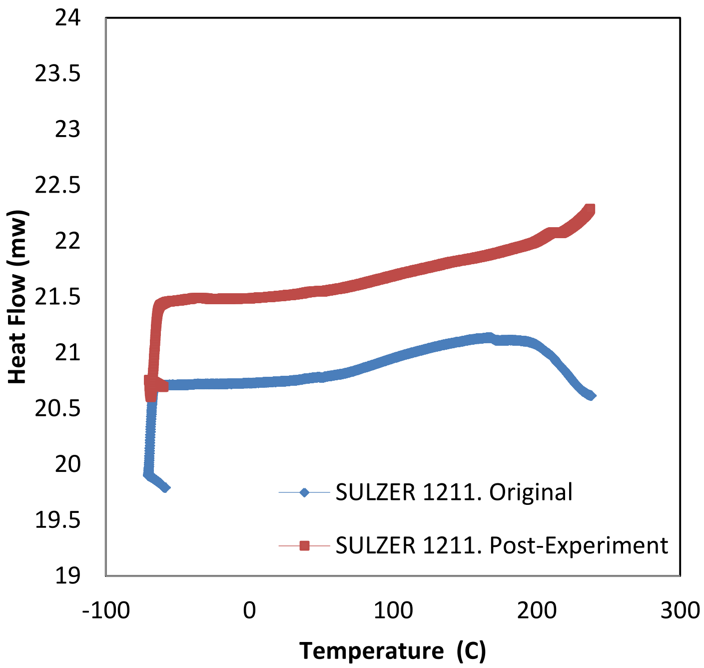

Figure 4.51. DSC results. PERVAP 1211, SULZER.

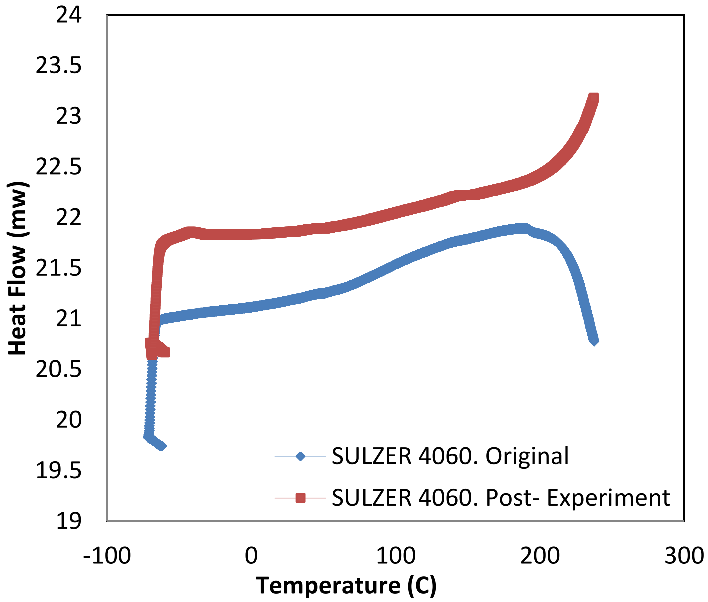

Figure 4.52. DSC results. PERVAP 4060, SULZER.

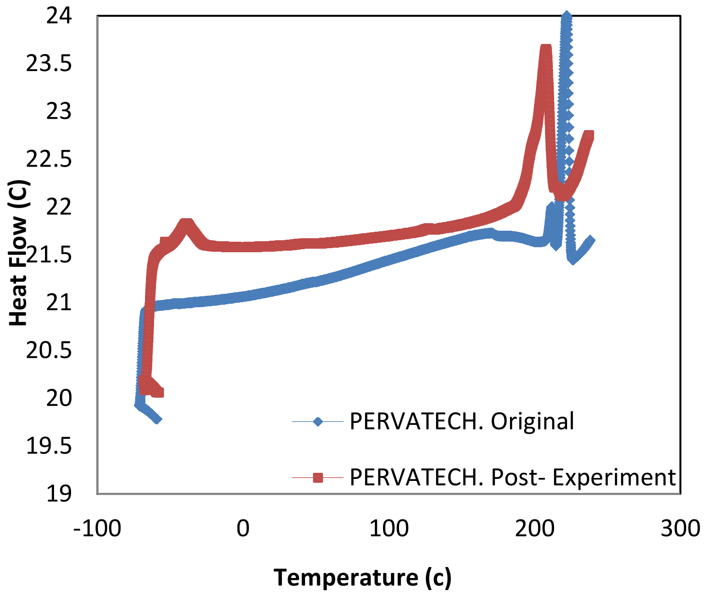

Figure 4.53. DSC results. PERVATECH.

4.2.4.3 SEM results

Top view and cross-section view images of PERVAP 4060 membrane are shown in Figure 4.54 and Figure 4.55 respectively.

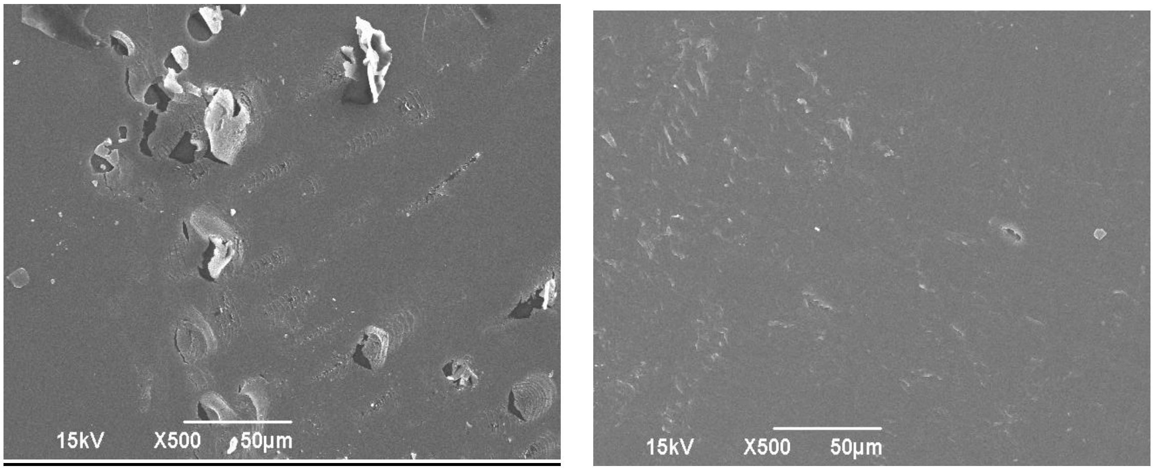

(a) **(b)**

Figure 4.54. PERVAP 4060 top view comparison. (a) Original Membrane (b) Post experiment Membrane.

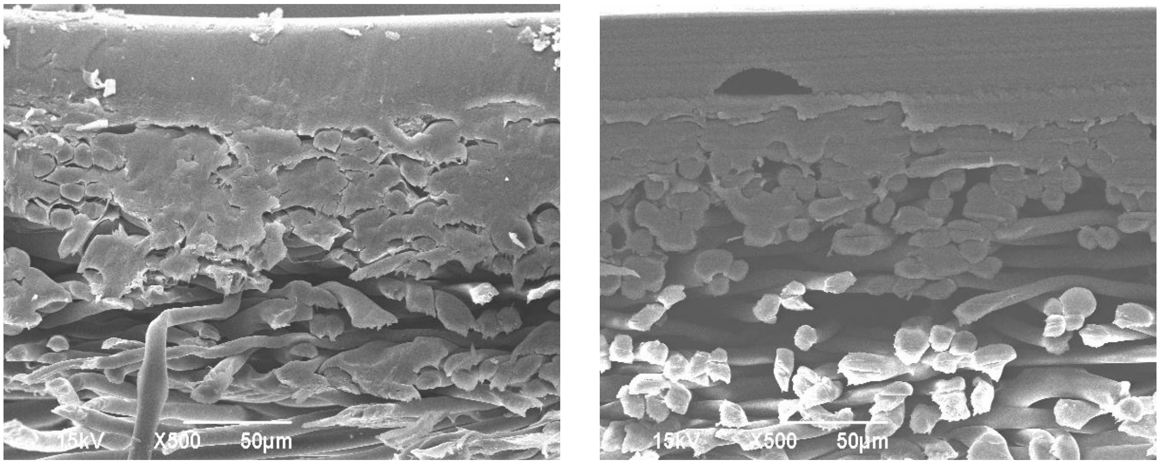

(a) (b)

Figure 4.55. PERVAP 4060 cross-section view comparison. (a) Original Membrane (b) Post experiment Membrane.

Comparison of the SEM images shows no significant changes of the membrane after being exposed to the high pressure solvent stream in the permeation setup. The pores of the membrane in the porous support section of the membrane as well as the top surface of the membrane appear to be essentially the same before and after the permeationexperiment.

5 Conclusions

5.1 Chemical Solvents

Porous membrane contactors were studied as an alternative to conventional strippers for CO_2 recovery from aqueous MEA solutions. An experimental system with a CO_2 absorption unit and regeneration unit based on membrane contactors was designed; constructed and validated. The following are the highlights of our research findings:

- We have verified the ability of our system to absorb CO_2 and recover a portion of that CO_2 using a porous membranes.
- Porous membranes of polypropylene (PP), polytetraflouroethylene (PTFE) were able to strip CO_2 from an MEA solution with high selectivity of CO2 over solvent.
- Cellulose acetate, PVDF, PES and nylon membranes were found to be unsuitable for this application without further modifications.
- In the regeneration loop of the experimental setup, an increase of temperature improved the flux of CO_2 through the membrane and thus improved the recovery of CO_2. However, it also resulted in higher solvent loss. Temperature was confirmed to be a significant factor for this process by both individual parametric study and design of experiment methodology.
- For regeneration, an increase in pressure on the retentate side of the membrane decreased the recovery of CO_2. This was possibly due to an increase in the mass resistance caused by the liquid film in contact with membranes, which was found to be the major resistance of this mass

transfer process.

- The CO_2 flux increased with feed flow rate until a sharp decrease at the flow rate of 300mL/min. This decrease is likely due to the membrane wetting caused by higher liquid pressure.
- Higher flow rates decreased the recovery of CO_2, but not linearly, resulting from a combination of the decreased residence time and improved mass transfer.
- In general, the recovery of CO_2 is relatively low in this system, suggesting that a large membrane surface area will be needed to obtain the high regeneration rate needed for this process to be commercially viable.
- Varying sweep gas rate resulted in no clear trend in the regeneration performance and did not influence the regeneration significantly.
- Laminar flow was found to be the primary flow regime in the membrane module. The laminar boundary layer adds significant mass transfer resistance.
- At regeneration process temperatures of 80 ºC and above, the temperature polarization coefficient measured is around 0.5, which is close the reported value for laminar flow in membrane distillation.
- MEA degradation residues are observed to adsorb into the membrane over time, altering the surface properties, reducing the hydrophobicity of the membrane and slowing down the mass transfer process.
- Membrane module design and configuration are important factors affecting the membrane performance. CO_2 regeneration in this particular module was

found to be very sensitive to the orientation.

- For the pore size study, the PP membrane with pore size 0.6 µm was identified with best selectivity, allowing substantial CO_2 flux and high rejection of liquid flux through the membrane.
- Membranes with pore size smaller than 2.5 µm showed excellent hydrophobicity with no wetting or fouling. Membranes with pore size of 5 µm and 10 µm became wetted during the process.
- The mass transfer coefficients were calculated under the assumption that all the porous membranes are operated in non-wetted mode. The results confirmed the controlling mass transfer resistance comes from the liquid phase boundary layer, accounting for roughly 90%-93% of the overall mass transfer resistance. Membrane mass transfer resistance accounts for roughly 0.5%-4% and gas phase mass transfer resistance has a contribution of 5% to 6%, respectively.

5.2 Physical Solvents

The feasibility of the application of composite polymeric membranes for efficient regeneration of physical solvents was also studied. A bench-scale high pressure permeation setup was built and used to study the capacity of common commercial membranes for separating CO_2 from the pre-saturated solvent. The primary conclusions from this work are as follows:

- During absorption using Selexol solvent, CO_2 mole fraction in the solvent was measured using the sampling module. As the pressure of the system is elevated, the mole fraction of CO_2 in the solvent increased. Additionally, the concentration of CO_2 in the solvent reached a steady state value approximately 2 hours after the absorber pressurization.

- CO_2 profile in the sweep gas of the membrane regeneration contactor reached its steady state condition roughly two hours after the absorber pressurization.
- PDMS-based membranes (PERVATECH and PERVAP 4060) have higher CO_2 permeability compared to PVOH-based membranes (PERVAP 1211 and PERVAP 1201).
- PERVAP 4060 was chosen as the candidate membrane for further analysis and experiments due to its high CO_2 flux and selectivity compared to the other membranes.
- Increasing the solvent temperature upstream of the PERVAP 4060 membrane module, did not enhance the rate of CO_2 permeation.
- Sweep gas flow rate did not significantly affect the rate of CO_2 permeation through the PERVAP 4060 membrane within the range of the experimental conditions in this study.
- Pressure appeared to have a significant effect on CO_2 flux across the PERVAP 4060 membrane. However, solvent flow rate had no significant effect. The primary conclusion based on this observation is that the mass transfer is controlled by the membrane.
- In terms of solvent flux, pressure was found to be significant, but feed flow rate did not have any influence.

- For the PERVAP 4060 membrane, neither the pressure of the system nor the solvent flow rate was found to have an effect on membrane selectivity.
- Both the system pressure and solvent flow rate had a significant effect on the recovery of CO_2.
- The post experiment characterization tests such as FTIR, DSC, and SEM were performed to study the chemical stability and structural integrity of the membranes after being exposed to the high pressure solvent stream in the permeation setup. None of these tests showed any major change of the membrane material or structure after experimental runs of up to ten hours.

6 References

1. Alexander Stern, S. (1994). Polymers for gas separations: The next decade. *Journal of Membrane Science, 94*(1), 1-65.

2. Alklaibi, A., & Lior, N. (2005). Membrane-distillation desalination: Status and potential. *Desalination, 171*(2), 111-131.

3. Alvarez, E., Rendo, R., Sanjurjo, B., Sanchez-Vilas, M., & Navaza, J. M. (1998). Surface tension of binary mixtures of water N-methyldiethanolamine and ternary mixtures of this amine and water with monoethanolamine, diethanolamine, and 2-amino-2-methyl-1-propanol from 25 to 50 C. *Journal of Chemical & Engineering Data, 43*(6), 1027-1029.

4. Baker, R. (2012). *Membrane technology and applications* Wiley.

5. Baker, R. W. (2002). Future directions of membrane gas separation technology. *Industrial & Engineering Chemistry Research, 41*(6), 1393-1411.

6. Basu, R., & Sirkar, K. (1991). Hollow fiber contained liquid membrane separation of citric acid. *AIChE Journal, 37*(3), 383-393.

7. Bessarabov, D. (1999). Membrane gas-separation technology in the petrochemical industry. *Membrane Technology, 1999*(107), 9-13.

8. Bhide, B., Voskericyan, A., & Stern, S. (1998). Hybrid processes for the removal of acid gases from natural gas. *Journal of Membrane Science, 140*(1), 27-49.

9. Bird, R. B., Stewart, W. E., & Lightfoot, E. N. (2006). *Transport phenomena* Wiley.

10. Breckenridge, W., Holiday, A., Ong, J. O., & Sharp, C. (2000). Use of SELEXOL® process in coke gasification to ammonia project. Paper presented at the *Proceedings of the Laurance Reid Gas Conditioning Conference,* 397-418.

11. Brunetti, A., Scura, F., Barbieri, G., & Drioli, E. (2010). Membrane technologies for CO_2 separation. *Journal of Membrane Science, 359*(1), 115-125.

12. Buckley-Smith, M. (2006). *The use of Solubility Parameters to Select Membrane Materials for Pervaporation of Organic Mixtures,*

13. Bucklin, R., & Schendel, R. (1985). *Comparison of physical solvents used for gas processing* Gulf Publishing Company, Houston, TX.

14. Burr, B., & Lyddon, L. (2008). A comparison of physical solvents for acid gas removal. Paper presented at the *Gas Processors' Association Convention, Grapevine, TX,*

15. Cath, T. Y., Adams, V. D., & Childress, A. E. (2004). Experimental study of desalination using direct contact membrane distillation: A new approach to flux enhancement. *Journal of Membrane Science, 228*(1), 5-16. doi:10.1016/j.memsci.2003.09.006

16. Chern, R., Sheu, F., Jia, L., Stannett, V., & Hopfenberg, H. (1987). Transport of gases in unmodified and arylbrominated 2, 6-dimethyl-1, 4-poly (phenylene oxide). *Journal of Membrane Science, 35*(1), 103-115.

17. Coleman, M., & Koros, W. (1990). Isomeric polyimides based on fluorinated dianhydrides and diamines for gas separation applications. *Journal of Membrane Science, 50*(3), 285-297.

18. Collins, J. P., Schwartz, R. W., Sehgal, R., Ward, T. L., Brinker, C., Hagen, G. P., & Udovich, C. A. (1996). Catalytic dehydrogenation of propane in hydrogen permselective membrane reactors. *Industrial & Engineering Chemistry Research, 35*(12), 4398-4405.

19. COONEY, D. O., & POUFOS, M. G. (1987). Liquid-liquid extraction in a hollow-fiber device. *Chemical Engineering Communications, 61*(1-6), 159-167.

20. Dastgir, M. G., Ferreira, F. C., Peeva, L. G., & Livingston, A. G. (2004). Recovery of 2, 4- dichlorophenol from acidic aqueous streams by membrane aromatic recovery system (MARS). *Journal of Chemical Technology and Biotechnology, 79*(4), 381-390.

21. Dastgir, M. G., Peeva, L. G., & Livingston, A. G. (2005). The performance of composite supported polymeric liquid membranes in the membrane aromatic recovery system (MARS). *Chemical Engineering Science, 60*(24), 7034-7044.

22. Davis, J. D. (2009). *Thermal degradation of aqueous amines used for carbon dioxide capture*

23. deMontigny, D., Tontiwachwuthikul, P., & Chakma, A. (2006). Using polypropylene and polytetrafluoroethylene membranes in a membrane contactor for CO_2 absorption. *Journal of Membrane Science, 277*(1), 99-107.

24. Doctor, R., Molburg, J., & Thimmapuram, P. (1994). *Gasification Combined Cycle: Carbon Dioxide Recovery, Transport,*

25. Eldridge, R. B. (1993). Olefin/paraffin separation technology: A review. *Industrial & Engineering Chemistry Research, 32*(10), 2208-2212.

26. Epps, R. (1994). Use of selexol solvent for hydrocarbon dewpoint control and dehydration of natural gas. Paper presented at the *Laurance Reid Gas Conditioning Conference, Norman, OK,*

27. Epps, R. Union Carbide Chemicals & Plastics Technology Corporation. (1992). Processing of landfill gas for commercial applications: The SELEXOL solvent process. Washington D. C.

28. Erbil, H. Y., Demirel, A. L., Avci, Y., & Mert, O. (2003). Transformation of a simple plastic into a superhydrophobic surface. *Science, 299*(5611), 1377-1380.

29. Feron, P., & Jansen, A. (1995). Capture of carbon dioxide using membrane gas absorption and reuse in the horticultural industry. *Energy Conversion and Management, 36*(6), 411-414.

30. Franco, J. A., deMontigny, D., Kentish, S. E., Perera, J. M., & Stevens, G. W. (2009). Effect of amine degradation products on the membrane gas absorption process. *Chemical Engineering Science, 64*(18), 4016-4023.

31. Freeman, B., Yampolskii, Y., & Pinnau, I. (2006). *Materials science of membranes for gas and vapor separation* Wiley.

32. Freeman, S. A., Davis, J., & Rochelle, G. T. (2010). Degradation of aqueous piperazine in carbon dioxide capture. *International Journal of Greenhouse Gas Control, 4*(5), 756-761.

33. Fu, D., Xu, Y., Wang, L., & Chen, L. (2012). Experiments and model for the surface tension of carbonated monoethanolamine aqueous solutions. *Science China Chemistry, 55*(7), 1467-1473.

34. Gabelman, A., & Hwang, S. (1999). Hollow fiber membrane contactors. *Journal of Membrane Science, 159*(1–2), 61-106. doi:10.1016/S0376-7388(99)00040-X

35. Gainar, I., & Anitescu, G. (1995). The solubility of CO_2, N_2 and H_2 in a mixture of dimethylether polyethylene glycols at high pressures. *Fluid Phase Equilibria, 109*(2), 281-289.

36. Garcia-Payo, M., Izquierdo-Gil, M., & Fernandez-Pineda, C. (2000). Wetting study of hydrophobic membranes via liquid entry pressure measurements with aqueous alcohol solutions. *Journal of Colloid and Interface Science, 230*(2), 420-431.

37. Goff, G. S., & Rochelle, G. T. (2006). Oxidation inhibitors for copper and iron catalyzed degradation of monoethanolamine in CO2 capture processes. *Industrial & Engineering Chemistry Research, 45*(8), 2513-2521.

38. Han, S., Ferreira, F. C., & Livingston, A. (2001). Membrane aromatic recovery system (MARS)—a new membrane process for the recovery of phenols from wastewaters. *Journal of Membrane Science, 188*(2), 219-233.

39. Han, S., Puech, L., Law, R. V., Steinke, J. H., & Livingston, A. (2002). Selection of elastomeric membranes for the separation of organic compounds in acidic media. *Journal of Membrane Science, 199*(1), 1-11.

40. Heintz, Y. J., Sehabiague, L., Morsi, B. I., Jones, K. L., & Pennline, H. W. (2008). Novel physical solvents for selective CO2 capture from fuel gas streams at elevated pressures and temperatures†. *Energy & Fuels, 22*(6), 3824-3837.

41. Hellums, M., Koros, W., Husk, G., & Paul, D. (1991). Gas transport in halogen-containing aromatic polycarbonates. *Journal of Applied Polymer Science, 43*(11), 1977-1986.

42. Henis, J. M., & Tripodi, M. K. (1980). A novel approach to gas separations using composite hollow fiber membranes. *Separation Science and Technology, 15*(4), 1059-1068.

43. Henni, A., Tontiwachwuthikul, P., & Chakma, A. (2006). Solubility study of methane and ethane in promising physical solvents for natural gas sweetening operations. *Journal of Chemical & Engineering Data, 51*(1), 64-67.

44. Hoff, K. A. (2003). *Modeling and Experimental Study of Carbon Dioxide Absorption in a Membrane Contactor,*

45. Hook, R. J. (1997). An investigation of some sterically hindered amines as potential carbon dioxide scrubbing compounds. *Industrial & Engineering Chemistry Research, 36*(5), 1779-1790.

46. Hu, L., Xu, X., & Coleman, M. R. (2007). Impact of H ion beam irradiation on matrimid®. II. evolution in gas transport properties. *Journal of Applied Polymer Science, 103*(3), 1670-1680.

47. Ilinitch, O., Semin, G., Chertova, M., & Zamaraev, K. (1992). Novel polymeric membranes for separation of hydrocarbons. *Journal of Membrane Science, 66*(1), 1-8.

48. Itoh, N. (1987). A membrane reactor using palladium. *AIChE Journal, 33*(9), 1576-1578.

49. Ji, L., Miksche, S., Rimpf, L., & Farthing, G. (2009). CO_2 chemical solvent screening. Paper presented at the *8th Annual Conference on Carbon Conference and Sequestration. Pittsburgh, PA, USA,* 4-7.

50. Jia, J., & Baker, G. L. (1998). Cross- linking of poly [1 (trimethylsilyl) 1 propyne] membranes using bis (aryl azides). *Journal of Polymer Science Part B: Polymer Physics, 36*(6), 959-968.

51. Judd, D. K. (1978). Selexol unit saves energy. *Journal of Hydrocarbon Processing, 57*(NO. 4, April), 122-124.

52. Kelman, S. D., Rowe, B. W., Bielawski, C. W., Pas, S. J., Hill, A. J., Paul, D., & Freeman, B. (2008). Crosslinking poly [1-(trimethylsilyl)-1-propyne] and its effect on physical stability. *Journal of Membrane Science, 320*(1), 123-134.

53. Kesting, R., Fritzsche, A., Murphy, M., Cruse, C., Handermann, A., Malon, R., & Moore, M. (1990). The second- generation polysulfone gas- separation membrane. I. the use of lewis acid: Base complexes as transient templates to increase free volume. *Journal of Applied Polymer Science, 40*(9- 10), 1557-1574.

54. Khaisri, S., deMontigny, D., Tontiwachwuthikul, P., & Jiraratananon, R. (2009). Comparing membrane resistance and absorption performance of three different membranes in a gas absorption membrane contactor. *Separation and Purification Technology, 65*(3), 290-297.

55. Khaisri, S., deMontigny, D., Tontiwachwuthikul, P., & Jiraratananon, R. (2011). CO_2 stripping from monoethanolamine using a membrane contactor. *Journal of Membrane Science, 376*(1), 110-118.

56. Kikuchi, E. (1995). Palladium/ceramic membranes for selective hydrogen permeation and their application to membrane reactor. *Catalysis Today, 25*(3), 333-337.

57. Kim, T., Koros, W., Husk, G., & O'brien, K. (1988). Relationship between gas separation properties and chemical structure in a series of aromatic polyimides. *Journal of Membrane Science, 37*(1), 45-62.

58. Kittel, J., Idem, R., Gelowitz, D., Tontiwachwuthikul, P., Parrain, G., & Bonneau, A. (2009). Corrosion in MEA units for CO_2 capture: Pilot plant studies. *Energy Procedia, 1*(1), 791-797.

59. Kohl, A. L., & Nielsen, R. (1997). *Gas purification* Gulf Professional Publishing.

60. Korens, N., Simbeck, D. R., Wilhelm, D. J., Longanbach, J. R., & Stiegel, G. J. (2002). SFA pacific, inc.

61. Koros, W., & Fleming, G. (1993). Membrane-based gas separation. *Journal of Membrane Science, 83*(1), 1-80.

62. Kumar, P., Hogendoorn, J., Feron, P., & Versteeg, G. (2002). New absorption liquids for the removal of CO_2 from dilute gas streams using membrane contactors. *Chemical Engineering Science, 57*(9), 1639-1651.

63. Lawson, K. W., & Lloyd, D. R. (1997). Membrane distillation. *Journal of Membrane Science, 124*(1), 1-25.

64. Lebo, J., Zajicek, J., Huckins, J., Petty, J., & Peterman, P. (1992). Use of semipermeable membrane devices for in situ monitoring of polycyclic aromatic hydrocarbons in aquatic environments. *Chemosphere, 25*(5), 697-718.

65. Li, J., & Chen, B. (2005a). Review of CO_2 absorption using chemical solvents in hollow fiber membrane contactors. *Separation and Purification Technology, 41*(2), 109-122.

66. Li, J., & Chen, B. (2005b). Review of CO_2 absorption using chemical solvents in hollow fiber membrane contactors. *Separation and Purification Technology, 41*(2), 109-122. doi:10.1016/j.seppur.2004.09.008

67. Matsuura, T. (1994). *Synthetic membranes and membrane separation processes* CRC PressI Llc.

68. Mccabe, W. L., Smith, J. C., & Harriott, P. (2005). *Unit operation of chemical engineering* (6th ed.)

69. *Meeting staged CO2 capture requirements with the UOP SELEXOL™ process.* (2009). ().UOP. A Honeywell company.

70. Meindersma, G., & Kuczynski, M. (1996). Implementing membrane technology in the process industry: Problems and opportunities. *Journal of Membrane Science, 113*(2), 285-292.

71. Miller, M. B., Chen, D., Xie, H., Luebke, D. R., Karl Johnson, J., & Enick, R. M. (2009). Solubility of CO2 in CO2-philic oligomers; COSMOtherm predictions and experimental results. *Fluid Phase Equilibria, 287*(1), 26-32. doi:10.1016/j.fluid.2009.08.022

72. Mulder, M. (1991). Basic principles of membrane technology.

73. Muruganandam, N., & Paul, D. (1987). Evaluation of substituted polycarbonates and a blend with polystyrene as gas separation membranes. *Journal of Membrane Science, 34*(2), 185-198.

74. National Energy Technology Laboratory. (May 2011). Advanced carbon dioxide capture R&D program: Technology update. http://www.netl.doe.gov/technologies/coalpower/ewr/pubs/CO2Handbook/CO2-Capture-Tech-Update-2011_Front-End%20Report.pdf

75. Newman, S. (1985). *Acid and sour gas treating processes* Gulf Publishing Co., Houston, TX.

76. Nunes, S. P., & Peinemann, K. (2006). *Membrane technology: In the chemical industry* Wiley-VCH.

77. Okamoto, K., Tanihara, N., Watanabe, H., Tanaka, K., Kita, H., Nakamura, A., . . . Nakagawa, K. (1992). Vapor permeation and pervaporation separation of water-ethanol mixtures through polyimide membranes. *Journal of Membrane Science, 68*(1), 53-63.

78. Okamoto, K., Semoto, T., Tanaka, K., & Kita, H. (1991). Application of pervaporation to Phenol–Acetone condensation reaction. *Chemistry Letters, 20*(1), 167-170.

79. Pankhania, M., Stephenson, T., & Semmens, M. J. (1994). Hollow fibre bioreactor for wastewater treatment using bubbleless membrane aeration. *Water Research, 28*(10), 2233-2236.

80. Park, Y. S., Won, J., & Kang, Y. S. (2001). Facilitated transport of olefin through solid PAAm and PAAm-graft composite membranes with silver ions. *Journal of Membrane Science, 183*(2), 163-170.

81. Percec, S. (1987). Chemical modification of poly (2, 6 dimethyl 1, 4phenylene oxide) by friedel–crafts reactions. *Journal of Applied Polymer Science, 33*(1), 191-203.

82. Perry, R. H., Green, D. W., & Maloney, J. O. (2008). *Perry's chemical engineers' handbook* McGraw-Hill New York.

83. Phattaranawik, J., Jiraratananon, R., & Fane, A. (2003). Effect of pore size distribution and air flux on mass transport in direct contact membrane distillation. *Journal of Membrane Science, 215*(1), 75-85.

84. Pixton, M., & Paul, D. (1994). *Relationships between structure and transport properties for polymers with aromatic backbones* CRC Press, Boca Raton, FL.

85. Porter, K., Sitthiosoth, S., & Jenkins, J. (1991). Designing a solvent for gas absorption. *Chemical Engineering Research & Design, 69*(A3), 229-236.

86. *Power plant carbon capture with CHEMCAD.* (No. rev. 031109).CHEMCAD.

87. Prasad, R., & Sirkar, K. (1987). Microporous membrane solvent extraction. *Separation Science and Technology, 22*(2-3), 619-640.

88. Prasad, R., & Sirkar, K. (1990). Hollow fiber solvent extraction: Performances and design. *Journal of Membrane Science, 50*(2), 153-175.

89. Prasad, R., & Sirkar, K. (1989). Hollow fiber solvent extraction of pharmaceutical products: A case study. *Journal of Membrane Science, 47*(3), 235-259.

90. Puri, P. S. (1996). Gas separation membranes-current status. *Membrane Journal, 6*(3), 117-126.

91. Raney, D. R. (1976). Remove carbon dioxide with selexol. *Journal of Hydrocarbon Processing, 55*(4), 73.

92. Rousseau, R., Matange, J., & Ferrell, J. (1981). Solubilities of carbon dioxide, hydrogen sulfide and nitrogen mixtures in methanol. *AIChE Journal, 27*(4), 605-613.

93. Sciamanna, S. F., & Lynn, S. (1988). Solubility of hydrogen sulfide, sulfur dioxide, carbon dioxide, propane, and n-butane in poly (glycol ethers). *Industrial & Engineering Chemistry Research, 27*(3), 492-499.

94. Simioni, M., Kentish, S. E., & Stevens, G. W. (2011). Membrane stripping: Desorption of carbon dioxide from alkali solvents. *Journal of Membrane Science, 378*(1), 18-27.

95. Spillman, R. W. (1989). Economics of gas separation membranes. *Chemical Engineering Progress, 85*(1), 41-62.

96. Srisurichan, S., Jiraratananon, R., & Fane, A. (2006). Mass transfer mechanisms and transport resistances in direct contact membrane distillation process. *Journal of Membrane Science, 277*(1), 186-194.

97. Stanojević, M., Lazarević, B., & Radić, D. (2003). Review of membrane contactors designs and applications of different modules in industry. *FME Transactions, 31*(2), 91-98.

98. Stern, S., Mi, Y., Yamamoto, H., & Clair, A. K. S. (1989). Structure/permeability relationships of polyimide membranes. applications to the separation of gas mixtures. *Journal of Polymer Science Part B: Polymer Physics, 27*(9), 1887-1909.

99. Story, B. J., & Koros, W. (1992). Sorption and transport of CO_2 and CH_4 in chemically modified poly (phenylene oxide). *Journal of Membrane Science, 67*(2), 191-210.

100. Strube, R., & Manfrida, G. (2011). CO_2 capture in coal-fired power plants—Impact on plant performance. *International Journal of Greenhouse Gas Control, 5*(4), 710-726.

101. Sweny, J. W. (1976). The SELEXOL process in fuel gas treating. *81st National Meeting of the American Institute of Chemical Engineers,*

102. Sweny, J. W. (1980). High CO_2- high H_2S removal with selexol solvent. *59th Annual GPA Convention,*

103. Sweny, J. (1976). Synthetic fuel gas purification by the SELEXOL process. *Am.Chem.Soc., Div.Fuel Chem., Prepr.;(United States), 18*(2)

104. Toshima, N. (1992). *Polymers for gas separation* VCH Weinheim.

105. VAN DEN, B., & Smolders, C. (1988). Flux decline in membrane processes. *Filtration & Separation, 25*(2), 115-121.

106. Wallace, J. S. (2006). Development of a carbon dioxide continuous scrubber (CDOCS) system for alkaline fuel cells.

107. Wankat, P. C. (2006). *Separation process engineering* Prentice Hall.

108. Wijmans, J. G., & Baker, R. W. (1995). The solution-diffusion model: A review. *Journal of Membrane Science, 107*(1–2), 1-21. doi:10.1016/0376-7388(95)00102-I

109. Wikol, M. J., Kobayashi, M., & Hardwick, S. J. (1998). Application of PTFE membrane contactors to the infusion of ozone into ultra-high purity water. *Contamination Control,* , 172-177.

110. Yan, S., Fang, M., Zhang, W., Wang, S., Xu, Z., Luo, Z., & Cen, K. (2007). Experimental study on the separation of CO_2 from flue gas using hollow fiber membrane contactors without wetting. *Fuel Processing Technology, 88*(5), 501-511. doi:10.1016/j.fuproc.2006.12.007

111. Yeh, J. T., Pennline, H. W., & Resnik, K. P. (2001). Study of CO_2 absorption and desorption in a packed column. *Energy & Fuels, 15*(2), 274-278.

112. Zhang, J. (2011). *Theoretical and Experimental Investigation of Membrane Distillation,*

113. Zhu, Y., Minet, R. G., & Tsotsis, T. T. (1996). A continuous pervaporation membrane reactor for the study of esterification reactions using a composite polymeric/ceramic membrane. *Chemical Engineering Science, 51*(17), 4103-4113. doi:10.1016/0009-2509(96)00252-7

7 Appendices

7.1 Physical solvent Sample Calculations

7.1.1 Sample calculation of CO_2 mole fraction in the solvent.

The detail of the sampling module was explained in section 3.5.7. A sample calculation of the CO_2 mole fraction in the Selexol at 400 psi is given here.

The following parameters were used in all calculations:

Universal Gas Constant:	1205.91	(cm^3.psi/gmol.k)
Solvent Density:	1.03	(gr/cm^3)
Solvent Average Molecular weight	250	(gr)
Sampling Module Total Volume:	1010	(cm^3)

For the sample taken from the absorber at an equilibrium pressure of 400 psi, the following data were collected from the sampling module:

Initial Pressure of the sampling module	2.16 (psi)
Final Equilibrium Pressure of the sampling module	5.07 (psi)
Sample Weight	2.57911(gr)
Temperature	291.15 (k)

The following equations are used to calculate the mole fraction of CO_2 in the solvent sample.

$$n_{CO2} = \frac{[P_2(V_T - V_S) - P_1 V_T]}{RT}$$

$$X_{CO2} = \frac{n_{CO2}}{n_{CO2} + \frac{m_s}{M_n}}$$

so the mole fraction of CO_2 at 400 psi can be calculated as follows:

$$n_{CO2} = \frac{[5.07(1010 - 2.57911/1.03) - 2.16 \times 1010]}{1205.91 \times 291.15} = 8.3349 \times 10^{-3}$$

$$X_{CO2} = \frac{8.3349 \times 10^{-3}}{8.3349 \times 10^{-3} + \frac{2.57911}{250}} = 0.4468$$

7.1.2 Sample calculation of CO_2 flux and permeability.

The calculation procedure for PERVAP 4060 membrane at 300 psi and Selexol flow rate of160 (mL/min) is given here. Table 7.1 summarizes the peaks area of CO_2 and N_2, given by the GC, with respect to the time.

Table 7.1. CO_2 and N_2 peaks areas with respect to time.

Time(min)	Area CO_2	Area N_2	Area (CO_2/N_2)	Flow (CO_2/N_2)	Flow CO_2 (sccm)
30	677.50	9457.36	0.072	0.082	41.1487
60	842.91	9338.77	0.090	0.104	51.8454
90	832.58	9293.28	0.090	0.103	51.4607
120	862.21	9321.43	0.092	0.106	53.1308
135	780.96	9391.40	0.083	0.096	47.7658
150	817.39	9353.19	0.087	0.100	50.1983
165	886.39	9278.80	0.096	0.110	54.8718
180	945.70	9282.52	0.102	0.117	58.5204
210	927.07	9254.31	0.100	0.115	57.5420
240	989.97	9264.24	0.107	0.123	61.3805
280	932.14	9266.83	0.101	0.116	57.7784
300	923.95	9299.85	0.099	0.114	57.0680
315	897.86	9320.06	0.096	0.111	55.3363
330	903.34	9293.90	0.097	0.112	55.8305
345	923.38	9284.28	0.099	0.114	57.1284
360	919.38	9276.89	0.099	0.114	56.9257
				Average Flow	55.8622

The first 120 minutes were excluded in taking the average of the CO_2 flow. Conversion of the peak area ratio to flow ratio was done using the calibration curve.

$$\mathrm{CO_2\ Flux} = \frac{\text{Average CO2 Flow}}{\text{Membrane Area}} \times \frac{1}{60} = \frac{55.862}{9.6} \times \frac{1}{60} =$$

0.09698 (cm^3 (STP) CO$_2$/cm^2.s)

Average solvent leak = 4.1×10 $^{(-5)}$

Selectivity = (CO$_2$ Flux) / (Solvent Flux) = 2365.43

Using the same procedure explained in section, mole fraction of CO$_2$ was calculated to be 0.3694.

Molar flow rate of solvent=

(solvent flow rate) × (solvent density)/(M.W. solvent)= 0.01098 (moles/sec)

Moles of CO$_2$ entering the membrane module = N$_{in}$=

$$\frac{\mathrm{X_{CO2}} \times (\text{ Molar flow rate of solvent})}{(1-\mathrm{X_{CO2})}} = 0.006435(\text{moles CO2/sec})$$

Moles of CO$_2$ permeating through the membrane= N$_{permeation}$

$$1(\text{atm}) \times \frac{(\text{CO2 flux}) \times (\text{Membrane Area})}{\big(82.057 \times (273.15 + 21.1)\big)} = 3.85 \times 10^{(-5)}\ (\text{moles CO2/sec})$$

Percent Recovery= (N$_{permeation}$) / (N$_{in}$) ×100= 0.599 %

7.2 Chemical Solvent Mass Transfer Coefficient Calculation

7.2.1 Liquid phase mass transfer coefficient (k_L)

The CO_2 diffusivity in liquid phase can be determined from N_2O analogy by the following equation (Khaisri et al., 2011):

$$D_{CO_2} = D_{N_2O}(\frac{D_{CO_2,H_2O}}{D_{N_2O,H_2O}})$$

Eqn (17)

T = 77 ºC = 350 K, C_{MEA} = 15 wt.% = 2.45 mol L^{-1}, α = 0.45 mol CO_2/ mol amine, and μ_{H_2O}= 1 mPa·s

$$D_{CO_2,H_2O} = 2.35 \times 10^{-2} \exp\left(\frac{-2119}{T}\right) = 2.35 \times 10^{-2} \exp\left(\frac{-2119}{350}\right) = 5.5 \times 10^{-5} cm^2 s^{-1}$$

Eqn (18)

$$D_{N_2O,H_2O} = 5.07 \times 10^{-2} \exp\left(\frac{-2371}{T}\right) = 5.07 \times 10^{-2} \exp\left(\frac{-2371}{350}\right) = 5.8 \times 10^{-5} cm^2 s^{-1}$$

Eqn (19)

$$D_{N_2O,MEA} = (5.07 \times 10^{-2} + 8.65 \times 10^{-3} C_{MEA} + 2.78 \times 10^{-3} C_{MEA}^2) \exp\left(\frac{-2371 - 93.4 C_{MEA}}{T}\right)$$

$$= (5.07 \times 10^{-2} + 8.65 \times 10^{-3} \times 2.45 + 2.78 \times 10^{-3} \times 2.45^2) \exp\left(\frac{-2371 - 93.4 \times 2.45}{350}\right) = 5.3 \times 10^{-5} cm^2 s^{-1}$$

Eqn (20)

$$D_{CO_2} = D_{N_2O}\left(\frac{D_{CO_2,H_2O}}{D_{N_2O,H_2O}}\right) = 5.3 \times 10^{-5}\left(\frac{5.5 \times 10^{-5}}{5.8 \times 10^{-5}}\right) = 5.0 \times 10^{-5} cm^2 s^{-1}$$

Eqn (21)

$$\frac{\mu_{MEA}}{\mu_{H_2O}} = \exp\frac{[21.186\Omega + 2373][\alpha(0.01015\Omega + 0.0093T - 2.2589) + 1]\Omega}{T^2} = 1$$

$$\mu_{MEA} = 1 \text{ mPa·s}$$

Eqn (22)

v_L = 120 mL/min = 120 cm^3/[π(0.25 inch/2)^2]/60 s = 6.3 cm s^{-1}
d_h = 2.45 mm = 0.245 cm
L = 4.7 cm (The average liquid path is approximated as the diameter of the membrane)

$$k_L = \frac{D_L}{d_h} 1.62 \left(\frac{d_h^2 v_L}{L D_L}\right)^{\frac{1}{3}} = \frac{5.0\times10^{-5}\text{cm}^2\text{s}^{-1}}{0.245\text{ cm}} 1.62 \left(\frac{0.245\text{ cm } \times 6.3\text{ cm s}^{-1}}{5.0\times10^{-5}\text{cm}^2\text{s}^{-1}}\right)^{\frac{1}{3}} = 1.037\times10^{-2}\text{ cm}\cdot\text{s}^{-1}$$
$$= 1.037\times10^{-4}\text{ m}\cdot\text{s}^{-1}$$

Eqn (23)

7.2.2 Gas phase mass transfer coefficient (k_G)

The CO_2 diffusivity in gas phase can be determined by the following equation (Khaisri et al., 2011):

$$D_G = \frac{0.001858 T^{3/2}[(1/M_A + 1/M_B)]^{1/2}}{P\sigma_{AB}^2 \Omega_G}$$

Eqn (24)

Parameters included can be calculated accordingly (Chern et al., 1987).

T = 65 ^oC = 338 K

M_A = 44, M_B = 28, and P = 1 atm = 1.01325 bar

$\sigma_{AB} = 0.5(\sigma_A + \sigma_B) = 0.5(4.63\text{Å} + 3.76\text{Å})$ = 4.195 Å

$\varepsilon_{AB}/\kappa = [(\varepsilon_A/\kappa)(\varepsilon_B/\kappa)]^{1/2} = [195.2\times71.4]^{1/2}$ = 118 K

$T^* = \kappa T/\varepsilon_{AB}$ = 338 K/118 K = 2.8

$$\Omega_G = \frac{1.06036}{(T^*)^{0.15610}} + \frac{0.19300}{\exp(0.47635T^*)} + \frac{1.03587}{\exp(1.52996T^*)} + \frac{1.76474}{\exp(3.89411T^*)}$$
$$= \frac{1.06036}{(2.8)^{0.15610}} + \frac{0.19300}{\exp(0.47635\times2.8)} + \frac{1.03587}{\exp(1.52996\times2.8)} + \frac{1.76474}{\exp(3.89411\times2.8)} = 0.97$$

Eqn (25)

$$D_G = \frac{0.001858 T^{3/2}[(1/M_A + 1/M_B)]^{1/2}}{P\sigma_{AB}^2 \Omega_G} = \frac{0.001858\times338^{3/2}[(1/44 + 1/28)]^{1/2}}{1\times4.195^2\times0.97}$$
$$= 0.164\text{ cm}^2\text{s}^{-1}$$

Eqn (26)

$$\frac{k_G d_h}{D_G} = 0.023(\frac{d_h \rho v_G}{\mu_G})^{0.8}(\frac{\mu_G}{D_G \rho})^{0.33}$$

Eqn (27)

$\rho_{mixture} \approx 1.0101\ kg\cdot m^{-3} = 10^{-3}\ g\cdot cm^{-3}$ (at 338 K, 1 atm)

$\mu_{mixture} \approx 19\times10^{-6}\ Pa\cdot s = 19\times10^{-5}\ g\cdot cm^{-1}\cdot s$ (at 338 K, 1 atm, and $1\ Pa\cdot s = 10\ g\cdot cm^{-1}\cdot s$)

$v_G = 500\ cm^3\cdot min^{-1} = 500\ cm^3/[\pi(0.25\ inch/2)^2]/60\ s = 26.25\ cm\cdot s^{-1}$

$$k_G = \frac{D_G}{d_h} \times 0.023 \left(\frac{d_h \rho v_G}{\mu_G}\right)^{0.8} \left(\frac{\mu_G}{D_G \rho}\right)^{0.33}$$

$$= \frac{0.164\ cm^2 s^{-1}}{0.245\ cm}$$

$$\times 0.023(\frac{0.245\ cm \times 10^{-3}\ g\cdot cm^{-3} \times 26.25\ cm\cdot s^{-1}}{19\times10^{-5}\ g\cdot cm^{-1}\cdot s^{-1}})^{0.8}(\frac{19\times10^{-5}\ g\cdot cm^{-1}\cdot s^{-1}}{0.164\ cm^2 s^{-1}\times10^{-3}\ g\cdot cm^{-3}})^{0.33}$$

$$= 0.27\ cm\cdot s^{-1} = 2.7\times10^{-3}\ m\cdot s^{-1}$$

Eqn (28)

7.2.3 Membrane Mass Transfer Coefficient (k_M)

$$k_M = \frac{D_e \varepsilon}{\tau \delta}$$

Eqn (29)

$$\frac{1}{D_e} = \frac{1}{D_k} + \frac{1}{D_G}$$

Eqn (30)

where D_e is the combination of Knudsen and molecular diffusivity coefficient. D_k is the Knudsen diffusivity coefficient, and D_G is the diffusivity of CO_2 in the gas phase (Khaisri et al., 2011).

$D_G = 0.164\ cm^2\ s^{-1}$, T =0.5(77 +65) = 71 ºC = 344 K

Eqn (31)

$$\mathrm{D_k = 4850\ d_{pore}}\sqrt{\frac{\mathrm{T}}{\mathrm{M_A}}}$$

Eqn (32)

For $PP_{0.1}$, d_{pore} = 0.5×0.1 μm = 0.5×10^{-5} cm, ε = 0.76, τ = 2.04, δ = 0.1 mm = 0.01 cm,

$$\mathrm{D_k = 4850\ d_{pore}}\sqrt{\frac{\mathrm{T}}{\mathrm{M_A}}} = 4850 \times 0.5 \times 10^{-5}\ \mathrm{cm} \times \sqrt{\frac{344}{44}} = 0.0678\ \mathrm{cm^2 s^{-1}}$$

Eqn (33)

$$\mathrm{D_e} = \frac{1}{\frac{1}{\mathrm{D_k}} + \frac{1}{\mathrm{D_G}}} = \frac{1}{\frac{1}{0.0678} + \frac{1}{0.164}} = 0.0479\ \mathrm{cm^2 s^{-1}}$$

Eqn (34)

$$\mathrm{k_M} = \frac{\mathrm{D_e}\varepsilon}{\tau\delta} = \frac{0.0479\ \mathrm{cm^2 s^{-1}} \times 0.76}{2.04 \times 0.01} = 1.78\ \mathrm{cm \cdot s^{-1}} = 1.78 \times 10^{-2}\mathrm{m \cdot s^{-1}}$$

Eqn (35)

7.2.4 Enhancement Factor

The enhancement factor can be determined by equation as shown below (Khaisri et al., 2011):

$$\mathrm{E} = 1 + \frac{(\mathrm{D_{MEACOO^-}}/\mathrm{D_{CO_2}})\sqrt{\mathrm{K}}\mathrm{C^B_{MEA}}}{\left(1 + 2(\mathrm{D_{MEACOO^-}}/\mathrm{D_{MEA}})\sqrt{\mathrm{K C_{CO_2,i}}}\right)(\sqrt{\mathrm{C_{CO_2,i}}} + \mathrm{C^B_{CO_2}})}$$

Eqn (36)

where $\mathrm{C^B_{MEA}}$ and $\mathrm{C^B_{CO_2}}$are the bulk concentration of free MEA and CO_2.

$\mathrm{C^B_{MEA}} = 2.45\ \mathrm{mol/L}$

$\mathrm{C^B_{CO_2}} = 1.10\ \mathrm{mol/L}$

$\mathrm{D_{CO_2}}$ is the CO_2 diffusivity in MEA solution.

$\mathrm{D_{CO_2}} = 5.0 \times 10^{-5}\mathrm{cm^2 s^{-1}}$

$\mathrm{D_{MEACOO^-}}$ and $\mathrm{D_{MEA}}$are diffusivity of carbamate and MEA.

$\mathrm{D_{MEACOO^-}} \approx \mathrm{D_{MEA}} = 5.3 \times 10^{-5}\mathrm{cm^2 s^{-1}}$

K is the equilibrium constant

$$\mathrm{K} = \frac{1}{\mathrm{C}_{\mathrm{CO_2,e}}}\left(\frac{\alpha}{1-2\alpha}\right)^2$$

Eqn (37)

$\mathrm{C}_{\mathrm{CO_2,e}} \approx \mathrm{C}_{\mathrm{CO_2}}^{\mathrm{B}} = 1.10\ \mathrm{mol/L}$, $\alpha = 0.45$

K = 18.4 L/mol

Assume $\mathrm{C}_{\mathrm{CO_2,e}} \approx \mathrm{C}_{\mathrm{CO_2,e}} \approx \mathrm{C}_{\mathrm{CO_2}}^{\mathrm{B}} = 1.10\ \mathrm{mol/L}$

Therefore,

$$\mathrm{E} = 1 + \frac{\left(\frac{5.3\times10^{-5}\mathrm{cm^2s^{-1}}}{5.0\times10^{-5}\mathrm{cm^2s^{-1}}}\right)\sqrt{18.4\frac{\mathrm{L}}{\mathrm{mol}}}\times 2.45\ \mathrm{mol/L}}{\left(1+2(1)\sqrt{18.4\frac{\mathrm{L}}{\mathrm{mol}}\times 1.1\ \mathrm{mol/L}}\right)(\sqrt{1.1\ \mathrm{mol/L}}+\sqrt{1.1\ \mathrm{mol/L}})} = 1.53$$

Eqn (38)

7.2.5 Henry's Constant

Henry's constant can be described as following equation (Khaisri et al., 2011):

$$\mathrm{H}_{\mathrm{CO_2}} = \mathrm{H}_{\mathrm{N_2O}}\left(\frac{\mathrm{H}_{\mathrm{CO_2,H_2O}}}{\mathrm{H}_{\mathrm{N_2O,H_2O}}}\right)$$

Eqn (39)

The unit of H_{CO2} is kPa·L·mol^{-1}

T = 65 ^{o}C = 338 K

$$\mathrm{H}_{\mathrm{CO_2,H_2O}} = 2.82\times10^6\exp\left(\frac{-2284}{\mathrm{T}}\right) = 2.82\times10^6\exp\left(\frac{-2284}{338}\right) = 3277\ \mathrm{kPa\cdot dm^3\cdot mol^{-1}}$$

Eqn (40)

$$\mathrm{H}_{\mathrm{N_2O,H_2O}} = 8.55\times10^6\exp\left(\frac{-2284}{\mathrm{T}}\right) = 8.55\times10^6\exp\left(\frac{-2284}{338}\right) = 9935\ \mathrm{kPa\cdot dm^3\cdot mol^{-1}}$$

Eqn (41)

$$H_{N_2O,MEA} = 1.207 \times 10^5 \exp\left(\frac{-1136.5}{T}\right) = 1.207 \times 10^5 \exp\left(\frac{-1136.5}{338}\right)$$

$$= 4188\ \mathrm{kPa \cdot dm^3 \cdot mol^{-1}}$$

Eqn (42)

The two body interaction parameter for MEA and H_2O is calculated as below, where Φ_{H_2O} is volume percentage of water.

$$\lambda_{H_2O-MEA} = 4.793 - 7.44 \times 10^{-3}T - 2.201\Phi_{H_2O}$$

$$= 4.793 - 7.44 \times 10^{-3} \times 338 - 2.201 \times 0.85 = 0.32$$

Eqn (43)

The excess Henry's constant is calculated as below:

$$H^E = \Phi_{MEA}\Phi_{H_2O}\lambda_{H_2O-MEA} = 0.15 \times 0.85 \times 0.32 = 0.041$$

Eqn (44)

$$\ln H_{N_2O} = H^E + \Phi_{MEA}H_{N_2O,\text{pure MEA}} + \Phi_{H_2O}\ln H_{N_2O,H_2O}$$

$$= 0.041 + 0.15 \times \ln 4188 + 0.85 \times \ln 9935 = 9.1$$

Eqn (45)

$$H_{N_2O} = 9092\ \mathrm{kPa \cdot dm^3 \cdot mol^{-1}}$$

Therefore,

$$H_{CO_2} = H_{N_2O}\left(\frac{H_{CO_2,H_2O}}{H_{N_2O,H_2O}}\right) = 9092\left(\frac{3277}{9935}\right) = 1381\ \mathrm{kPa \cdot dm^3 \cdot mol^{-1}}$$

$$= 3000\ \mathrm{kPa \cdot dm^3 \cdot mol^{-1}} = 3000\ \mathrm{kPa \cdot L \cdot mol^{-1}}$$

Eqn (46)

The dimensionless H of CO_2 is

$$H = \left(\frac{1}{H_{CO_2}}\right)RT = \left(\frac{8.314\ \mathrm{kPa \cdot L \cdot K^{-1} \cdot mol^{-1}} \times 338\ \mathrm{K}}{3000\ \mathrm{kPa \cdot L \cdot mol^{-1}}}\right) = 0.94$$

Eqn (47)

7.3 Materials and Equipment List

7.3.1 Chemical Solvent system

A detailed list of equipment and materials is given below:

Equipment:

- Membrane unit: Millipore 47mm Stainless Steel Membrane Holder XX4404700
- Pump: Cole-Parmer digital gear pump, pumping speed 0-330 ml/min, ± 1 ml/min
- Two Cartridge heaters: Stainless steel construction, 3 feet leads, ¼" diameter, 8" length, ¼" NPT thread, 600 W from Omega engineering Inc.
- Alternative heater: Low flow air process and liquid circulation heater AHPF-121, 120VAC, 1200W, stainless stain, outlet temperature up to 430 °C, flow rate up to 15 CFM, pressure up to 100 psi from Omega.
- Heater controller: Cal controller 9400
- Pressure transducer: Omega, 0-300 psi, 5 VDC regulated input, 0-100 mV output.
- Pressure gauges: Omega 0-300 psi, unknown origin
- Thermocouple: 1/8", 1/4" diameter, K type from Omega
- Mass flow controller: Brooks 4800 series, CO_2 (0-10 SLPM), N_2 (0-10 SLPM).
- Swagelok tubing and fittings
- Liquid and particulate filter: Parker coalescing filter (Cole Parmer)

Data logger:

- National Instruments USB-9219 4-Channel Universal Analog Input Module

CO_2 analyzers:

- LI-COR 820 Non-Dispersive Infrared CO_2 analyzer, 0-20,000 ppm, ± 1ppm
- Agilent 7850A GC- FID with methanizer, TCD

Computers and Software:

- Computer: Dell Precision T3200, Microsoft^{TM} Windows 7
- Data acquisition: Labview^{TM} software, version 2010 from National Instruments
- GC control and analysis: Chemstation, Agilent
- CO_2 analyzer: LI-820 v2.0.0

7.3.2 Physical solvent system

The following equipment and materials were used for building the high pressure permeation setup.

Pervaporation equipment

- Membrane unit: Millipore® 47 mm High Pressure Stainless Steel Membrane Holder XX4504700
- Pump head: Micropump high-flow pressure-loaded pump compatible with type 56 c-face motors from Cole-Parmer, Part Number: EW-07003-41
- Pump motor: Leeson NEMA Type 56C-face TEFC motor, 1/3 hp, 1750 rpm, 90 VDC from Cole-Parmer, Part Number: EW-70071-00

- Motor speed controller: Basic Variable-Speed DC Motor Controller for 1/4 to 2 hp motors, from Cole-Parmer, Part Number: EW-70100-10
- Cartridge heaters: Stainless steel construction, ¼” diameter, 6” length, ¼” NPT thread, 400 W, 120V, ID Number: HR25060R from Big Chief, Inc.
- Heater controller: Cal controller 9400
- Pressure transducer: Omega, 0-1000psi, 5 VDC regulated input, 0-100mV output, Part Number : PX309-1KGV
- Pressure gauges: Cole-Parmer, Part number: PGI-63C-PG800-LAOX
- Thermocouple: 1/8”, 1/4” diameter, K type from Omega
- Mass flow controller: Brooks 4800 series, N2 (0-10 SLPM).
- Swagelok tubing and fittings
- Liquid and particulate filter: Parker coalescing filter from Cole-Parmer, ¼” NPT Ports, Part Number: EW-02917-00
- Rotameter: Brooks Metal Tube Rotameter Model 3750CA5A11DCAAAAA0, Valve on Inlet, +/- 5% full scale accuracy.

7.3.2.1 Data logger

- National Instruments 9219 4 CH-CH ISOLATED, 24-BIT, +/-60V, UNIVERSAL AI MODULE, Part Number: 779781-01.
- National Instruments USB SINGLE MODULE CARRIER FOR C SERIES MODULES, Part Number: 779471-01.

7.3.2.2 CO_2 Analyzer

- LI-COR 820 Non-Dispersive Infrared CO_2 analyzer, 0-20,000 ppm ± 1ppm

- Agilent 7850A GC- FID with methanizer, TCD

7.3.2.3 Computers and software

- Computer: Dell Precision T3200, Microsoft^{TM} Windows 7
- Data acquisition: Labview^{TM} software, version 2010 from National Instruments
- GC control and analysis: Chemstation, Agilent
- CO_2 analyzer: LI-820 v2.0.0

7.3.2.4 Absorption vessel

The 4 liter absorption vessel was built by the University of North Dakota Chemical Engineering Department workshop from a 6” stainless steel pipe. Two class 300 raised-face (?) flanges coupled with gaskets are used to seal the absorption tank. This absorption vessel is equipped with a home-made cooling water coil to maintain the absorption temperature at a certain value. A pressure transducer is mounted on top of the absorber to record the pressure inside the absorber. CO_2 is injected into the solvent via a sparger installed at the bottom of the absorber to increase the contact time between the liquid and gas bubbles. To discharge the air during the period when absorber is loaded with solvent and also to regenerate the physical solvent inside the absorption tank at the end of the experiment, a relief valve is mounted on top of the absorber. Using a 1/4” diameter, K type thermocouple, the absorber temperature is measured and recorded continuously.

7.3.2.5 Membrane Module

The membrane module is modified from the original Millipore® 47 mm stainless steel membrane holder XX4504700. **Error! Reference source not found.** shows different parts of the original filter holder. This membrane holder can hold filters of 47 mm diameter and the inlet pressure is rated up to 10000 psi. Its diameter and height is 8.6 cm and 4.4 cm respectively. It is sealed by a fluoroelastomer O-ring. The inlet and outlet fittings are 7/16 in.-20 (UNF-3B) female. To apply this filter holder to our application, the central inlet and outlet adaptors on top and bottom plates were plugged and two new 1/8” holes were drilled on each plate for the solvent recirculation in the upper chamber and sweep gas line in the bottom chamber of the membrane holder.

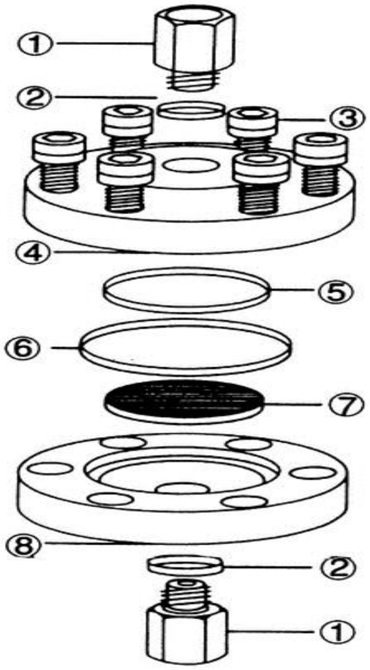

Figure 7.1. (Adopted from www.millipore.com/catalogue/module/C263) Original configuration of the membrane holder (Upper and bottom plates were modified with an inlet and outlet) 1. Inlet/Outlet Adapter, 2. Adapter O-ring, 3. Hex-cap Screw, 4. Top plate, 5. Inner O-ring, 6. Outer O-ring, 7. Support Screen, 8. Bottom plate.

7.3.2.6 Pumping system

Initially, a reciprocating pump was implemented to circulate the solvent through the setup. The pump was a 500-A-N3 stainless steel pump from Neptune (Available at UND Chemical Engineering Research Lab). Two major difficulties were identified with this pump. First, the flow rate of the Neptune pump was very limited, 3.7 LPH at 100 psi. The system is supposed to operate at significantly high pressures and since the flow rate decreases by 10% for each 100 psi pressure increase (based on personal communication with the factory), it is realized that using this pump would prevent us from looking into different flow rates at different pressures.

The second important issue regarding the Neptune pump was its pumping method. Neptune pumps are reciprocating pumps, and thus much pulsation is expected in the flow. Such pulsations made the flow rate measurements difficult and inaccurate. The rotameter calibration needs rather a smooth flow with much lower level of fluctuations. On the other hand, if the flow is pulsing in the membrane chamber, it will be expected to see fluctuations in the sweep gas CO_2 concentration.

A container filled with solvent and pressurized air on top of the liquid was added to the solvent line to dampen flow fluctuations. However, later investigations of the system indicated that running the system would deplete the dampener and eventually pump cavitation occurs. Additionally, it was assumed that the liquid CO_2 loading is not equal to the CO_2 loading of the solvent circulating in the system and this could decrease the accuracy of the calculations.

For the mentioned difficulties, a new gear pump that delivers the fluid more smoothly with a wider range of flow rates was purchased. The new installed pump includes the following items:

- Micropump® high-flow pressure-loaded pump head. This pump head is a magnetically driven, precision-geared pump which delivers the fluid smoothly and with very low pulsation and an acceptable range of flow rates (0.85 ml/revolution). The pump head was purchased through Cole Parmer, part No: EW-07003-41.

- Leeson NEMA Type 56C-face TEFC motor, 1/3 hp, 1750 rpm, 90 VDC. (Purchased through Cole Parmer, part No: EW-70071-00)
- Basic Variable-Speed DC Motor Controller to adjust the speed of the motor and thus the desirable flow rate. (Purchased through Cole Parmer, part No: EW-70100-10).

7.3.3 Physical solvent System Materials list

- Poly (Ethylene Glycol) Dimethyl Ether, Average Mn CA. 250, 10L from SIGMA-ALDRICH, SKU No: 445878).
- PREVAP TM 1201/2235 Polymeric Membrane Sheets, Sulzer Chemtech.
- PREVAP TM 1211/2203 Polymeric Membrane Sheets, Sulzer Chemtech.
- PERVAP TM 4060 Polymeric Membrane Sheets, Sulzer Chemtech.
- PDMS Selective Layer Polymeric Membrane Sheet, PERVATECH.
- SYLGARD 184® silicon elastomer base and silicon elastomer curing agent, from SIGMA-ALDRICH, SKU No: 761036-5EA.
- Membrane holder inner O-ring (TFE packed VITON) from Millipore®, part No: XX4504705.
- Membrane holder inner O-ring (Perfluoroelastomer) from CHEMRAZ®, part No: 9030-SD505.
- Membrane Holder Outer O-ring (VITON), from Millipore®, part No: XX4504713.

7.4 Procedures

7.4.1 Chemical Solvents

1. Use the digital micrometer/caliper to measure and record the thickness at five points on the membrane, four along the outside and one in the middle, measure membrane diameter and membrane mass as shown below, calculate and record average value, standard deviation and variance.

2. Turn on the power switch; let the MFCs, CO_2 analyzer and other devices to warm up.

3. Rinse absorption tank using tap water.

4. Mount membrane in the membrane holder, place O-ring on the membrane and then top plate, tighten the three hex-nuts gradually and try to keep it balanced.

5. Open CO_2 gas tank, N_2 gas tank, adjust the secondary regulator at 50 psi or slightly higher. Turn on the pump, adjust the pumping speed if necessary. Turn on N_2 MFC at desired flow rate, check leaks. Make sure all the valves are open and in the right direction.

6. Calculate and make up the desired concentration and amount of solution into the absorption tank, turn on the pump to help it mix well. Record make-up volumes and calculate theoretical concentrations. (Density of DI water 1012 g/L, density of MEA 997 g/L) And then take 20 ml sample and save it in a sample vial and label it.

7. Stop the pump, keep N_2 sweep gas MFC set at desired flow rate. Open Li-820 program at desktop, record the baseline CO_2 concentration for 5 minutes at steady state, calculate average, standard deviation.

8. Turn on Labview program, check temperature and pressure reading is normal. The temperature reading should be room temp at 22 to 23 ^{o}C, pressure reading should be close to 0. If normal, name the file using date and time, for example: 062311am1045.

9. Turn on the pump set at desired pumping speed, make sure gear set should be set at T23. It just takes 20-30 sec for pump to reach steady state. Turn on the heater, set at 50 C for the first stage, 70 C for the second stage and 90 C if 90 C is the desired set point, it takes about 20- 30 minutes to reach steady state.

Turn off procedure:

1. Stop LI-820 CO_2 concentration recording, disconnect the data communication interface, and close the program.
2. Stop Labview program.
3. Adjust temperature controller set point below the room temperature.
4. When temperature controller reading approaches room temperature, turn off the pump and MFC, and power off.

7.4.2 Physical solvents

The following procedure was used to measure the permeation rate of CO_2 for different polymeric membranes:

- Membranes are cut using a variable diameter circular cutter to the radius of 47mm.
- Membrane holder O-rings are inspected visually to make sure they can seal the membrane properly. If any corrosion or defect is observed, the O-rings will be replaced.

- Membrane sheet is placed on top of the screen in the bottom chamber of the filter holder.
- The upper chamber is placed over the bottom chamber and screwed down tightly. For even sealing, the screws are tightened with the same number of turns.
- The pump motor speed controller is set to 10% and the pump is turned on.
- N_2 mass flow controller is set to 500 (sccm/min) and N_2 tank pressure regulator is opened and set to 50 psi (The allowed pressure for the mass flow controller).
- Checking the sweep gas coalescing filter to make sure no crazy leaking is occurring in the membrane chamber.
- Running the Data Acquisition program using NI LabView.
- Opening the relief valve mounted on the absorber vessel
- Opening the CO_2 tank and set the pressure as low as 30 psi for five minutes (This is to flush the absorber with CO_2 to ensure no air is trapped in the system).
- Closing the relief valve.
- Pressurizing the absorber to the desirable pressure by increasing the outlet pressure of the CO_2 tank pressure regulator and monitoring the readings of the absorber pressure transducer via LabView. (This step has to be done slowly to make sure no hydraulic shock happens to the membrane sealing and the pump).

- Setting the desired solvent flow rate by adjusting the DC motor speed controller and using the calibration charts for any pressure.
- Confirming the solvent flow rate by measuring it via the pump calibration module.
- Diverting the sweep gas to the CO_2 analyzer and running the LI-820 v2.0.0 to monitor and store the measured CO_2 concentration in the sweep gas (Two measurements per second).
- If the CO_2 analyzer readings are over the analyzer limit (20000 ppm), then the sweep gas CO_2 concentration should be measured using the GC.
- Measuring the CO_2 mole fraction via the sampling module and procedure explained in section 3.5.7.
- Running the permeation experiment for about 6-8 hours.
- Draining the sweep gas filter once per hour for the “membrane selectivity calculations”.
- Depressurizing the system by opening the relief valve, stopping the pump, opening the chamber and removing the membrane for post-experiment characterization tests.

7.5 Membrane material candidates

Table 7-2 Membrane Material Candidates

Rank	Polymer	Abbreviation	$P(CO_2)$ (barrer)	T_g (C)	T_m(C)	Water Absorption (%)	Solvents	Vender	Notes
1	poly(1-trimethylsilyl-1-propyne)	PTMSP	3520[2]	262[2]	323[2]				
2	polydimethylsiloxane	PDMS	3100[5],4553[7]	-128[4]	-40[3]		Benzene, Toluene		Rubbery Polymer
3	6FDA-based polyimides	6FDA–durene	456[1], 24.2[5]	300-350[9]	N/A				
4	Poly(phenylene oxide)	PDMPO (60.0% brominated)	159.9[1]	184[2]	279-285[2]				
5	cis-polyisoprene	cis-PIP	134[5],191[7]	99[2]	156[2]		Hydrocarbon		Rubbery Polymer
6	Polycarbonates	TMHFPC	111[1]	217[2]	270[2]			GE,	
7	Polysulfones	PSF	110[1], 5.6[5]4.6[7]	237[2]186-190[9]	N/A		grade reagent alcohol (Fisher	Amoco Performance Products	P-1700
8	Poly(ether-b-amide)	PEBAX[6]	30-104[15]	-60 to -70[2] -30to 160[9]	120-210[2]		weight mixture of 1-propanol and 1-butanol at	ATOFINA Chemical, Inc. (Philadelphia, PA.)	grade 2533,hydrophobic
9	Polyarylates	TBHFBPA/tBIA	85.1[1]	N/A	N/A				Similar to polyester aromatics

Table 7-2 Membrane Material Candidates continued

Rank	Polymer	Abbreviation	$P(CO_2)$ (barrer)	T_g (C)	T_m(C)	Water Absorption (%)	Solvents	Vender	Notes
10	Poly(4-methyl-1-pentene)	PMP	83[5]	151-162[2]	270[2]		Xylene (>100C)		
11	Polyester	PE	HDPE 76.4[12] LDPE 13.4[12]	-20[8]	166-249[2]	0.1-0.5[2]		GE, Sigma-Aldrich	
12	Poly(2,6-dimethyl phenylene oxide)	PPO	61[5]	249-259[2]	282[2]		Benzene, Toluene		
13	Poly(pyrrolone)	6FDA–TAB	54.0[1]	N/A	273(?)[2]				
14	Polypropylene	PP	13.4,34[11]	-10[8]	135-165[8]				P477
15	Poly(arylene ether)	6FPPy–6FBPA	29.46 [1]	N/A	82-96[8]	0.06[2]			Similar to Poly(phenylene ether) V13P21
16	poly(tertbutylacetylene)	PTBA	5.0-27.4[13]	-77[13]	126-204[13]		isopropanol		
17	Poly(tetrafluoroethylene)	PTFE	21.3[11]	204[2]	316[2]		Perfluorinated Materials, >573K	GE, Dupont-NEN, Millipore,Advantec.	
18	Polystyrene	PS	12.4	98[8,9]			Acetone, Benzene		

Table 7-2 Membrane Material Candidates continued

Rank	Polymer	Abbreviation	P(CO_2) (barrer)	T_g (C)	T_m(C)	Water Absorption (%)	Solvents	Vender	Notes
19	Polyimides	PMDA–BAPHF	11.8[1]	230-330[9]	N/A				
20	Cellulose acetate	CA	5.5[7]	117-245[2]	304[2]	0.6[2]			
21	polyethersulfone	PES	4.2[2]	259[2]	N/A		0.43	GE	
22	Poly(vinyl acetate)	PVAC	3.1[10]	150[2]34.8[9]	231[2]	3-6[2]	Acetone,ethanol, methanol, benzene, toluene		
23	Polyamide	Nylon Hydrophobic	1.5[11]	160[2]	231-234[2]	1.0[2]		GE	Nylon 12
24	Poly(vinyl chloride)	PVC	1.3[12]	71[9]173-188[2]			Toluene, Acetone		Poisonous, p157
25	poly(ethylene terephthala	PET	0.5[12]	172-198[2]	281[2]	0.5[2]			
26	Polyvinyl fluoride	PVF	0.06[11]					GE	
27	Polyvinylidene fluoride	PVDF	0.05[14]	114[2]	227[2] 155-192[8]	0.025[2]	Acetone	GE, Dupont-NEN, Millipore,	V17P537

Table 7-2 Membrane Material Candidates continued

Rank	Polymer	Abbreviation	$P(CO_2)$ (barrer)	T_g (C)	T_m(C)	Water Absorption (%)	Solvents	Vender	Notes
28	poly(amide-imide)	PAI		287[2]	N/A	0.33[2]			
29	Nitrocellulose	cellulose nitrate CN	2.1[2]	163[2]	N/A	1.0[2]	Acetone,water	GE,Bio-Rad,Dupont-NEN, Millipore, S&S	
30	Polyvinylpyrrolidone	PVP		194-233[2]	N/A		Water,alcohol	Fluka Chemika	
31	Polyvinyl alcohol	PVA	161[10]	181[2]	281[2]		water		
32	Poly(acetylene)	Poly(trimethyl-prop-1-ynyl-silane)	19000 [1]	145[2]	420[2]				Degrades, not stable
33	Poly(ethylene oxide)	PEO	773[1]	70-112[2],-60[6]	99-171[2]		water	Sigma-Aldrich	Hydrophobic, Flash point 270C